

# Fragmentation of fully heavy tetraquarks: The TQ4Q1.1 functions as a case study

Francesco Giovanni Celiberto <sup>1,\*</sup>

<sup>1</sup>*Universidad de Alcalá (UAH), Departamento de Física y Matemáticas, E-28805 Alcalá de Henares, Madrid, Spain*

We extend the study of exotic matter formation via the **TQ4Q1.1** set of collinear, variable-flavor-number-scheme fragmentation functions for fully charmed or bottomed tetraquarks in three quantum configurations: scalar ( $J^{PC} = 0^{++}$ ), axial vector ( $J^{PC} = 1^{+-}$ ), and tensor ( $J^{PC} = 2^{++}$ ). We adopt single-parton fragmentation at leading power and implement a nonrelativistic QCD factorization scheme tailored to tetraquark Fock-state configurations. Short-distance inputs at the initial scale are modeled using updated calculations for both gluon- and heavy-quark-initiated channels. A threshold-consistent DGLAP evolution is then applied via **HF-NRevo**. We provide the first systematic treatment of uncertainties propagated from the color-composite long-distance matrix elements that govern the nonperturbative hadronization of tetraquarks. To support phenomenology, we compute NLL/NLO<sup>+</sup> cross sections for tetraquark-jet systems at the HL-LHC and FCC using **(sym)JETHAD**, incorporating angular multiplicities as key observables sensitive to high-energy QCD dynamics. This work connects the investigation of exotic hadrons with state-of-the-art precision QCD.

## CONTENTS

## I. INTRODUCTION

I. Introduction	1
II. Fragmentation of fully heavy tetraquarks	5
A. Heavy-flavor fragmentation: Key concepts	5
B. NRQCD from quarkonia to tetraquarks	6
C. Initial-scale FF inputs	8
D. TQ4Q1.1 functions from HF-NRevo	12
III. Hadron-collider phenomenology	20
A. Rapidity distributions	21
B. Angular multiplicities	24
IV. Summary and new directions	29
Acknowledgments	31
Data availability	31
A. Analytic expressions for the SDCs	32
B. Tetraquark-jet systems in NLL/NLO <sup>+</sup> HyF	35
References	38

Understanding how matter organizes itself beyond the conventional meson and baryon structure remains one of the central open challenges in hadron physics. Exotic configurations such as tetraquarks and pentaquarks—genuine multiquark states—invite us to rethink the underlying mechanisms of color confinement and hadronization, due to their beyond-minimal valence content and possible internal complexity.

High-energy experiments at the Large Hadron Collider (LHC), and future projects like the Electron-Ion Collider (EIC) [1–6] and the Future Circular Collider (FCC) [7–9], provide access to unprecedented kinematic regimes where such exotic hadrons can be produced and studied. These machines offer a clean testing ground for probing multiquark formation, resolving their inner quark-gluon structure, and isolating the dominant production mechanisms.

Recent advances in QCD factorization and the development of all-order resummation techniques have expanded the theoretical reach of precision calculations for exotic-matter observables [10–21]. Accurate predictions of cross sections and differential distributions, validated against experimental measurements, are now possible, enabling a more refined understanding of the interplay between perturbative dynamics and nonperturbative hadron formation.

\* francesco.celiberto@uah.es

A comprehensive physics program that combines exotic spectroscopy with state-of-the-art QCD approaches could shed light on the effective degrees of freedom at play in strongly interacting systems and help reveal the organizing dynamics of multi-quark states. Such insights would enhance our grasp of QCD in the nonperturbative regime and contribute to clarifying the mechanisms that drive the formation of bound hadronic matter.

Exotic hadrons are generally classified into two categories: gluon-rich states, such as quark-gluon hybrids [22–24] and glueballs [25–29], and multi-quark states, such as tetraquarks, pentaquarks, and hexaquarks [30–42]. While hybrids and glueballs contain explicit gluonic degrees of freedom, compact multi-quarks are modeled as leading Fock-state combinations of four or five quarks, respectively.

The observation of the  $X(3872)$  particle by the Belle experiment at KEKB in 2003 [43], later confirmed by several Collaborations [44–47], marked the beginning of what is often referred to as the “Exotic-matter Revolution” or Second Quarkonium Revolution”. It followed the earlier “Quarkonium Revolution” of the 1970s, which had been ignited by the historic discovery of the first doubly charmed hadron, the  $J/\psi$  meson [48–50]. The  $X(3872)$ , identified as a hidden-charm state with a  $[c\bar{c}]$  component, is widely interpreted as the first experimentally observed candidate for a hidden-charm tetraquark [51, 52]. This milestone was followed in 2021 by the LHCb detection of the  $X(2900)$  [53], representing the first exotic hadron observed with open-charm flavor and thus expanding the landscape of exotic spectroscopy.

Despite exhibiting conventional quantum numbers, the  $X(3872)$  features decay modes that explicitly violate isospin conservation. Such anomalies point to a structural complexity that cannot be captured by the standard quarkonium picture, motivating a wealth of theoretical interpretations framed within the tetraquark paradigm.

Among the most explored frameworks is the compact diquark model, where the  $X(3872)$  is envisioned as a tightly bound diquark-antidiquark configuration, distinct from the standard quark-antiquark composition of mesons [54–62]. An alternative view is offered by the meson molecule scenario, which interprets the  $X(3872)$  as a loosely bound system of two mesons held together

by residual strong interactions, in analogy with molecular binding in atomic physics [62–69]. A third possibility is the hadroquarkonium picture, where the  $X(3872)$  is described as a compact quarkonium core surrounded by a light mesonic cloud, bearing similarities to a hadronic analogue of an atomic system [40, 70–74].

These models aim to disentangle the subtleties of the  $X(3872)$  inner dynamics, and to shed light on the broader class of exotic hadrons sharing similar features. Further insight into its nature may be gleaned through phenomenological investigations in high-multiplicity proton collisions [75], as well as via theoretical analyses of its thermal behavior in a hadronic medium [76].

In 2021, the LHCb Collaboration reported the first observation of a doubly charmed tetraquark,  $T_{cc}^+$  [77, 78]. This state is interpreted as a near-threshold  $|DD\rangle$  molecular configuration, and its dynamics have been theoretically investigated using the XEFT effective field theory framework [79–87].

Until recently, the  $X(3872)$  was the only exotic hadron clearly observed in prompt proton-proton collisions. This picture evolved with the detection of both the  $T_{cc}^+$  and a broad resonance in the di- $J/\psi$  invariant mass spectrum [88], now dubbed  $X(6900)$  and believed to correspond either to the  $0^{++}$  scalar state or, more likely, to the  $2^{++}$  tensor excitation of a fully charmed  $T_{4c}$  tetraquark [89].

The CMS Collaboration has recently advanced our understanding of fully charmed tetraquarks by performing the first spin-parity determination of the states observed in the  $[J/\psi]$  and  $[J/\psi, \psi(2S)]$  channels. The initial observation of a family of three resonances in the  $4m_c < M < 7\text{ GeV}$  region was reported in Refs. [90] (see also Ref. [91]), and has now been complemented by a new angular analysis [92] favoring a  $[J^{PC} = 2^{++}]$  assignment for the leading signal. This result disfavors loosely bound molecular interpretations and supports a compact diquark-antidiquark structure, where spin-1 diquarks naturally produce  $[J = 2]$  configurations. Such spin constraints do not apply to mixed-flavor exotics such as  $X(3872)$  or  $Z_c(3900)$ , which remain consistent with lower spin and molecular descriptions. The CMS findings thus provide crucial input for modeling the internal dynamics of fully tetraquarks.

From a theoretical viewpoint, doubly and fully heavy tetraquarks,  $X_{Q\bar{Q}q\bar{q}}$  and  $T_{4Q}$ , represent particularly accessible systems for probing the strong force. In  $X_{Q\bar{Q}q\bar{q}}$  states, nonrelativistic heavy quarks interact with light degrees of freedom, often via diquark-like substructures, enabling a clean test of QCD in a mixed-mass regime. Similarly,  $T_{4Q}$  hadrons consist solely of heavy quarks and antiquarks in a  $|Q\bar{Q}Q\bar{Q}\rangle$  configuration, devoid of valence light quarks or active gluon fields, thus resembling a doubled, exotic quarkonium.<sup>1</sup>

Given the nonrelativistic dynamics of their constituents and the Fock-space structure, these exotic states can be analyzed using techniques developed for quarkonia. While charmonia are often described as QCD analogues of hydrogen atoms [100],  $X_{Q\bar{Q}q\bar{q}}$  and  $T_{4Q}$  tetraquarks may be seen as QCD nuclei or molecules, depending on the modeling approach [101].

Despite major progress in understanding exotic hadrons' mass spectra and decay modes since the  $X(3872)$  discovery, their production mechanisms remain poorly understood. Only a few model-dependent approaches, based on color evaporation [102] or hadron-quark duality [103–105], have been proposed so far.

Complementary efforts explored the role of multiparticle interactions in tetraquark production at hadron colliders [106, 107] and investigated potential signatures of high-energy dynamics in exotic formation [108]. Additional studies focused on exclusive radiative decays of  $T_{4Q}$  at bottom factories [11] and on  $T_{4Q}$  photoproduction in lepton-hadron collisions [13]. A deep neural network approach to multi-quark bound states was recently proposed [109].

In the bottom sector, our knowledge is still limited. The BELLE Collaboration first reported two charged bottomoniumlike structures in  $\Upsilon(5S)$  decays [110], hinting at exotic contributions. However, no  $|b\bar{b}b\bar{b}\rangle$  or  $|b\bar{b}q\bar{q}\rangle$  tetraquarks have yet been confirmed.

A recent observation by the ANDY Collaboration at RHIC of a resonance near 18.15 GeV in copper-gold collisions [111] matches predictions for  $T_{4b}$  states [112]. On the lattice side, bottom-charmed and doubly bottomed

tetraquarks have been investigated in Refs. [113, 114] and [115–117], respectively.

The unexpectedly high cross sections for  $X(3872)$  at large transverse momenta, reported by ATLAS, CMS, and LHCb [118–120], point to a fragmentation-based production mechanism. These findings offer a key opportunity to refine theoretical descriptions rooted in high-energy QCD.

To this end, in Ref. [18] we introduced the first-generation fragmentation functions (FFs) for fully charmed tetraquarks, the TQ4Q1.0 sets, focused on scalar ( $J^{PC} = 0^{++}$ ) and tensor ( $J^{PC} = 2^{++}$ ) fully charmed states. These FFs incorporate initial-scale inputs from both gluon and charm fragmentation, respectively modeled using quark-potential nonrelativistic QCD (NRQCD) [121–127] and spin-physics inspired prescriptions [16, 128–130].

The evolution to energy scales covered by experiments is performed using the novel *Heavy-flavor nonrelativistic-evolution* (HF-NRevo) method [131–133], which enables a DGLAP-consistent treatment of multi-step heavy-flavor thresholds, including gluon and charm activation.

The scalar and tensor channels provide valuable benchmarks in the study of fully heavy tetraquarks. Recent experimental efforts, notably the CMS analysis [90, 92], have favored a  $2^{++}$  assignment for observed all-charm tetraquark peaks. This supports the picture of a compact configuration with internal spin-1 diquark constituents, where the tensor channel emerges as the natural ground-state candidate due to symmetry and dynamical constraints. Such findings reinforce the relevance of these channels as targets for phenomenological modeling and experimental comparison.

Subsequently, in Ref. [19], the FFs were extended to the TQ4Q1.1 sets, which represent the successors of the 1.0 versions and include updated initial-scale inputs derived from NRQCD for both gluon [10] and charm [14] channels. Remarkably, the TQ4Q1.1 framework includes both fully charmed and fully bottomed tetraquark states, thus generalizing the fragmentation picture across different heavy-flavor sectors.

A further step was achieved in Ref. [20], with a dedicated study of axial-vector ( $J^{PC} = 1^{+-}$ ) tetraquarks, also marking the first time that LDME uncertainties

<sup>1</sup> For analogous studies on fully stranded tetraquarks, the “cousins” of the  $T_{4Q}$  states, see Refs. [93–99].

were consistently propagated into the FFs. These states are of particular interest in hadron physics, as they offer a relatively clean window into multiquark dynamics. Although light  $1^{+-}$  tetraquarks can undergo strong mixing with conventional mesons due to chiral symmetry breaking and meson-tetraquark couplings [134, 135], fully heavy systems behave differently. Heavy-quark spin symmetry (HQSS) [136, 137] implies weak spin-dependent interactions among charm and bottom quarks, thus suppressing  $[1^{++} \leftrightarrow 1^{+-}]$  mixing [138, 139]. This leads to more rigid spin structures and nearly pure physical eigenstates in the heavy sector, allowing for precise theoretical control and a clean separation from molecular-like admixtures.

The axial-vector states are further distinguished by their production characteristics. Due to Landau-Yang constraints [140, 141] and  $C$ -parity selection rules, they are suppressed at leading order (LO) in gluon fusion, making them excellent probes of nonperturbative QCD effects [105, 142]. Their selective dynamics and reduced mixing enhance their diagnostic value, especially when compared to scalar and tensor configurations, which may suffer from overlapping resonant interpretations.

Taken together, the scalar, tensor, and axial-vector components of the TQ4Q1.1 sets embody a unified, evolution-consistent framework for modeling the fragmentation of fully heavy tetraquarks. This modular infrastructure, grounded in QCD and responsive to experimental input, is well suited for future developments such as *multimodal* modeling and comparative studies across flavor sectors.

In this work, we extend and complete the phenomenological study of collinear fragmentation to fully heavy tetraquarks, presenting a detailed examination of the TQ4Q1.1 family of functions. This comprehensive update includes collinear FFs in a variable-flavor number scheme (VFNS) [143–145] for both charmed and bottomed tetraquarks, across all three spin-parity configurations: scalar ( $J^{PC} = 0^{++}$ ), axial-vector ( $J^{PC} = 1^{+-}$ ), and tensor ( $J^{PC} = 2^{++}$ ). As mentioned, the construction of these FFs is grounded in the HF-NRevo methodology.

By embedding all spin channels within a unified formalism, the TQ4Q1.1 framework, we provide a systematic treatment of collinear fragmentation for compact four-quark bound states, allowing for controlled com-

parisons across quantum numbers and heavy-flavor sectors.

A novel aspect of this study is the implementation of a quantitative treatment of nonperturbative uncertainties. For the first time, we propagate theoretical errors from long-distance matrix elements (LDMEs) into the FFs themselves. These LDMEs are defined on a color-composite basis, consistent with diquark-antidiquark clustering, and are extracted from potential NRQCD calculations for the scalar and tensor channels and from a model-averaged prescription in the axial-vector case.

By incorporating uncertainty bands, TQ4Q1.1 serves not only as a functional tool for high-energy predictions, but also as a diagnostic instrument to assess the model dependence of exotic hadron formation. Designed as a case study within a broader strategy, this work lays the foundation for future *multimodal* fragmentation frameworks, where perturbative and nonperturbative ingredients of different nature can be jointly explored and validated against upcoming experimental results.

As a test case for our fragmentation framework, we examine the inclusive production of fully heavy tetraquarks accompanied by a jet in proton-proton collisions at energies relevant for the High-Luminosity LHC (HL-LHC) and FCC. Our reference reaction is studied within a NLL/NLO<sup>+</sup> hybrid formalism (HyF) that combines next-to-leading order (NLO) collinear factorization with the resummation of high-energy logarithms beyond NLL accuracy.

This setup allows us to access observables that are particularly sensitive high-energy dynamics, including rapidity intervals and azimuthal-angle multiplicities, the latter being novelly introduced as discriminators of energy-flow patterns—resummed versus fixed order—in QCD radiation. All predictions are obtained using the JETHAD numerical infrastructure supplemented by its symbolic extension `symJETHAD` [146–150].

This work contributes to the broader effort of establishing a systematic, evolution-consistent framework for the fragmentation of fully heavy tetraquarks, bridging the flexible modeling strategies typical of hadron-structure studies with the most advanced tools from precision QCD. By addressing multiple spin-parity channels and both charm and bottom flavors, it provides a unified reference for the entire family of compact four-



quark states. It sets the stage for future investigations and cross-validations with potential-model predictions, lattice QCD results, and heavy-flavor phenomenology at current and next-generation colliders.

The structure of this article is as follows. In Section II, we begin with a brief overview of the general features of heavy-flavor fragmentation, including how the NRQCD framework—originally developed for quarkonia—can be extended to the case of fully heavy tetraquarks. We then present the technical foundation underlying the construction of the TQ4Q1.1 functions for both fully charmed and fully bottomed systems. In Section III, we discuss our phenomenological analysis for tetraquark-jet systems at HL-LHC and FCC energies and within the HyF framework. In Section IV we presents our conclusions and outlook.

## II. FRAGMENTATION OF FULLY HEAVY TETRAQUARKS

In the first part of this section, we briefly outline the main features of heavy-flavor fragmentation, focusing on heavy-light hadrons, quarkonium states, and exotic bound systems (Section II A). We then discuss the application of NRQCD to model initial-scale inputs for gluon and constituent heavy-quark fragmentation channels to  $T_{4Q}$  tetraquarks (Sections II B and II C). Finally, in Section II D, we study the timelike DGLAP evolution within the HF-NRevo framework of the complete TQ4Q1.1 family of FFs, as a case study for a modular and consistent approach to the fragmentation of fully heavy tetraquarks.

### A. Heavy-flavor fragmentation: Key concepts

Contrariwise to their light-flavor counterpart, heavy-flavor hadrons entail a fragmentation mechanism partially rooted in perturbative QCD. Unlike light hadrons, heavy-flavor hadronization involves additional complexity due to the large mass of heavy quarks, which places them within the perturbative QCD domain. As a result, while FFs for light hadrons are entirely nonperturbative, those for heavy hadrons must include perturbative

elements at the initial scale.

For singly heavy-flavored hadrons like  $D$ ,  $B$ , or  $\Lambda_{c,b}$ , the fragmentation process can be modeled as a two-step mechanism [144, 151–155]. First, a highly energetic parton  $i$  fragments into a heavy quark  $Q$ , a process calculable in perturbative QCD since the coupling at the heavy-quark mass scale is small. This short-distance coefficient (SDC), describing the  $[i \rightarrow Q]$  subprocess, occurs over a shorter timescale than hadronization. The first NLO computations for such SDCs appeared in Refs. [143, 156], with further next-to-NLO developments in Refs. [157–162].

The second, nonperturbative stage involves the hadronization of the heavy quark into a physical hadron, typically modeled through phenomenological functions [163–168] or effective theories [137, 152, 169–171]. To build a full VFNS FF set, one then evolves these initial inputs through DGLAP equations, using numerical methods to incorporate scaling violations at the desired perturbative accuracy.

This two-stage strategy also applies to quarkonium fragmentation. However, the presence of a  $[Q\bar{Q}]$  pair in the leading Fock state makes the dynamics more involved. This is addressed within the framework of NRQCD [121–127], whose foundations and phenomenological implications are extensively reviewed in Refs. [172–176].

In NRQCD, heavy quarks and antiquarks are treated as nonrelativistic degrees of freedom, enabling a factorization between SDCs, describing the perturbative production of a  $[Q\bar{Q}]$  pair, and LDMEs, which model nonperturbative hadronization. A physical quarkonium is expressed as a linear combination of Fock states, ordered via a double expansion in  $\alpha_s$  and the relative velocity  $v_Q$  of the constituent quarks.

NRQCD accommodates both low and high transverse-momentum ( $p_T$ ) production. At low  $p_T$  values, the dominant mechanism is the direct production of the  $[Q\bar{Q}]$  pair in the hard scattering, followed by nonperturbative hadronization. At higher  $p_T$ , fragmentation of a single parton into the hadron plus radiation becomes dominant. While this single-parton process corresponds to a VFNS governed by DGLAP evolution, the low- $p_T$  short-distance channel aligns with a fixed-flavor number scheme (FFNS) [177],

involving two-parton fragmentation and higher-power corrections [131–133, 178–181].

Early LO calculations for gluon and heavy-quark fragmentation into  $S$ -wave vector quarkonia in color-singlet states were provided in Refs. [182, 183]. NLO order results became available later [184, 185], enabling the development of the first pioneering VFNS DGLAP-evolved FFs, known as the ZCW19<sup>+</sup> sets [148, 186]. This was extended to  $B_c(^1S_0)$  and  $B_c(^3S_1)$  mesons via the ZCFW22 sets [187, 188].

Predictions using ZCFW22 aligned with LHCb data [188–190], confirming that  $B_c(^1S_0)$  production stays below 0.1% relative to singly bottomed  $B$  mesons [188], thereby validating the use of the VFNS scheme at large  $p_T$ .

Recent studies suggest that the NRQCD factorization also applies to exotic states, such as double  $J/\psi$  signals observed at the LHC [88, 90, 191], interpreted as compact tetracharms [192, 193]. Here,  $T_{4c}$  formation proceeds from the short-distance production of two charm and two anticharm quarks, at a scale  $\sim 1/m_c$ . As in the quarkonium case, fragmentation is modeled as a two-step convolution: a perturbative stage followed by nonperturbative hadronization.

The first NRQCD-based calculation of the initial input for gluon fragmentation into color-singlet  $S$ -wave  $T_{4c}$  states was carried out in Ref. [10]. Building on that framework, the first VFNS FF sets for heavy-light tetraquarks, TQHL1.0, were introduced in Ref. [17] (see also the review in [149]). Reference [19] expanded upon this effort by releasing the successor families TQ4Q1.1 and TQHL1.1, featuring NRQCD-based modeling also for the  $[Q \rightarrow T_{4Q}]$  input [14], improved treatment of doubly-heavy tetraquark fragmentation, and inclusion of bottomoniumlike states.

Then, a prime dedicated study of axial-vector ( $1^{+-}$ ) states was presented in Ref. [20], also marking the first time that composite LDME uncertainties were propagated into the FFs.

As a direct application of our exploration on exotic-matter production, FF determinations for fully charmed pentaquarks and rare  $\Omega$  baryons were presented in Refs. [21] and [194], respectively, leading to the release of the PQ5Q1.0 and OMG3Q1.0 sets.

## B. NRQCD from quarkonia to tetraquarks

In this subsection, we outline the NRQCD-based approach to collinear fragmentation, detailing how it provides a systematic framework for describing the transition from a partonic state to the physical hadron. To ensure clarity and consistency, we first recall the structure of NRQCD-based fragmentation in the case of conventional quarkonium. This provides the necessary background for understanding the subsequent extension to exotic channels.

The derivation of FFs for tetraquark states follows the formalism presented in Refs. [10, 14], which we adapt to match the specific scope of our study. We refer the reader to those references for technical details on the NRQCD-based calculations and the modeling of both short-distance and long-distance contributions.

According to NRQCD, the FF of a parton  $i$  into a physical quarkonium state  $\mathcal{Q}$  with momentum fraction  $z$  at the initial energy scale  $\mu_{F,0}$  is given by the following expression

$$D_i^{\mathcal{Q}}(z, \mu_{F,0}) = \sum_{[n]} \mathcal{D}_i^{Q\bar{Q}}(z, [n]) \langle \mathcal{O}^{\mathcal{Q}}([n]) \rangle. \quad (1)$$

Here,  $\mathcal{D}_i^{Q\bar{Q}}(z, [n])$  is the perturbative SDC for the production of the intermediate  $[Q\bar{Q}]$  pair, expandable in  $\alpha_s$  and featuring DGLAP-type logarithms for resummation. The factor  $\langle \mathcal{O}^{\mathcal{Q}}([n]) \rangle$  represents the nonperturbative NRQCD LDME, containing suppression effects in the relative velocity  $v_{\mathcal{Q}}$  of the  $[Q\bar{Q}]$  system. These LDMEs must be determined through global fits or estimated via lattice or potential models. The  $[n] \equiv 2S+1 L_J^{(c)}$  label denotes the spectroscopic quantum numbers, with  $(c)$  indicating the color state, singlet (1) or octet (8).

Equation (1) reflects the two core assumptions of NRQCD: first, the physical quarkonium is described by a linear superposition of all contributing Fock states labeled by  $[n]$ ; second, all contributions are organized via a double expansion in  $\alpha_s$  and  $v_{\mathcal{Q}}$ .

A comparison between heavy-light-hadron and quarkonium fragmentation reveals both structural analogies and crucial differences. For singly heavy-flavored hadrons  $h_Q$ , the  $[i \rightarrow h_Q]$  FF at the initial

scale involves a convolution between a perturbative FF for  $[i \rightarrow h_Q]$  and a nonperturbative transition function that encodes the probability for  $Q$  to hadronize into  $h_Q$  [144, 151, 152]. This convolution reflects the dynamical sharing of momentum with soft constituents, and leads to an explicit  $z$ -dependence in the hadronization model.

In contrast, NRQCD expresses the  $[i \rightarrow \mathcal{Q}]$  FF as a sum over Fock states  $[n]$ , each term being a product of a perturbative SDC and a constant LDME. Since the heavy constituents of the quarkonium originate from the short-distance process itself, hadronization does not involve additional momentum redistribution. As a result, LDMEs are  $z$ -independent and represent fixed probabilities for the transition of a  $[Q\bar{Q}]$  pair into the physical state  $\mathcal{Q}$ . This fundamental difference explains why FFs for open-flavor hadrons require phenomenological  $z$ -dependent models, while NRQCD-based FFs are built from linear combinations of perturbative functions weighted by scalar LDMEs.

Although LDMEs are not known from first principles, they can be constrained by experimental data or estimated through nonperturbative approaches such as lattice QCD or potential models. However, specific assumptions may simplify their structure.

A notable assumption is the so-called *vacuum saturation approximation* (VSA) [123, 195, 196], which posits that intermediate states other than the vacuum are suppressed by powers of the relative velocity  $v_Q$  of the heavy quarks. Under this approximation, the LDME reduces to the product of matrix elements between the vacuum and the lowest Fock state  $|Q\bar{Q}\rangle$ . Symbolically, the VSA reads

$$\langle 0 | \chi^\dagger \Pi_n \psi \mathcal{P}_Q \psi^\dagger \Pi'_n \chi | 0 \rangle \simeq \langle 0 | \chi^\dagger \Pi_n \psi | \mathcal{Q} \rangle \langle \mathcal{Q} | \psi^\dagger \Pi'_n \chi | 0 \rangle \quad (2)$$

Here,  $\Pi_n$  and  $\Pi'_n$  are spin-color projectors for the relevant NRQCD state, while  $\mathcal{P}_Q$  denotes the projector onto the physical quarkonium  $\mathcal{Q}$ . The fields  $\chi$  and  $\psi$  represent nonrelativistic Pauli spinors that annihilate a heavy antiquark and create a heavy quark, respectively, within the NRQCD framework.

In analogy with Eq. (1), which describes the fragmentation of a parton  $i$  into a quarkonium  $\mathcal{Q}$  within the NRQCD factorization framework, the initial-scale FF of a parton  $i$  into a fully heavy tetraquark  $T_{4Q}$  can also be expressed as a weighted sum over different Fock

states. In this extended scenario, the nonperturbative formation of the physical tetraquark state is described by color-composite LDMEs that encode the probability of hadronization from a perturbatively produced four-quark configuration. The general structure of the initial-scale FF reads

$$D_i^{T_{4Q}}(z, \mu_{F,0}) = \sum_{[n]} \mathcal{D}_i^{4Q}(z, [n]) \langle \mathcal{O}^{T_{4Q}}([n]) \rangle, \quad (3)$$

where the role of the  $\mathcal{D}_i^{4Q}(z, [n])$  SDCs is to describe the production of a compact  $|QQ\bar{Q}\bar{Q}\rangle$  configuration in a definite spin, color, and orbital state  $[n]$ , and  $\langle \mathcal{O}^{T_{4Q}}([n]) \rangle$  are the color-composite LDMEs encoding the nonperturbative hadronization into the physical tetraquark.

The key distinction with respect to the quarkonium case lies in the complexity of the intermediate state. Instead of a two-body heavy-quark pair, the tetraquark system originates from a four-body configuration, subject to additional spin-color couplings and internal symmetries. This richer structure implies a larger number of contributing Fock states and, consequently, a more intricate pattern of LDMEs, reflecting the possible internal color-spin arrangements compatible with a color-singlet final state.

Moreover, while the NRQCD framework continues to apply thanks to the  $m_Q \gg \Lambda_{\text{QCD}}$  hierarchy, the reduced binding of the four-heavy-quark system and the possible coexistence of tightly- and loosely-bound configurations may influence the convergence of the velocity expansion and the size of subleading terms. Nevertheless, for low-lying  $S$ -wave compact tetraquarks, one expects the factorized structure of Eq. (3) to remain a valid starting point for constructing perturbative inputs at the initial energy scale, and for matching the evolution to high energies via DGLAP equations.

Considering a fully heavy tetraquark  $T_{4Q}(J^{PC})$ , with total angular momentum, parity, and charge  $J^{PC} = 0^{++}$ ,  $1^{+-}$ , or  $2^{++}$ , and retaining only the lowest-order terms in the velocity expansion, we can recast Eq. (3) as follows

$$D_i^{T_{4Q}(J^{PC})}(z, \mu_{F,0}) = \frac{1}{m_Q^9} \sum_{[n]} \tilde{\mathcal{D}}_i^{(J^{PC})}(z, [n]) \times \langle \mathcal{O}^{T_{4Q}(J^{PC})}([n]) \rangle, \quad (4)$$

with  $m_Q = m_c = 1.5$  GeV ( $m_Q = m_b = 4.9$  GeV) being the charm (bottom) mass. Furthermore, the composite

quantum number  $[n]$  runs over the combinations:  $[3, 3]$ ,  $[6, 6]$ ,  $[3, 6]$ , and  $[6, 3]$ . Throughout this work, we define the SDCs as dimensionless quantities, given by

$$\tilde{\mathcal{D}}_i^{(J^{PC})}(z, [n]) \equiv m_Q^9 \mathcal{D}_i^{(J^{PC})}(z, [n]) . \quad (5)$$

Finally, the following symmetry relations hold

$$\begin{aligned} \tilde{\mathcal{D}}_i^{(J^{PC})}(z, [3, 6]) &= \tilde{\mathcal{D}}_i^{(J^{PC})}(z, [6, 3]) , \\ \langle \mathcal{O}^{T_{4c}(J^{PC})}([3, 6]) \rangle &= \langle \mathcal{O}^{T_{4Q}(J^{PC})}([6, 3]) \rangle^* . \end{aligned} \quad (6)$$

### C. Initial-scale FF inputs

For the sake of clarity, this section is divided into four parts: we first introduce the dimensionless SDCs, then present the general strategy to construct the color-composite LDMEs, discuss the role of color-octet mechanisms, and finally specify the LDME values and their associated uncertainties.

**Dimensionless SDCs.** To calculate the SDCs entering Eq. (4), Authors of Refs. [10, 14] followed the standard perturbative matching procedure between pure QCD and NRQCD matrix elements. Within the standard NRQCD approach, the SCDs are determined by matching perturbative QCD and NRQCD matrix elements computed with fictitious, free multi-quark states that carry the same quantum numbers as the physical quarkonium [123, 197]. At present, analytic calculations for the initial-scale FF inputs of  $T_{4Q}$  states are available only at LO in both  $\alpha_s$  and the relative velocity  $v_Q$ .

As in the quarkonium case, SDCs for  $T_{4Q}$  states are insensitive to the long-distance dynamics of hadronization, and can thus be computed by replacing the physical tetraquark state  $T_{4Q}$  with an artificial, free four-quark configuration  $[[QQ][\bar{Q}\bar{Q}]]$  carrying the same quantum numbers.

The matching is performed at LO in  $\alpha_s$  and in the relative velocity  $v_Q$ , retaining only the lowest-order NRQCD operators and neglecting derivative contributions. The tetraquark is modeled as a diquark-antidiquark configuration, and the projection onto definite spin, parity, and color is achieved through the con-

struction of appropriate NRQCD four-quark operators.<sup>2</sup> These operators include both  $[3 \otimes 3]$  and  $[6 \otimes \bar{6}]$  color structures.

However, the allowed quantum numbers depend on the interplay between Fermi-Dirac statistics and the  $S$ -wave orbital structure of the system. Specifically, for scalar ( $0^{++}$ ) and tensor ( $2^{++}$ ) channels, both color configurations are in principle allowed, with the  $[6 \otimes \bar{6}]$  component contributing only to spin-0 states. In contrast, for the axial-vector state ( $1^{+-}$ ), Fermi-Dirac constraints eliminate the  $[6 \otimes \bar{6}]$  configuration, leaving only the  $[\bar{3} \otimes 3]$  contribution. Additionally, in the axial-vector case, the gluon-initiated channel is forbidden at LO due to the Landau-Yang theorem, which prohibits the coupling of a single on-shell gluon to a  $1^{+-}$  state. As a result, only the constituent heavy-quark fragmentation channel is retained in this case.

The analytic expressions for the dimensionless SDCs of our tetraquarks are reported in Appendix A. The gluon and heavy-quark NRQCD channels, first calculated in Refs. [10] and [14], and later independently rederived using the (sym)JETHAD [146–150] symbolic engine, are valid at LO accuracy and for color-singlet configurations (see Fig. 1).

**Building color-composite LDMEs.** As mentioned above, our approach provides analytic expressions for the SDCs at the initial energy scale, which are then matched to the corresponding NRQCD LDMEs. These matrix elements encode the nonperturbative transition of the  $[[QQ][\bar{Q}\bar{Q}]]$  configuration into the physical tetraquark state and must be either extracted from experimental data or modeled through phenomenological assumptions.

In analogy with the quarkonium case, a commonly adopted simplification is provided by the VSA, which reduces the LDMEs to the product of matrix elements between the vacuum and the lowest Fock component

<sup>2</sup> The diquark-antidiquark configuration simplifies the NRQCD matching by reducing the four-body problem to two-body building blocks, making the projection onto spin, parity, and color quantum numbers more tractable. References [10, 14] adopt this approach to construct gauge-invariant operators and extract the corresponding SDCs.

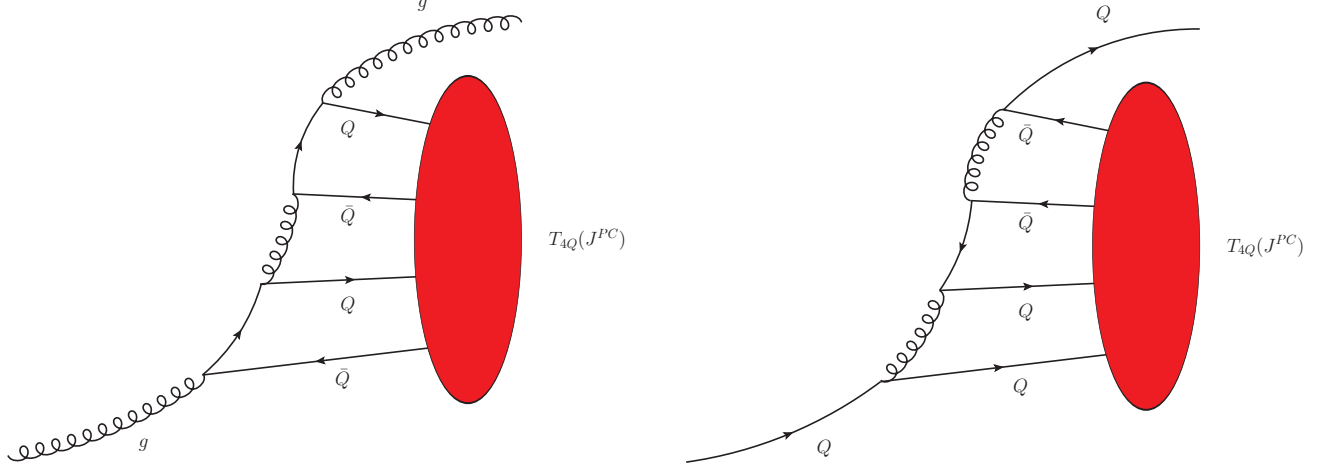


FIG. 1. LO diagrams illustrating the collinear fragmentation of a gluon (left) and a heavy quark (right) into a fully heavy  $S$ -wave tetraquark in a color-singlet configuration. Parton interactions on the left-hand side of each diagram depict the perturbative short-distance coefficients (SDCs), while red blobs on the right-hand side portray the nonperturbative long-distance matrix elements (LDMEs) describing the final hadronization step.

of the physical state. For tetraquarks, this structure is more intricate due to the presence of two color-connected diquark and antidiquark subsystems. Following Refs. [10, 14], we adopt the so-called color-composite LDMEs, where the physical tetraquark state is expanded in a diquark-antidiquark basis and projected onto definite color-singlet operators.

This decomposition enables the classification of the long-distance matrix elements according to the color configuration of the constituent clusters, namely  $[3, 3]$ ,  $[6, 6]$ , and the mixed  $[3, 6]/[6, 3]$  components, as previously introduced in Eq. (4). These LDMEs describe the probability amplitude for hadronizing a perturbatively produced four-quark state into the physical bound state, and must be specified for each spin and color configuration. For completeness, here we report the color composite operators associated with the  $T_{4Q}$  LDMEs, and refer the reader to Section IV of Ref. [10] for technical details. We write

$$\begin{aligned} \mathcal{O}_{3\otimes 3}^{(0)} &= -\frac{1}{\sqrt{3}} [\psi_a^T(i\sigma^2)\sigma^i\psi_b] [\chi_c^\dagger\sigma^i(i\sigma^2)\chi_d^*] \mathcal{C}_{3\otimes 3}^{ab;cd}, \\ \mathcal{O}_{3\otimes 3}^{\alpha\beta;(2)} &= [\psi_a^T(i\sigma^2)\sigma^m\psi_b] [\chi_c^\dagger\sigma^n(i\sigma^2)\chi_d^*] \Gamma^{\alpha\beta;mn} \mathcal{C}_{3\otimes 3}^{ab;cd}, \\ \mathcal{O}_{6\otimes 6}^{(0)} &= [\psi_a^T(i\sigma^2)\psi_b] [\chi_c^\dagger(i\sigma^2)\chi_d^*] \mathcal{C}_{6\otimes 6}^{ab;cd}, \end{aligned} \quad (7)$$

with  $\sigma^2$  standing for the second Pauli matrix, and  $\psi$  and  $\chi$  representing the standard NRQCD fields, as in Eq. (2). The rank-4 Lorentz tensor is defined as

$$\Gamma^{kl;mn} \equiv \frac{1}{2} \left( \delta^{km}\delta^{ln} + \delta^{kn}\delta^{lm} - \frac{2}{3}\delta^{kl}\delta^{mn} \right), \quad (8)$$

and the rank-4 color tensors take the form

$$\begin{aligned} \mathcal{C}_{3\otimes 3}^{ab;cd} &= \frac{1}{(\sqrt{2})^2} \epsilon^{abm} \epsilon^{cdn} \frac{\delta^{mn}}{\sqrt{N_c}} \\ &= \frac{1}{2\sqrt{3}} (\delta^{ac}\delta^{bd} - \delta^{ad}\delta^{bc}), \\ \mathcal{C}_{6\otimes 6}^{ab;cd} &= \frac{1}{2\sqrt{6}} (\delta^{ac}\delta^{bd} + \delta^{ad}\delta^{bc}), \end{aligned} \quad (9)$$

where we have introduced the rank-3 Levi-Civita tensors  $\epsilon^{ijk}$  and the Kronecker delta  $\delta^{mn}$  to construct color-singlet combinations.

We note that the adopted diquark-antidiquark basis is formally equivalent, via Fierz rearrangements, to a molecular-like decomposition with color structure  $[1 \otimes 1]$  or  $[8 \otimes 8]$ . However, this choice is not meant to imply a literal bound-state interpretation of the diquark-antidiquark configuration. Rather, it reflects the structural assumptions of our proxy model, where



the tetraquark formation is driven by dominant color and spin correlations between tightly coupled diquark and antidiquark pairs. Such a representation is fully consistent with the nature of a fragmentation production inherently based on the direct formation of compact, multi-quark bound states.

**On the role of color-octet mechanisms.** The inclusion of color-octet channels in the NRQCD modeling of initial-scale FFs remains a challenging task, both conceptually and phenomenologically. In the present work, following the strategy adopted in Refs. [10, 14], we restrict our analysis to color-singlet configurations only. This choice reflects the current status of reliable input for the LDMEs associated with color-octet channels, which are notoriously difficult to constrain. As discussed in those studies, a consistent treatment of such contributions will require dedicated efforts to obtain trustworthy estimates of octet LDMEs, possibly through lattice simulations or advanced potential models. Until such inputs become available, any attempt to include color-octet terms would rely on uncontrolled modeling assumptions.

However, it is instructive to assess the potential relevance of color-octet mechanisms by drawing an analogy with the well-known “quarkonium production puzzle” in (semi-)inclusive reactions (see Refs. [198, 199] and references therein). In the case of  $J/\psi$  production, extensive phenomenological evidence has shown that color-singlet mechanisms alone fail to describe high- $p_T$  data at hadron colliders. Prediction within the dominant singlet contribution, proceeding through  $^3S_1^{(1)}$  configurations, underestimate the observed rates. In contrast, the inclusion of fragmentation processes involving gluons or heavy quarks into color-octet  $|c\bar{c}\rangle$  states, (particularly  $^3S_1^{(8)}$ ,  $^1S_0^{(8)}$ , and  $^3P_J^{(8)}$ ) yields a more accurate description [124, 125, 182, 200–203]. These observations have led to the widely accepted conclusion that a complete description of vector charmonia requires the inclusion of color-octet channels.

For other quarkonia, however, the situation is different. For pseudoscalar states like  $\eta_c$  and  $\eta_b$ , NRQCD predicts the dominance of the  $^1S_0^{(1)}$  singlet channel, with octet contributions strongly suppressed by symmetry constraints [182, 204]. The available data (especially for  $\eta_c$  [205, 206]) can be reproduced by singlet-only ap-

proaches, confirming this prediction. A similar pattern holds for  $\Upsilon(nS)$  states [207], where the larger mass scale and reduced soft-gluon sensitivity limit the impact of octet mechanisms [208], although minor corrections may still be allowed at high transverse momentum [209].

Turning our attention to fully heavy tetraquarks, the applicability of a singlet-only approximation is highly sensitive to the quantum numbers  $J^{PC}$  of the bound state. In the scalar channel ( $0^{++}$ ), the internal color-spin wavefunction receives contributions from multiple diquark-antidiquark configurations, most notably the  $[3, 3]$  and  $[6, 6]$  color combinations. These components can interfere and mix, leading to a fragmentation structure that is inherently model dependent. In this case, the interplay of color configurations and their sensitivity to the assumed potential model may render color-octet mechanisms necessary to account for transitions that cannot be captured by the singlet component alone. As a consequence, predictions for scalar tetraquark fragmentation could be particularly vulnerable to theoretical uncertainties.

The situation is structurally simpler in the tensor channel ( $2^{++}$ ), where only the  $[3, 3]$  configuration contributes. This channel is  $S$ -wave and fully symmetric in spin, and Fermi-Dirac statistics permit just one allowed color-spin coupling. Despite the absence of internal mixing, the resulting predictions still retain a moderate level of model dependence, especially through the specific shape and normalization of the bound-state wavefunction. In addition, the lack of strict symmetry constraints on the spinor structure leaves more room for ambiguity in modeling the wavefunction, thereby increasing the sensitivity to potential-model assumptions. Moreover, while a singlet-only treatment may be justified in first approximation, the possibility of subleading octet contributions cannot be fully excluded at the quantitative level.

A qualitatively different scenario emerges in the axial-vector channel ( $1^{+-}$ ), which stands out for its structural clarity. Here, the  $S$ -wave nature of the bound state, combined with the antisymmetric requirements of Fermi-Dirac statistics, constrains the internal color-spin wavefunction to a single configuration: the  $[3, 3]$  component. This eliminates the possibility of interference between different color structures and leads to a much cleaner factorization scheme. The resulting fragmen-

tation dynamics are largely insensitive to the details of the potential model, and the singlet-only approximation proves to be not only sufficient but also phenomenologically robust. This is supported by the observed stability of predictions across different modeling frameworks, as reported in Refs. [14, 20].

It is tempting to draw a parallel between the axial-vector tetraquark and the  $J/\psi$ , both being spin-1 states. However, such a comparison can be misleading. The  $J/\psi$  is a vector  $^3S_1$  quarkonium with well-understood spin and parity assignments, while the  $1^{+-}$  tetraquark is an exotic multiquark system with different symmetry properties and a different color-spin composition. Unlike the  $J/\psi$ , whose singlet contribution is insufficient at high  $p_T$ , the  $1^{+-}$  tetraquark can, in many cases, be well described by the singlet term alone, particularly in gluon fragmentation.

From a structural viewpoint, the difference stems from the dominance of a single color configuration in the diquark-antidiquark basis adopted within the NRQCD color-decomposition framework. The fragmentation process itself further enhances this compactness, favoring the formation of correlated subsystems with minimal color rearrangement. In this context, the role of color-octet contributions becomes increasingly model-specific: relevant in some configurations, negligible in others.

In light of this analysis, our choice to restrict the present implementation of FFs to color-singlet channels is well motivated, particularly for the axial-vector channel. At the same time, our discussion outlines the path for future improvements: once reliable determinations of color-octet LDMEs become available, their inclusion will allow for a more comprehensive and quantitatively accurate modeling of tetraquark production across all quantum number sectors.

**LDME values and uncertainties.** As mentioned, the LDMEs  $\langle \mathcal{O}^{T_{4Q}(J^{PC})}([n]) \rangle$  represent the genuinely non-perturbative inputs to our initial-scale FFs. As in our previous works [18, 19], and in the absence of experimental data or lattice inputs for fully heavy tetraquarks, we extract estimates of these matrix elements from quark potential models.

This approach follows the strategy introduced in

Ref. [10], where the radial wave functions at the origin are computed for fully charmed states by solving the Schrödinger equation with a Cornell-like potential [210, 211], and then related to LDMEs through the VSA. In that work, three models were proposed [212–214]: the first and third adopt nonrelativistic quark fields, while the second includes relativistic corrections.

The first model tends to significantly overestimate the cross section when compared to CMS data on  $J/\psi$  production at  $\sqrt{s} = 13$  TeV [215], which are in any case expected to exceed the actual  $T_{4c}$  yield. Moreover, numerical tests (not shown here) revealed that the third model leads to severe instabilities: FFs constructed with its LDMEs exhibit large numerical fluctuations under minimal parameter variations, on the order of 0.1%. For these reasons, in Refs. [18, 19] we discarded both the first and third models and selected the second model [213] as default reference.

A further extension was introduced in Ref. [14], where two additional LDME models, denoted as Models IV and V in that work, were incorporated into the NRQCD-based construction of heavy-quark FFs. From the inspection of Table 1 of Ref. [14], it clearly emerges that Model IV [216] predicts values for the  $1S$  axial-vector channel that are numerically close to those in [213], whereas Model V [217] yields results that are suppressed by roughly one order of magnitude. In light of this results, and aiming to reduce model dependence while avoiding overconservative suppression, in Ref. [20] we based our analysis of the  $T_{4c}(1^{+-})$  case on the average of the LDMEs from Refs. [213] and [216], taking the spread between them as a measure of the theoretical uncertainty.

The axial-vector channel stands out as a particularly clean benchmark for this purpose. As already explained, due to Fermi-Dirac statistics and the  $S$ -wave nature of the state, its internal color-spin wavefunction is dominated by a single configuration,  $[3, 3]$ , with no interference or mixing among color structures. This leads to a much cleaner factorization structure, reduces sensitivity to model assumptions, and enhances prediction stability. As observed in Ref. [20], the  $1^{+-}$  channel displays remarkable robustness under variations of the LDME model—particularly for Models I, II, and IV in Ref. [14]—unlike the scalar and tensor channels.

In contrast, the scalar ( $0^{++}$ ) and tensor ( $2^{++}$ ) states suffer from stronger model dependence. As discussed in Ref. [10] and revisited in Refs. [18, 19], the  $0^{++}$  state receives contributions from multiple interfering components in the diquark-antidiquark basis, notably the  $[3, 3]$ ,  $[6, 6]$ , and mixed  $[3, 6]$  channels. These induce destructive or constructive interference patterns that vary with the potential model, making the resulting LDMEs unstable. The  $2^{++}$  channel is structurally simpler, since it involves only a  $[3, 3]$  component, but still displays significant sensitivity to the shape and normalization of the radial wavefunction.

Given these considerations, in the present study we adopt a conservative prescription for estimating uncertainties on the scalar and tensor LDMEs. Since no direct uncertainty estimate is available for these channels, we take the relative uncertainty extracted in Ref. [20] for the axial-vector LDME as a reference and double it to reflect the enhanced model dependence.

Then, in the absence of first-principles determinations for the LDMEs of fully bottomed tetraquarks, we rely on a phenomenological *Ansatz* inspired by physical arguments. We consider the  $T_{4b}$  system to behave as a compact diquark-antidiquark bound state, whose internal dynamics are predominantly governed by attractive color-Coulomb interactions. Under this assumption, a dimensional analysis allows us to relate the four-body Schrödinger wave function at the origin for  $T_{4b}$  and  $T_{4c}$  states. This strategy, originally proposed in Ref. [12], leads to the following scaling relation

$$\frac{\langle \mathcal{O}^{T_{4b}(J^{PC})}([n]) \rangle}{\langle \mathcal{O}^{T_{4c}(J^{PC})}([n]) \rangle} = \frac{\langle \mathcal{O}_{[C]}^{T_{4b}} \rangle}{\langle \mathcal{O}_{[C]}^{T_{4c}} \rangle} \simeq \left( \frac{m_b \alpha_s^{[b]}}{m_c \alpha_s^{[c]}} \right)^9 \simeq 400. \quad (10)$$

In this expression,  $\alpha_s^{[Q=c,b]}$  represents the strong coupling constant evaluated at the characteristic scale  $m_Q v_Q$ , with  $v_Q$  denoting the typical relative velocity between the two constituent heavy quarks. The '[C]' label specifies that the associated LDME has been obtained using a potential model dominated by Coulomb-like interactions within the diquark subsystem.

We collect the numerical values of the color-composite LDMEs employed in our analysis in Tables I and II, for the  $T_{4c}(J^{PC})$  and  $T_{4b}(J^{PC})$  states, respectively. The quoted uncertainties reflect the model-dependent prescriptions detailed above.

$[n]$	$T_{4c}(0^{++})$ [GeV <sup>9</sup> ]	$T_{4c}(1^{+-})$ [GeV <sup>9</sup> ]	$T_{4c}(2^{++})$ [GeV <sup>9</sup> ]
$[3, 3]$	$0.0347 \pm 0.0076$	$0.0878 \pm 0.0098$	$0.0720 \pm 0.0158$
$[6, 6]$	$0.0128 \pm 0.0028$	0	0
$[3, 6]$	$0.0211 \pm 0.0046$	0	0

TABLE I. Color-composite LDMEs  $\langle \mathcal{O}^{T_{4c}(J^{PC})}([n]) \rangle$  for the  $T_{4c}(0^{++})$ ,  $T_{4c}(1^{+-})$ , and  $T_{4c}(2^{++})$  states. The uncertainties reflect the strategy described in the main text.

$[n]$	$T_{4b}(0^{++})$ [GeV <sup>9</sup> ]	$T_{4b}(1^{+-})$ [GeV <sup>9</sup> ]	$T_{4b}(2^{++})$ [GeV <sup>9</sup> ]
$[3, 3]$	$13.88 \pm 3.05$	$35.1 \pm 3.9$	$28.80 \pm 6.34$
$[6, 6]$	$5.12 \pm 1.13$	0	0
$[3, 6]$	$8.44 \pm 1.86$	0	0

TABLE II. Color-composite LDMEs  $\langle \mathcal{O}^{T_{4b}(J^{PC})}([n]) \rangle$  for the  $T_{4b}(0^{++})$ ,  $T_{4b}(1^{+-})$ , and  $T_{4b}(2^{++})$  states at the initial scale. The values are obtained via color-Coulomb scaling from the corresponding  $T_{4c}$  entries, as explained in the main text.

#### D. TQ4Q1.1 functions from HF-NRevo

The final ingredient in constructing the TQ4Q1.1 collinear FFs for fully heavy tetraquarks is the proper application of DGLAP evolution to the initial-scale inputs discussed in the previous subsection. Unlike the case of light-hadron fragmentation, a key feature here is that both the heavy-quark ( $Q$  or  $\bar{Q}$ ) and the gluon channels exhibit nontrivial evolution thresholds. This behavior arises directly from the kinematics of the perturbative splittings  $[g \rightarrow (Q\bar{Q}Q\bar{Q})]$  and  $[Q, \bar{Q} \rightarrow (Q\bar{Q}Q\bar{Q}) + Q, \bar{Q}]$ , which correspond to the left and right diagrams of Fig. 1, respectively, and are encoded in the relevant SDCs.

By kinematic constraints, the minimum invariant mass required for the gluon-induced splitting is  $\mu_{F,0}(g \rightarrow T_{4Q}) = 4m_Q$ , which we take as the evolution threshold for gluon fragmentation. Similarly, the lowest allowed invariant mass for the heavy-quark-induced splitting is  $\mu_{F,0}(Q \rightarrow T_{4Q}) = 5m_Q$ , which defines the corresponding threshold for the (anti)quark channel.

To properly account for the presence of both quark and gluon thresholds in the DGLAP evolution, we adopt a dedicated strategy rooted in the recently developed HF-NRevo scheme [131–133].

This methodology is specifically designed to govern the DGLAP evolution of heavy-hadron FFs built from nonrelativistic inputs, and it is structured around three foundational elements: physical interpretation, evolution dynamics, and uncertainty quantification. The interpretation step connects the low-transverse-momentum production mechanism to a two-parton fragmentation picture, as detailed in Section II A, thus enabling a consistent matching between FFNS and VFNS schemes. The uncertainty quantification component provides a systematic way to assess missing higher-order uncertainties (MHOUs) through controlled variations of the evolution thresholds.

Originally designed to connect precision QCD predictions with a hadron-structure-driven perspective on quarkonium fragmentation, the HF-NRevo framework has recently been extended to accommodate rare and exotic matter production, yielding promising results. Notable applications include initial studies of scalar ( $0^{++}$ ) and tensor ( $2^{++}$ ) tetraquarks using the TQ4Q1.0 functions [18, 19]—precursors to the TQ4Q1.1 sets—as well as rare triply heavy baryons such as  $\Omega_{3Q}$  [194], investigated through the OMG3Q1.0 determinations. There HF-NRevo has proven to be a versatile scheme for evolving FFs that feature both heavy-quark and gluon initial-scale inputs. This dual-channel nature requires a dedicated treatment of evolution thresholds, individually tailored to each partonic channel.

In the present study, which explores the HF-NRevo fragmentation of fully heavy tetraquarks, we defer the implementation of matching techniques and the assessment of theoretical uncertainties. Our primary focus is instead placed on developing a consistent and accurate strategy for performing DGLAP evolution under the presence of both quark and gluon thresholds.

According to HF-NRevo, the DGLAP evolution of a set of heavy-hadron FFs can be organized into two sequential steps. Focusing on the  $T_{4Q}$  case, the evolution begins from the partonic channel with the lowest threshold, namely the gluon. We take gluon-FF input calculated within NRQCD, evaluated at the initial scale  $\mu_{F,0}(g \rightarrow T_{4c}) = 4m_Q$ , and evolve it using

DGLAP equations governed solely by the LO  $P_{gg}$  kernel. This evolution proceeds up to the threshold for the constituent heavy-(anti)quark channel,  $\mu_{F,0}(Q \rightarrow T_{4Q}) = 5m_Q$ .

Within this range, the evolution exclusively generates collinear gluons. Since it involves a single channel and is expanded perturbatively in powers of  $\alpha_s$ , this step can be performed analytically using the `symJETHAD` plugin.

The second step starts at the heavy-quark threshold. Here, the gluon FF evolved up to  $Q_0 \equiv \mu_{F,0}(Q \rightarrow T_{4Q}) = 5m_Q$  is combined with the (anti)quark FF NRQCD input. Starting from this common scale, we carry out a full DGLAP evolution that includes all active channels, thereby generating the NLO TQ4Q1.0 functions released in LHAPDF format.

We refer to  $Q_0$  as the *evolution-ready* scale. It corresponds to the maximum threshold among the partonic species involved and marks the point where the numerical DGLAP evolution is initialized. For this second step, we employ the `APFEL++` library [218–220], while future implementations will consider interfacing with `EKO` [221, 222] as well.

While our two-step evolution framework focuses on gluon and constituent heavy-quark channels, one may question the absence of light- and nonconstituent-heavy-quark contributions. We have not included these channels at this stage. Although light-quark initiated fragmentation into fully heavy tetraquarks has recently been computed [15], their implementation is beyond the scope of the present study and is left for future developments aimed at completing the set of NRQCD inputs. As such, nonconstituent quarks are not assigned any initial-scale FFs and instead enter the evolution dynamically, being radiatively generated from the gluon and heavy-quark channels.

Nonetheless, insights from NRQCD studies on color-singlet pseudoscalar [182, 183, 223–226] and vector [182, 183, 227] charmonia suggest that such suppressed fragmentation modes are phenomenologically negligible compared to the dominant gluon and constituent heavy-quark ones.

**Momentum dependence.** In Figs. 2, 3 and 4 we present the dependence on the momentum fraction  $z$  of the TQ4Q1.1 FFs, multiplied by  $z$ , for the  $0^{++}$ ,  $1^{+-}$ ,

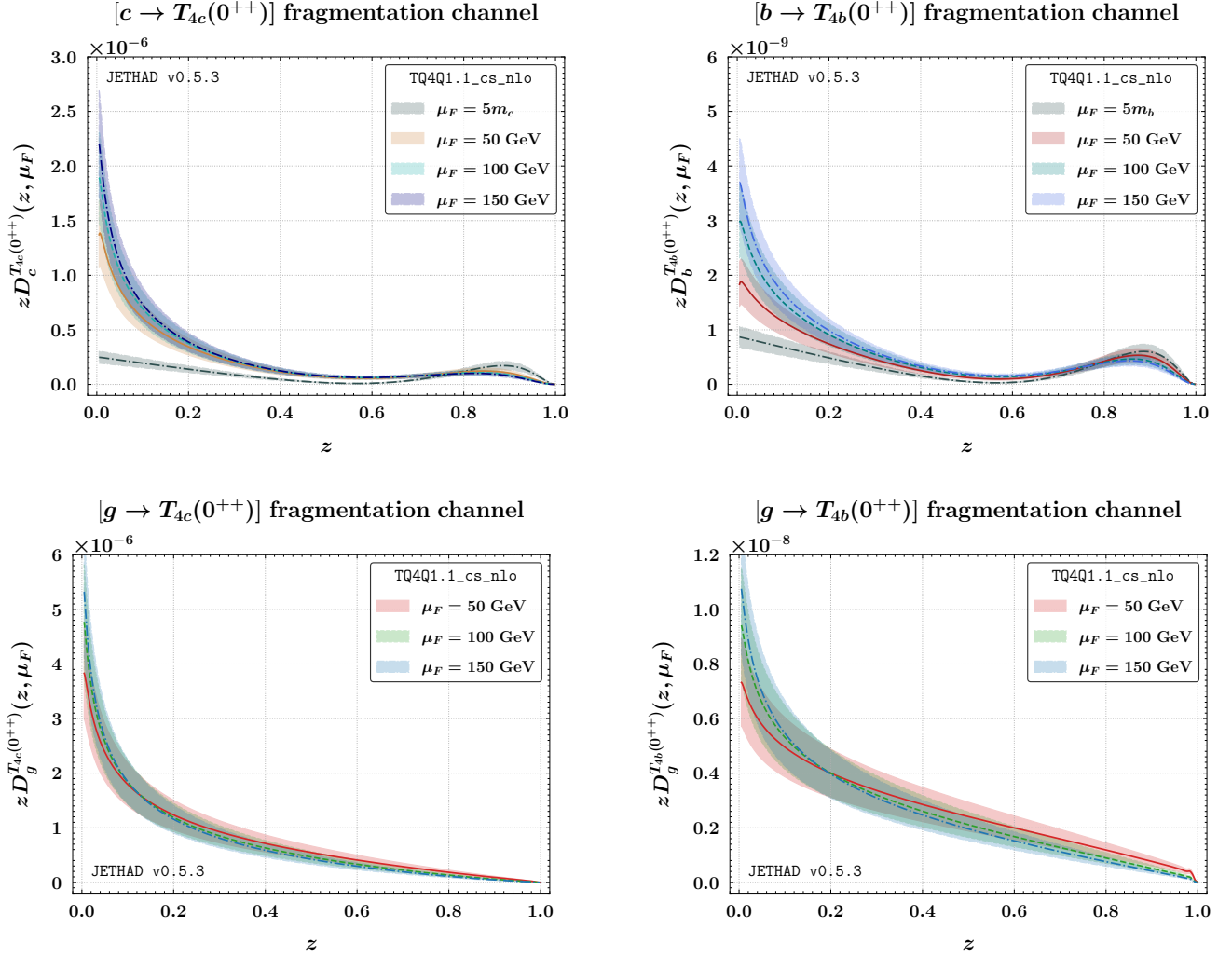


FIG. 2.  $z$ -shape of the TQ4Q1.1 FFs for scalar tetraquarks  $T_{4c}(0^{++})$  (left) and  $T_{4b}(0^{++})$  (right), evaluated at various energy scales. Upper (lower) panels refer to the heavy-quark (gluon) initiated channels. Filled bands represent the uncertainties associated with LDMEs.

and  $2^{++}$  tetraquarks. Each figure presents a double panel structure, where the left (right) columns refer to the charm (bottom) sector, and the upper (lower) rows correspond to the constituent heavy-quark (gluon) fragmentation channels. To highlight the role of the perturbative QCD evolution, we show FFs at four representative values of the factorization scale  $\mu_F$ : the evolution-ready scale  $Q_0 = 5m_Q$ , and the evolved scales  $\mu_F = 50$ ,

100, and 150 GeV. At  $Q_0$ , the  $[g \rightarrow T_{4Q}(1^{+-})]$  FF vanishes by construction, as it is generated radiatively through DGLAP evolution for  $\mu_F > Q_0$ . For the scalar and tensor cases, a nonzero gluon FF is already present at the input scale. However, for consistency across the plots, all gluon FFs are omitted at  $Q_0$  and shown only for  $\mu_F = 50$ , 100, and 150 GeV.

The momentum-fraction dependence of the  $[Q \rightarrow$



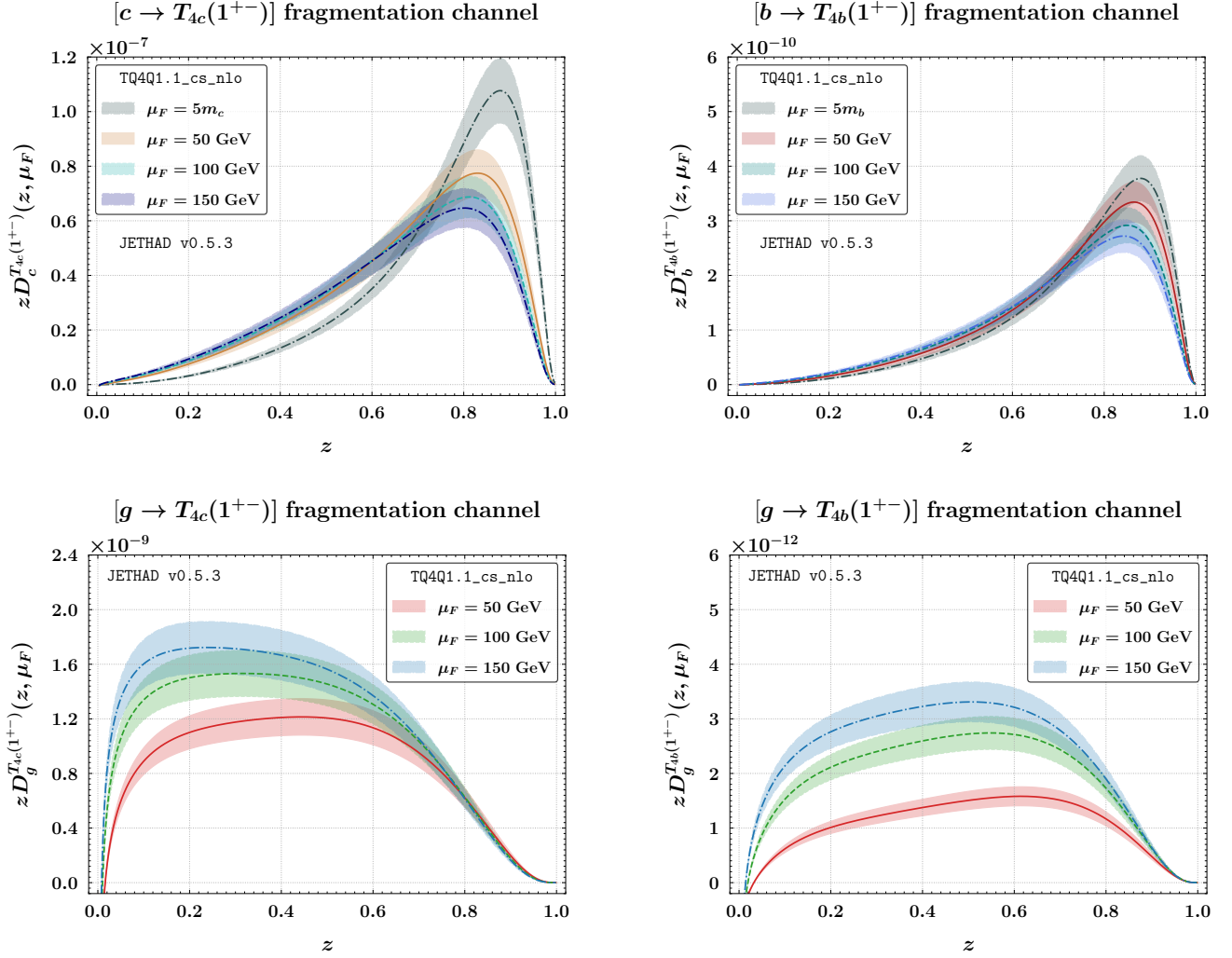


FIG. 3.  $z$ -shape of the TQ4Q1.1 FFs for axial-vector tetraquarks  $T_{4c}(1^{+-})$  (left) and  $T_{4b}(1^{+-})$  (right), evaluated at various energy scales. Upper (lower) panels refer to the heavy-quark (gluon) initiated channels. Filled bands represent the uncertainties associated with LDMEs.

$T_{4Q}$  FFs displays distinct features for each quantum number. In the scalar and tensor channels, the heavy-quark FFs show a characteristic two-phase structure: they start from a finite, nonzero value at  $z = 0$ , then decrease steeply with increasing  $z$ , before developing a moderate peak in the region around  $z \simeq 0.9$  for the charm case, slightly shifted toward lower  $z$  for the bottom case. The descending tail from  $z = 0$  becomes

increasingly steep with growing  $\mu_F$ , reflecting the enhancement of radiation at small momentum fractions induced by DGLAP evolution.

Despite this suppression, a small hump survives at large  $z$ , signaling a residual hard-fragmentation component. This behavior is consistent with expectations from the heavy-quark limit and reflects the typical hard fragmentation pattern observed in other heavy-flavor

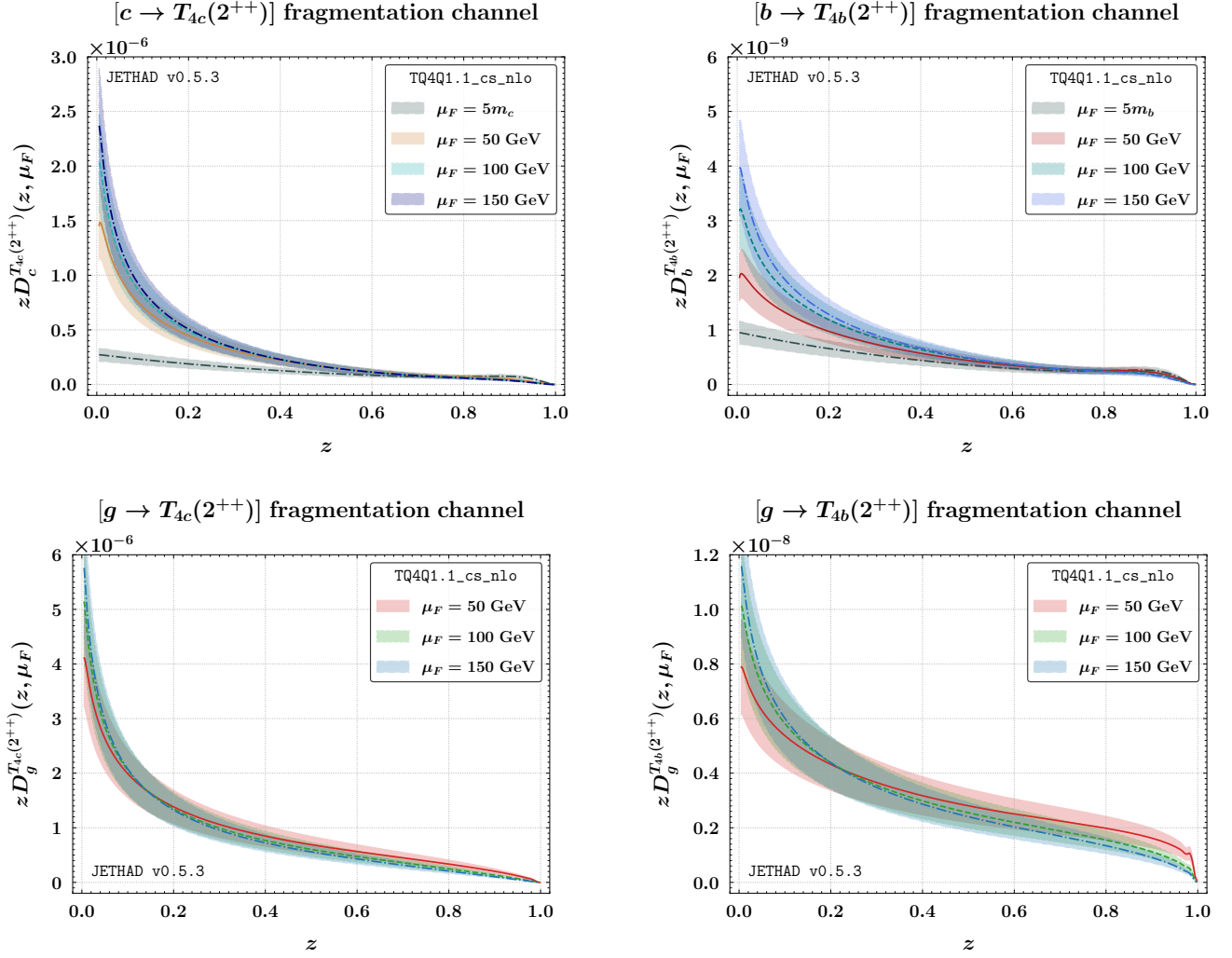


FIG. 4.  $z$ -shape of the TQ4Q1.1 FFs for tensor tetraquarks  $T_{4c}(2^{++})$  (left) and  $T_{4b}(2^{++})$  (right), evaluated at various energy scales. Upper (Lower) panels refer to the heavy-quark (gluon) initiated channels. Filled bands represent the uncertainties associated with LDMEs.

systems [128, 228], where the heavy constituent quark tends to carry a sizable fraction of the hadron momentum. It illustrates the soft-hard interplay characteristic of heavy-flavor fragmentation into multiquark bound states, where the fragmenting quark can retain either a small or a large share of the total momentum, depending on the configuration.

In our previous analysis of TQ4Q1.0 functions [18],

precursors of the 1.1 determinations, we modeled the initial condition of the FF using a simplified kinematic approach inspired by the Suzuki model [128], originally devised for heavy-light systems. There, we emphasized that for singly heavy-flavored hadrons, such as  $|Q\bar{q}\rangle$  mesons, the heavy quark and light antiquark must share the same velocity. This requirement leads to a momentum-fraction peak at  $\langle z \rangle \simeq 1 - \Lambda_q/m_Q$ , where  $\Lambda_q$

is a hadronic scale, thus enforcing a hard-fragmentation pattern directly from kinematics. However, we also pointed out that such an argument does not hold in general for multiply heavy-flavored states, like quarkonia and tetraquarks, where no light constituent is present in the lowest Fock component and no natural soft scale exists. In that context, we cautioned against using purely kinematic reasoning to predict the FF peak location.

Nevertheless, our present results show that, even in the absence of light quarks, a peak at large  $z$  still emerges dynamically in the scalar and tensor channels, especially for the charm case. This observation is in line with what is known for quarkonia [183], where the FF of a heavy quark into  $\eta_Q$  or  $J/\psi$  also displays a dominant peak at  $z \gtrsim 0.7$ , despite the absence of kinematic constraints. Hence, the presence of a high- $z$  structure in the FFs for  $T_{4Q}$  states can be interpreted as a genuine dynamical feature, reflecting the compactness of the bound state and the dominance of configurations where the fragmenting quark retains most of the momentum. In this sense, our result confirms and extends the expected behavior for heavy-quark fragmentation into systems made exclusively of heavy constituents.

In contrast, the axial-vector heavy-quark FFs exhibit a sharply localized peak in the intermediate-to-large  $z$  region, typically within  $0.75 \lesssim z \lesssim 0.9$ , and vanish in the limit  $z \rightarrow 0$ , for all values of  $\mu_F$ . These functions are steeper and more collimated than those of the scalar and tensor cases, highlighting a strong preference for hard-fragmentation configurations and the reduced phase space available for soft emission. The overall shape remains stable under scale evolution, especially in the peak region.

Finally, we observe that the FFs for the fully bottomed tetraquarks (right panels) are uniformly suppressed by approximately three orders of magnitude across the entire  $z$  spectrum, when compared to their fully charmed counterparts (left panels). This difference arises from the larger heavy-quark mass, which reduces the overall probability for fragmentation and shifts the dynamics toward even harder configurations. Such a suppression overcomes the enhancement expected from the corresponding LDMEs, which are roughly 400 times larger for bottomed states (see Section 10). This confirms that the dominant control over the FF normalization is exerted by the perturbative coefficient, rather

than by the nonperturbative matrix element.

Conversely, the  $[g \rightarrow T_{4Q}]$  FFs exhibit a broader distribution, with significant support at lower values of  $z$ . For scalar and tensor tetraquarks, the gluon FFs display a behavior that partially mirrors that of the corresponding heavy-quark FFs: they decrease monotonically with increasing  $z$ , starting from a finite value at  $z = 0$ , and do not develop any peak structure at large  $z$ . In contrast, the axial-vector gluon FFs exhibit a distinct profile, characterized by a broad hump in the intermediate region, approximately within  $0.15 \lesssim z \lesssim 0.7$ , with a peak that shifts slightly toward higher  $z$  as  $\mu_F$  increases. This structure becomes more pronounced under scale evolution, especially in the charm sector, and is accompanied by a strong suppression at both low and high  $z$ .

The qualitative difference between the axial-vector channel and the scalar or tensor ones is expected, since the gluon FF for  $1^{+-}$  states is entirely generated via DGLAP evolution. While this prevents us from probing the nonperturbative gluon input at the initial scale, it allows us to isolate and study the genuine effects of DGLAP dynamics. The emergent hump structure thus provides insight into the intrinsic shape generated radiatively by the evolution itself, unaltered by model-dependent boundary conditions.

Finally, a similar suppression is observed for gluon-initiated FFs: those associated with fully bottomed tetraquarks (right panels) are approximately three orders of magnitude smaller across the entire  $z$  spectrum compared to their fully charmed counterparts (left panels), consistently with what is found in the heavy-quark channel.

By comparing the relative magnitudes across the quantum numbers, we observe that the overall normalization of the axial-vector FFs is systematically lower than that of the scalar and tensor ones. This suppression affects both  $Q$  and  $g$  channels, where the fragmentation probabilities toward the  $1^{+-}$  state are reduced by more than one order of magnitude with respect to the scalar and tensor counterparts. This hierarchy is consistent with the NRQCD picture and the features discussed in Sec. II C. In particular, the antisymmetric spin-color configuration of the  $1^{+-}$  state leads to reduced overlap with the LO gluon production mechanisms and suppressed LDME values [12, 138]. Furthermore, the lack

of orbital excitation in the scalar and tensor channels enhances their compatibility with collinear NRQCD selection rules, unlike the axial-vector case [229–231].

As the factorization scale increases, all FFs experience a distortion of their  $z$ -shape. For  $Q$ -initiated channels, the peak is preserved but slightly reduced in magnitude, while the tail at low  $z$  becomes more populated. This behavior reflects the typical softening induced by DGLAP evolution. In the gluon channel, the growth of the low- $z$  tail with  $\mu_F$  is evident, especially in the axial-vector cases. Nevertheless, the shape distortion remains moderate even at the highest scale  $\mu_F = 150$  GeV, confirming that the leading features of the fragmentation pattern are set at the input and preserved under evolution.

Finally, we remark that our extended analysis includes uncertainty bands for all quantum states, accounting for LDME variation also in the scalar and tensor channels. This completes the partial picture offered in Ref. [20], where only the  $1^{+-}$  case featured error estimates. Uncertainty bands for all the considered channels are moderate, reflecting the conservative strategy described in Sec. II C.

**Energy dependence.** For completeness, Fig. 5 displays the energy dependence of the gluon, charm, and bottom  $TQ4Q1.1$  FFs, multiplied by  $z$ , as a function of the factorization scale  $\mu_F$ . The layout of the figure is organized by spin configuration, with scalar states shown in the upper panels, axial-vector in the middle, and tensor in the lower panels; the left columns correspond to fully charmed tetraquarks, while the right columns refer to fully bottomed ones. The FFs are evaluated at a representative value of the momentum fraction,  $z = \langle z \rangle \simeq 0.5$ , which is typical in high-energy hadroproduction processes [146, 186–188, 232, 233].

We first examine the scalar channel ( $0^{++}$ , upper row), where both the gluon and the constituent heavy quarks are active at the input scale  $Q_0$ . For the fully charmed case (left panel), the gluon FF dominates the spectrum across the full  $\mu_F$  range, remaining nearly constant with a value of order  $10^{-6}$ . This reflects the significant short-distance enhancement of the  $[g \rightarrow T_{4c}(0^{++})]$  SDC, and is consistent with the observed radiative stability under evolution. The charm FF lies about one order of magnitude below, with a slightly increasing trend in  $\mu_F$ ,

as expected from timelike DGLAP evolution with positive splitting contributions from gluon radiation. The evolution-generated bottom channel, although present, is further suppressed. The pattern is qualitatively preserved in the fully bottomed case (right panel), although all curves are rescaled downward by approximately two orders of magnitude due to the heavier quark mass, which reduces both phase space and coupling strength at the input. Here, the gluon FF retains its dominance, with the bottom FF as the subdominant contribution, and the evolution-generated charm FF being further suppressed, consistent with a mass-threshold origin.

Moving to the axial-vector channel ( $1^{+-}$ , middle row), a crucial structural difference emerges from the absence of the gluon initial-scale input, since no  $[g \rightarrow T_{4Q}(1^{+-})]$  operator can be constructed in the color-singlet NRQCD framework at LO [10, 216]. This feature manifests clearly in the  $T_{4c}(1^{+-})$  plot (left panel), where the gluon FF grows slowly through evolution, yet remains subdominant over the entire scale range. The dominant contribution here is from the charm quark, with a flat profile driven by the relatively large input LDME and timelike DGLAP evolution at fixed  $z$ . The  $[b(\bar{b}) \rightarrow T_{4c}(1^{+-})]$  component is strongly suppressed and exhibits a logarithmic-like growth with  $\mu_F$ . In the bottom sector (right panel), the pattern reverses, as expected: the bottom FF dominates, while the charm-induced one starts from zero and becomes visible only at  $\mu_F \gtrsim 100$  GeV. Analogously to the  $T_{4c}(1^{+-})$  case, the gluon FF remains two to one orders of magnitude subdominant across the full scale range, further confirming that gluon-initiated fragmentation into axial tetraquarks is a radiatively generated and genuinely subleading channel. This structural hierarchy, supported by the  $[3, 3]$  dominance in the color-spin basis [14], is a distinctive signature of the  $1^{+-}$  state and highlights its model-intrinsic stability.

Finally, the tensor channel ( $2^{++}$ , bottom row) exhibits a configuration broadly similar to the scalar one. In both the fully charmed (left panel) and fully bottomed (right panel) cases, the gluon FF is the leading function across  $\mu_F$ , starting from a nonzero value at  $Q_0$  and evolving very mildly. As emphasized in Ref. [234], this behavior stems from the large number of contributing diagrams in the  $[g \rightarrow T_{4Q}(2^{++})]$  SDC, due to the rich Lorentz structure of the final state. The quark-induced FFs follow the same hierarchy observed in the

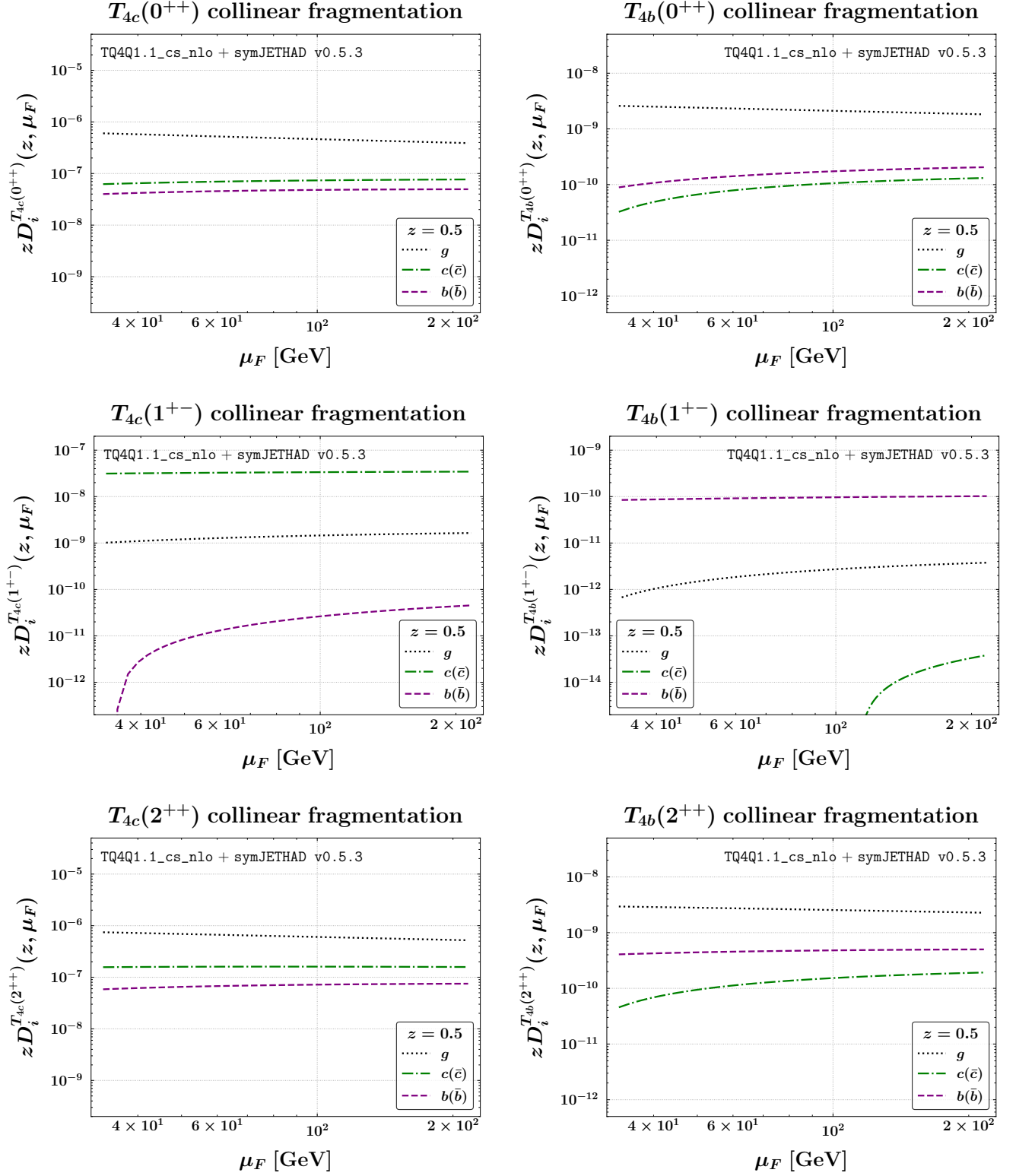


FIG. 5. Energy shape of the TQ4Q1.1 FFs for scalar (upper), axial-vector (central), and tensor tetraquarks (lower), evaluated at  $z = \langle z \rangle \simeq 0.5$ . Left (right) panels are for fully charmed (bottomed) states.



scalar channel: charm dominates over bottom in the  $T_{4c}(2^{++})$  case, and the order is reversed in  $T_{4b}(2^{++})$ , with cross-flavor contributions being significantly suppressed. The overall  $\mu_F$  dependence is again mild, with slightly steeper trends in the subdominant components, reflecting DGLAP-driven flavor mixing and radiative broadening at moderate  $z$ .

An overarching feature that emerges from Fig. 5 is the smooth behavior of the gluon FFs as the factorization scale  $\mu_F$  increases. In all spin configurations and for both charm and bottom sectors, the gluon FFs either show a mild growth with  $\mu_F$  or display, at most, a very soft suppression, especially in the scalar and tensor cases. This trend is not only theoretically expected from the structure of timelike DGLAP evolution, but it also plays a critical role in phenomenological stability. Indeed, gluon FFs with such a regular  $\mu_F$  pattern act as *natural stabilizers* [235] of high-energy distributions, particularly those sensitive to semi-inclusive emissions of heavy-flavored hadrons.

This concept of natural stability was first introduced in the context of singly charmed [232] and singly bottomed [233] mesons, and later confirmed in studies of vector quarkonia [186],  $B_c$ -like states [187, 188], and early precision-QCD analyses of exotic hadrons [17, 18, 20, 21]. Our results for the TQ4Q1.1 family reinforce this picture: the gluon channel, either initialized at the evolution-ready scale  $Q_0$  (as in the scalar and tensor cases) or radiatively generated above it (as in the axial-vector case), contributes in a smooth and controlled fashion across the full  $\mu_F$  range, ensuring robust theoretical predictions in the presence of NLO corrections and MHOUs (see Section III for our phenomenological applications).

To conclude, the energy profiles of the TQ4Q1.1 FFs provide insight into the relative strength and scale sensitivity of different fragmentation channels. The axial-vector configuration emerges as the cleanest and most theoretically stable scenario, due to its well-defined color-spin structure and radiative hierarchy. The scalar and tensor cases, while quantitatively richer, are more model-dependent and sensitive to the chosen LDME set. Altogether, this systematic characterization as a function of  $\mu_F$  complements the  $z$ -dependent analysis presented previously, and sets the stage for phenomenological applications exotic hadron production at large

transverse momenta.

### III. HADRON-COLLIDER PHENOMENOLOGY

To support phenomenology, we present predictions for rapidity and azimuthal-angle differential distributions sensitive to the inclusive production of tetraquark-jet systems at HL-LHC and FCC energies. As mentioned, our reference formalism is the NLL/NLO<sup>+</sup> HyF, where the standard collinear factorization at NLO is consistently enhanced by including the resummation of high-energy logarithms within the next-to-leading accuracy and going partially beyond.

This hybrid approach is particularly suited for semi-hard observables that probe QCD at next-generation hadron colliders. A comprehensive overview of the theoretical setup of the NLL/NLO<sup>+</sup> resummation formalism implemented in our analysis is provided in Appendix B.

The production of identified hadrons and jets provides a key window into the high-energy, semi-hard regime of QCD, where large logarithms of energy can disrupt standard perturbative expansions.<sup>3</sup> The Balitsky-Fadin-Kuraev-Lipatov (BFKL) framework [236–238] addresses this by resumming both leading ( $\alpha_s^n \ln s^n$ ) and next-to-leading ( $\alpha_s^{n+1} \ln s^n$ ) energy logarithms.

In this context, cross sections are expressed as transverse-momentum convolutions of a universal NLO BFKL Green's function [239, 240] with process-dependent emission functions (also known as forward impact factors) that embed collinear inputs, including PDFs and FFs. This straightforwardly leads to the aforementioned HyF scheme that unifies high-energy resummation and collinear dynamics [146, 241–243].

Over time, BFKL resummation has been widely applied to processes such as Mueller-

<sup>3</sup> The semi-hard regime of QCD is defined by the scale hierarchy  $\Lambda_{\text{QCD}}^2 \ll Q^2 \ll s$ , where  $Q^2$  denotes a process typical hard scale and  $s$  is the squared center-of-mass energy. In this regime, transverse momenta are large enough to allow for a perturbative treatment, but not asymptotically large. As a consequence, both collinear and high-energy logarithms can become sizable, and their joint resummation is required for reliable theoretical predictions.

Navelet jets [242, 244–253], dihadron systems [147, 243, 249, 254, 255], hadron-jet [146, 255–259] and multijet tags [249, 260–263], forward Higgs [264–274], Drell-Yan [275, 276], and heavy-flavor emissions [148, 186–188, 232, 233, 235, 277–283].

Studies of single-forward emissions have offered key insights into small- $x$  gluon dynamics through unintegrated gluon distributions (UGDs), with analyses performed at HERA [284–292] and the EIC [291, 293–296]. This has led to the development of resummed PDFs [297–302] and improved small- $x$  TMDs [303–313].

Heavy-flavor emissions, such as  $\Lambda_c$  [232] and  $b$ -hadron production [233], have revealed strategies to overcome difficulties in modeling semihard processes at natural scales. Unlike light-hadron emissions, which suffer from large NLL corrections and threshold effects [146, 256], heavy-flavored hadrons show a trend of *natural stabilization* [235], stemming from VFNS-based collinear fragmentation.

This behavior motivated the construction of VFNS DGLAP-evolved FFs using NRQCD inputs [182–185, 227, 314–318], extending from vector quarkonia [148, 186] to charmed  $B$  mesons [187, 188]. Stability at high energies also opened new directions in exotic-hadron phenomenology, enabling fragmentation studies of doubly [17, 19] and fully heavy tetraquarks [18–20], as well as charmed pentaquarks [21] and triply heavy baryons [194].

In Sections III A and III B we present present results for rapidity distributions and angular multiplicities, respectively. All numerical calculations were performed by making use of JETHAD [146–150], a hybrid PYTHON/FORTRAN multimodular interface designed for the computation, handling, and post-processing of physical observables across multiple theoretical formalisms.

### A. Rapidity distributions

The first class of observables investigated in our phenomenological study is the rapidity distribution, defined as the cross section differential with respect to the rapidity separation  $\Delta Y = y_1 - y_2$  between the two final-state

particles. One has

$$\frac{d\sigma(\Delta Y, s)}{d\Delta Y} \equiv C_{n=0}, \quad (11)$$

where  $C_{n=0}$  stands for the  $\varphi$ -summed azimuthal-angle coefficient, integrated over the rapidity and momentum final-state phase space, and taken at fixed  $\Delta Y$  (see Appendix B). By isolating the  $n = 0$  conformal spin, we suppress all transverse-angle modulations and retain the leading energy-dependent component of the cross section, which is particularly sensitive to resummation effects.

The phenomenological analysis of rapidity-interval distributions offers a direct insight into the interplay between high-energy dynamics and the collinear structure of hadrons, especially in semi-inclusive topologies involving a fully heavy tetraquark and a recoiling jet. The transverse momentum of the  $T_{4Q}(J^{PC})$  tetraquark is varied between 30 and 120 GeV, while the accompanying light jet spans from 40 to 120 GeV. These ranges align with those employed in current and future LHC analyses involving hadronic and jet final states [319, 320]. The use of *asymmetric* transverse momentum cuts magnifies high-energy resummation effects over the fixed-order baseline [146, 242, 247].

Our selection of rapidity intervals reflects the acceptance criteria in ongoing LHC measurements. Tetraquarks are assumed to be detected within the barrel calorimeter coverage, following the CMS configuration [321], which restricts their rapidity to the range  $-2.5 < y_1 < +2.5$ . Jets, which can also be reconstructed in the endcap calorimeters [319], are allowed within a wider rapidity window of  $|y_2| < 4.7$ .

In Figs. 6 to 8 we show our theoretical predictions for  $d\sigma/d\Delta Y$  in the production of scalar ( $0^{++}$ ), axial-vector ( $1^{+-}$ ), and tensor ( $2^{++}$ ) tetraquarks with charm (left) or bottom content (right), in association with a light jet. Upper and lower panels refer to HL-LHC ( $\sqrt{s} = 14$  TeV) and FCC ( $\sqrt{s} = 100$  TeV) configurations, respectively. Each plot displays the absolute differential cross section in the main panel and the ratio of LL and HE-NLO<sup>+</sup> to NLL/NLO<sup>+</sup> results in the ancillary panel below. Uncertainty bands in the main plots combine MHOUs, LDMEs, and multidimensional phase-space integration errors, while bands in the lower panels reflect only the variation due to MHOUs. The bin width in  $\Delta Y$  is set to 0.5 throughout.

We note a universal trend across all final states: the cross section decreases with increasing  $\Delta Y$ . This behavior stems from a balance between two competing mechanisms. On the one hand, the resummed partonic coefficient grows with energy (*i.e.*, with  $\Delta Y$ ), as predicted by the BFKL formalism. On the other hand, this growth is counteracted by the convolution with collinear PDFs and FFs, which are strongly suppressed at large momentum fractions. As a result, the observable exhibits a relatively moderate decrease at small  $\Delta Y$  values, say  $\Delta Y \sim 2.5 \div 3$ , and a steady decline thereafter.

Despite this shared trend, some differences emerge when comparing the three channels.

**Scalar channel ( $0^{++}$ ).** Predictions for the  $T_{4c}(0^{++})$  and  $T_{4b}(0^{++})$  states are shown in Fig. 6. Here, we observe the highest overall cross sections among all considered cases, with values ranging from around  $10^{-2}$  to  $10$  pb for charm and from  $10^{-5}$  to  $10^{-2}$  pb for bottom, depending on  $\Delta Y$  and  $\sqrt{s}$ . This is in line with expectations, given the absence of spin suppression and the compactness of the wave function for scalar  $S$ -wave configurations.

The uncertainty bands due to MHOUs are modest, remaining well below a 1.5 relative size. The LL/LO curves tend to overestimate the NLL/NLO<sup>+</sup> result in the low- $\Delta Y$  region, while the two predictions become closer at large  $\Delta Y$ . This convergence indicates a good resummation control and validates the use of NLL-improved hybrid factorization in this context. The rise in the cross section from HL-LHC to FCC is significant—roughly an order of magnitude—suggesting excellent prospects for observing such states at future colliders.

A closer inspection of the lower panels in Fig. 6 reveals a nontrivial pattern in the ratio between fixed-order HE-NLO<sup>+</sup> predictions and the resummed NLL/NLO<sup>+</sup> result. At small values of  $\Delta Y$ , the HE-NLO<sup>+</sup> versus NLL/NLO<sup>+</sup> ratio is close to unity for both HL-LHC and FCC setups, confirming that high-energy effects are mild and under control in this domain. However, as  $\Delta Y$  increases, we observe opposite behaviors at the two energies: at 14 TeV HL-LHC, the HE-NLO<sup>+</sup> result tends to overestimate the NLL/NLO<sup>+</sup> one, while at 100 TeV FCC, the opposite happens—the HE-NLO<sup>+</sup> curve lies systematically below the NLL/NLO<sup>+</sup> predic-

tion.

This inversion strongly suggests that genuine BFKL resummation effects become increasingly relevant as the available rapidity interval enlarges and the energy grows. We interpret this as a threefold indication of the potential impact of high-energy logarithms at future hadron colliders:

1. The suppression of the HE-NLO<sup>+</sup> cross section relative to NLL/NLO<sup>+</sup> at large  $\Delta Y$  and 100 TeV points to an enhanced role of resummation terms, which dominate over fixed-order ones when  $\log s$  becomes sizable.
2. Under current fiducial cuts, such behavior implies that it will be feasible to isolate the genuinely resummed signal at FCC energies and large  $\Delta Y$ , even without the need to tune additional observables or selection strategies.
3. These features are consistent with prior findings on Higgs production at high energies [322, 323], where BFKL effects were shown to become essential to achieve accurate predictions beyond fixed-order.

Consequently, our results provide yet another data point in support of the idea that the high-energy limit of QCD, when coupled to proper collinear evolution and heavy-flavor fragmentation, is not only theoretically consistent but also phenomenologically accessible, especially at next-generation hadron colliders like the FCC.

**Axial-vector channel ( $1^{+-}$ ).** The  $T_{4c}(1^{+-})$  and  $T_{4b}(1^{+-})$  cases, detailed in Fig. 7, feature substantially lower rates, due to the suppression in the nonperturbative transition from a fragmenting parton to a spin-1 tetraquark, as discussed in Sec. II C. Event yields span from  $10^{-4}$  to about  $10^{-2}$  pb for charm and from  $10^{-7}$  to about  $10^{-5}$  pb for bottom.

Despite these low rates, the axial-vector channel stands out for its distinctive theoretical features, particularly concerning uncertainty control and the structure of radiative corrections. Among all the spin configurations considered, the  $1^{+-}$  exhibits the smallest uncertainty bands over the full  $\Delta Y$  range. This stability is driven by two intertwined effects:

1. As illustrated in Fig. 5, the gluon FF grows significantly with the factorization scale in the axial-vector case, unlike the scalar and tensor ones, where it tends to decrease slightly. This trend amplifies the *natural stabilization* power of the HyF resummation: the faster the FF evolves, the more it compensates higher-order instabilities and MHOU-related uncertainties [232, 233, 235].
2. As discussed in Section II C, the initial-scale FF for the  $1^{+-}$  state is built upon a single heavy-quark fragmentation channel, and thus the LDME-induced uncertainties propagate from a unique, localized source, rather than combining multiple contributions as in the other spin channels.

The comparison between the HE-NLO<sup>+</sup> and the NLL/NLO<sup>+</sup> curves reveals closer proximity in the axial-vector case, especially at  $\sqrt{s} = 14$  TeV. This is clearly visible in the ancillary panels, where the HE-NLO<sup>+</sup> versus NLL/NLO<sup>+</sup> ratio stays systematically nearer to one, with deviations remaining below 50% across the entire  $\Delta Y$  spectrum. This behavior implies that, in the  $1^{+-}$  channel, the unresummed high-energy limit already captures a relevant portion of the NLL-enhanced corrections. Still, the role of subleading logarithms is far from negligible, as evidenced by the LL/LO versus NLL/NLO<sup>+</sup> separation. At 100 TeV, all channels display a similar gap between HE-NLO<sup>+</sup> and NLL/NLO<sup>+</sup>, reinforcing the conclusion that BFKL-type resummation becomes increasingly relevant at higher energies, and the axial-vector case is no exception.

In summary, although the  $1^{+-}$  signal is intrinsically weaker, it displays the cleanest radiative structure, and the most robust separation of resummation dynamics. Thus, it offers a promising laboratory to validate the HyF formalism and probe subleading high-energy corrections. The favorable perturbative convergence and reduced uncertainty bands observed at the FCC make the axial-vector channel a promising candidate for precision tests of high-energy resummation effects.

**Tensor channel ( $2^{++}$ ).** The tensor case, presented in Fig. 8, lies in between the scalar and axial-vector extremes. Cross sections are lower than in the  $0^{++}$  channel, due to the angular-momentum barrier in the formation of a spin-2 bound state, but larger than in

the  $1^{+-}$  case. The overall pattern of  $\Delta Y$  dependence follows that of the scalar state, with a mild decrease around  $\Delta Y \sim 2.5$  and more rapid falloff at large rapidity separations.

Uncertainty bands under NLL/NLO<sup>+</sup> remain controlled and competitive, and the gap between LL/LO and NLL/NLO<sup>+</sup> is qualitatively similar to the scalar case. This suggests that subleading logarithms have the same impact on both scalar and tensor productions, especially at lower  $\Delta Y$ . Interestingly, we observe that HE-NLO<sup>+</sup> curves tend to lie between LL/LO and NLL/NLO<sup>+</sup> throughout the kinematic range, validating their interpretation as a fixed-order limit of the resummed approach.

Overall, the tensor channel confirms the broader narrative: heavy tetraquark production via fragmentation is *naturally stable* under resummation, but sensitive enough to reveal slight differences between spin structures.

**Comparative summary and phenomenological outlook.** The detailed inspection of all rapidity distributions across spin states allows us to draw several key conclusions.

First, resummation effects are visible and under control across all channels, with NLL/NLO<sup>+</sup> offering a stable and physically motivated baseline. Second, the impact of spin is twofold: it modulates the absolute normalization of the cross section through FF suppression and shapes the  $\Delta Y$  profile via the scale evolution of the underlying FFs. Third, among all channels, the axial-vector one provides the clearest window to isolate subleading logarithmic corrections, due to the combination of low rate, strong scale evolution, and mild contamination from higher-spin or orbital-momentum mixing.

From an experimental point of view, these findings suggest that searches for heavy tetraquarks at high-energy colliders should prioritize inclusive observables such as  $\Delta Y$  distributions. Although suppressed, axial-vector channels could act as clean indicators of genuine high-energy behavior, whereas scalar and tensor channels offer higher yields and complementarity.

We emphasize that these patterns hold across both  $T_{4c}$  and  $T_{4b}$  sectors and persist from 14 to 100 TeV, confirming their universality and robustness.

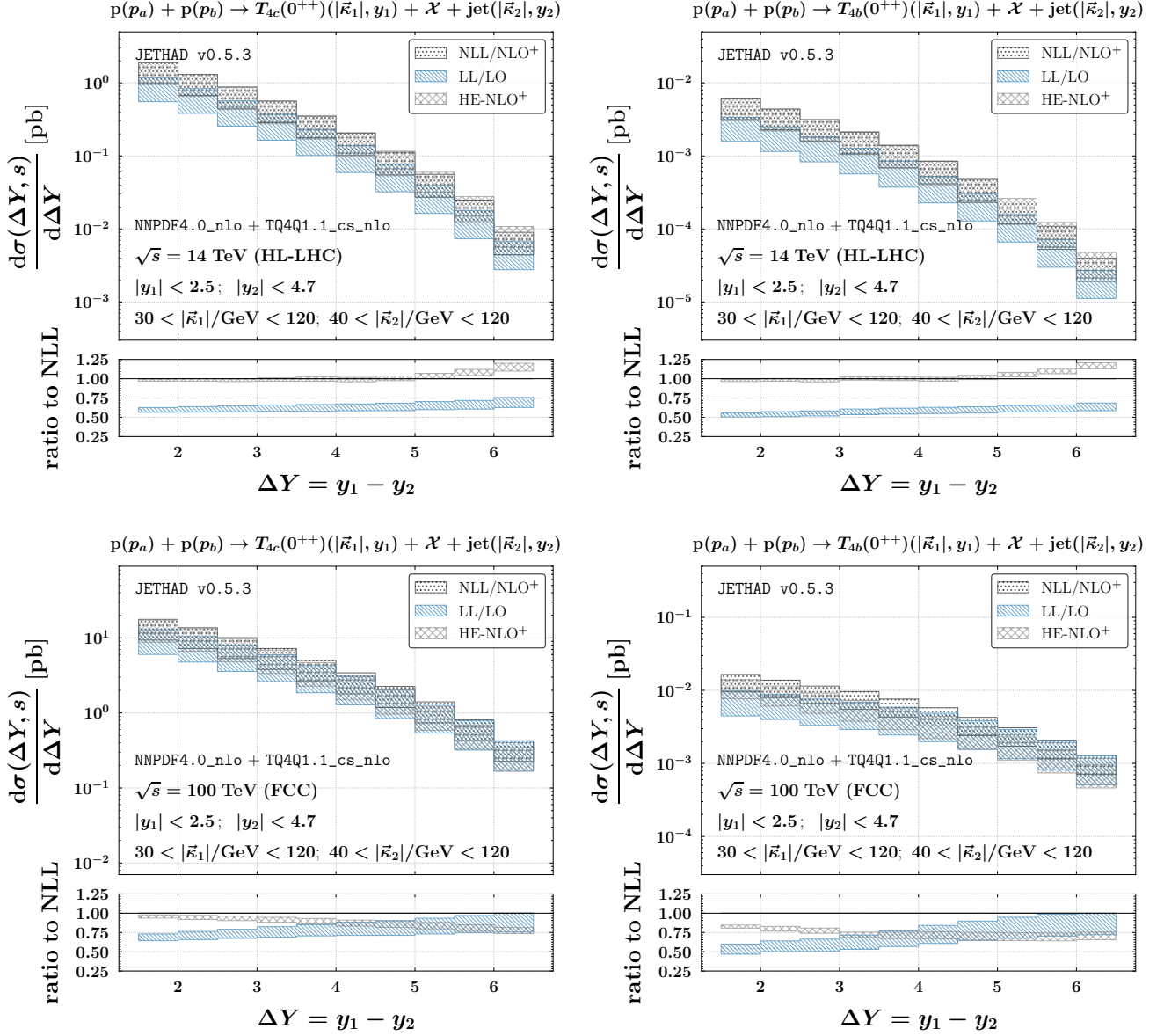


FIG. 6. Rapidity distributions for scalar tetraquarks  $T_{4c}(0^{++})$  (left) and  $T_{4b}(0^{++})$  (right) produced in association with a jet at  $\sqrt{s} = 14$  TeV (HL-LHC, top) and 100 TeV (nominal FCC, bottom). Filled bands in the main panels indicate the total uncertainty, combining contributions from MHOUs, LDMEs, and multidimensional phase-space integration. The lower panels show the ratios of LL/LO and HE-NLO<sup>+</sup> predictions to the NLL/NLO<sup>+</sup> result, with uncertainty bands accounting for MHOUs only.

### B. Angular multiplicities

The second focal point of our phenomenological investigation is the angular distribution. We perform, for

the first time, a detailed analysis of this observable fully heavy tetraquark states. In particular, we study the fol-



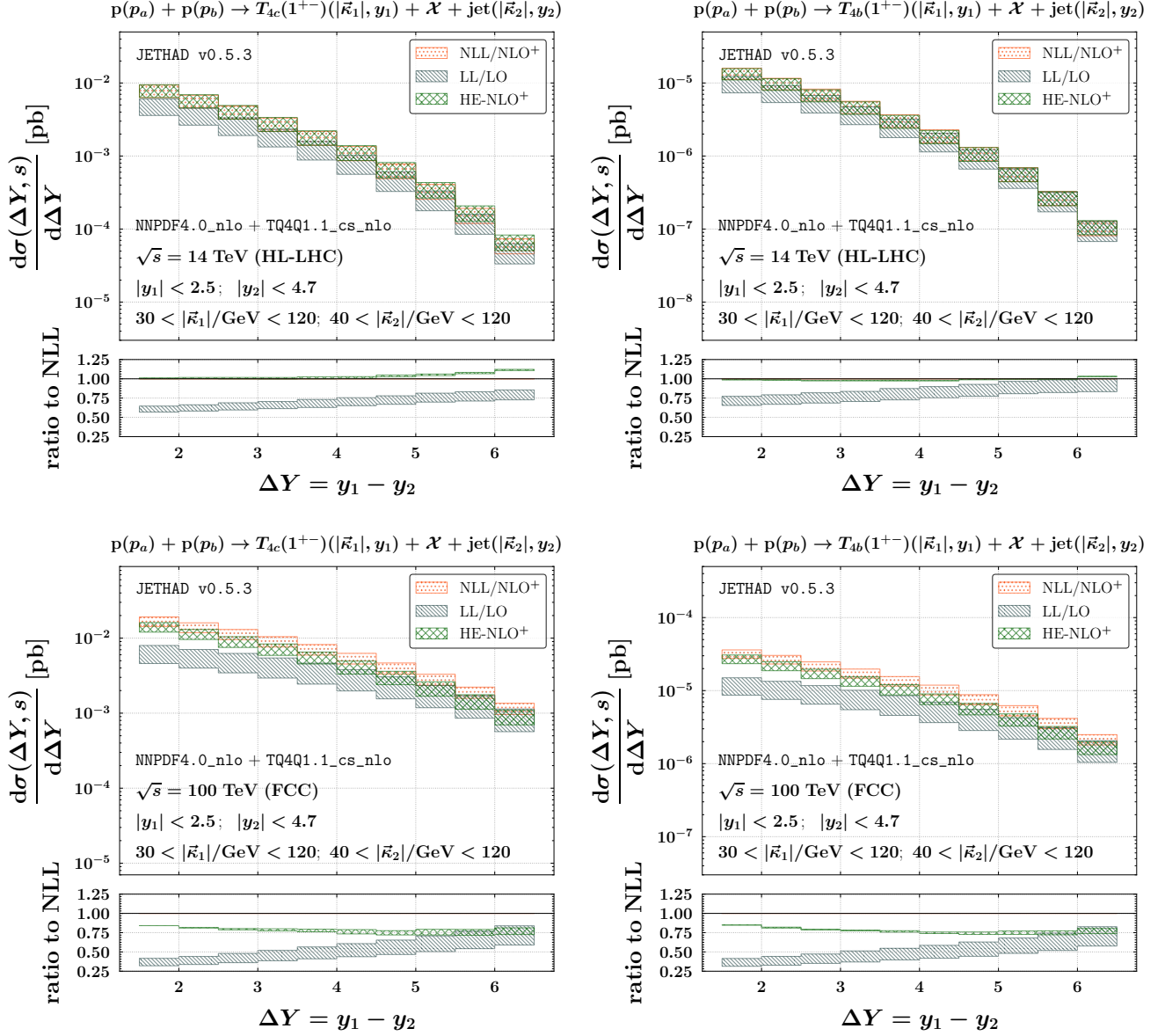


FIG. 7. Rapidity distributions for axial-vector tetraquarks  $T_{4c}(1^{+-})$  (left) and  $T_{4b}(1^{+-})$  (right) produced in association with a jet at  $\sqrt{s} = 14$  TeV (HL-LHC, top) and 100 TeV (nominal FCC, bottom). Filled bands in the main panels indicate the total uncertainty, combining contributions from MHOUs, LDMEs, and multidimensional phase-space integration. The lower panels show the ratios of LL/LO and HE-NLO<sup>+</sup> predictions to the NLL/NLO<sup>+</sup> result, with uncertainty bands accounting for MHOUs only.

lowing normalized multiplicities

$$\frac{1}{\sigma} \frac{d\sigma(\varphi, s)}{d\varphi} = \frac{1}{\pi} \left[ \frac{1}{2} + \sum_{n=1}^{\infty} \langle \cos(n\varphi) \rangle \cos(n\varphi) \right], \quad (12)$$

with  $\varphi = \phi_1 - \phi_2 - \pi$ ,  $\phi_{1,2}$  the azimuthal angles of the two outgoing objects,  $C_n$  the azimuthal coefficients

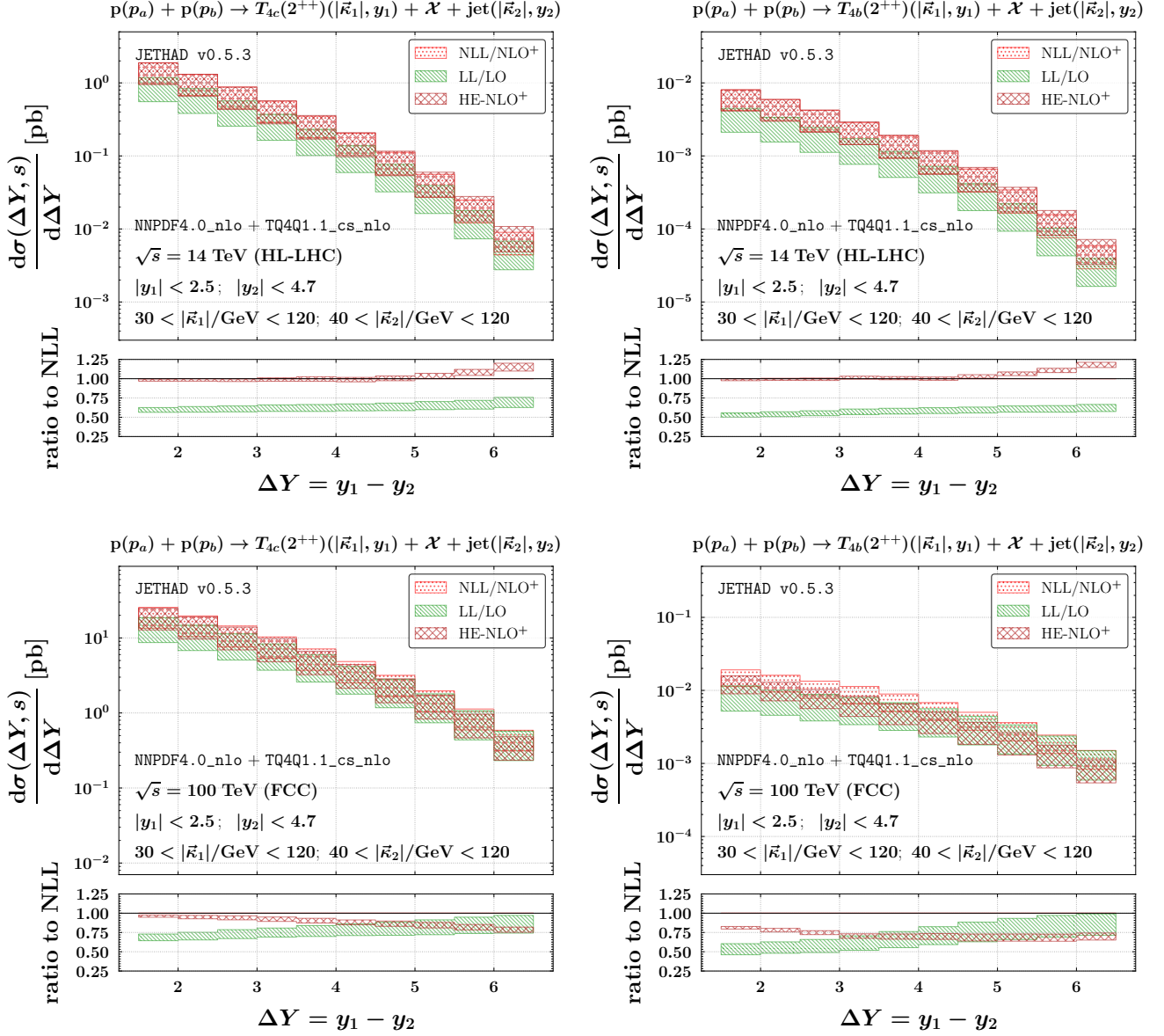


FIG. 8. Rapidity distributions for tensor tetraquarks  $T_{4c}(2^{++})$  (left) and  $T_{4b}(2^{++})$  (right) produced in association with a jet at  $\sqrt{s} = 14$  TeV (HL-LHC, top) and 100 TeV (nominal FCC, bottom). Filled bands in the main panels indicate the total uncertainty, combining contributions from MHOUs, LDMEs, and multidimensional phase-space integration. The lower panels show the ratios of LL/LO and HE-NLO<sup>+</sup> predictions to the NLL/NLO<sup>+</sup> result, with uncertainty bands accounting for MHOUs only.

(see Appendix B) and  $\langle \cos(n\varphi) \rangle = C_n/C_0$  standing for the corresponding azimuthal correlation moments. The

coefficients  $C_n$  are integrated in the full rapidity and transverse momentum windows as in Section III A, and

integrated over fixed bins of the rapidity interval  $\Delta Y$ .

Originally developed to investigate the azimuthal decorrelation in light dijet systems [245, 324], these angular multiplicities have proven to be powerful observables for probing the dynamics of QCD in the high-energy limit. They encapsulate contributions from all azimuthal harmonics and offer a sensitive handle on the internal structure of the partonic interactions.

Their differential dependence on the azimuthal angle  $\varphi$  makes them particularly suitable for experimental analyses, allowing for straightforward comparison with detector data even in the presence of nonuniform azimuthal acceptance over the full  $2\pi$  range. A recent investigation on dijet angular multiplicities highlighted two key advantages [252]. First, it helps alleviate persistent resummation instabilities observed in light-flavored final states at natural scales [146, 256]. Second, it improves the agreement with CMS data at  $\sqrt{s} = 7$  TeV [319].

For the sake of simplicity, we consider only the fully charmed tensor resonance,  $T_{4c}(2^{++})$ , which, as mentioned, represents the most favorable candidate for the  $X(6900)$  state [88]. However, numerical tests have not shown significant discrepancies when considering the fully bottom counterpart,  $T_{4b}(2^{++})$ .

In Fig. 9 we compare HyF predictions within NLL/NLO<sup>+</sup> accuracy (upper plots) with the corresponding LL/LO accuracy (central plots) and the HE-NLO<sup>+</sup> background (lower plots). Left and right columns show multiplicities taken at 14 TeV HL-LHC and 100 TeV FCC, respectively. The rapidity distance  $\Delta Y$  is scanned over the interval from three to six units, and results are shown for three representative, nonoverlapping bins of unit width.

Due to the intrinsic symmetry of the azimuthal distributions defined in Eq. (12) under the transformation  $[-\varphi \rightarrow \varphi]$ , we display them only within the range  $0 < \varphi < \pi$ . To facilitate future experimental comparisons, the multiplicities are averaged over fixed-size  $\varphi$  bins. Since these distributions are defined as normalized ratios of cross sections, uncertainties from LDMEs and from the multidimensional phase-space integration effectively cancel out. As a result, the error bands displayed in the plots reflect only the impact of MHOUs.

Our multiplicities display a pronounced peak located

at  $\varphi = 0$ , corresponding to nearly back-to-back configurations between the final-state tetraquark and the jet. This back-to-back enhancement is a standard feature of semihard final states produced with large rapidity separation because it reflects momentum conservation and the suppression of hard-gluon emissions at lowest order. At the same time, the  $\Delta Y$ -shape of these multiplicities offers insight into the interplay between collinear and high-energy logarithmic dynamics.

For all panels and all accuracy levels, we observe that the height of the peak at  $\varphi = 0$  diminishes as  $\Delta Y$  grows. This reduction is particularly pronounced in the NLL/NLO<sup>+</sup> and  $-LL/LO$  case. Such a trend reveals the increasing influence of BFKL-driven decorrelation effects, which become more visible as the rapidity span enlarges and more phase space opens for the emission of undetected gluons. These secondary emissions tend to balance the transverse momentum between the final-state objects, thereby degrading their azimuthal alignment.

In contrast, HE-NLO<sup>+</sup> predictions show a comparatively weaker sensitivity to  $\Delta Y$ . The corresponding curves display a sharper peak at small  $\varphi$ , with only a mild flattening at larger separations. This behavior is consistent with what is expected from a pure DGLAP-like evolution, where gluon radiation is collinear and less capable of inducing large-angle decorrelation. This LL/LO versus NLL/NLO<sup>+</sup> and HE-NLO<sup>+</sup> separation mirrors the classical “BFKL versus DGLAP” dichotomy, which has been extensively analyzed in the context of Mueller-Navelet jets, hadron-jet and dihadron systems [146, 147, 186, 232, 242]. In particular, according to BFKL dynamics, increasing  $\Delta Y$  leads to a broadening of the angular distribution and a suppression of the back-to-back peak, whereas in DGLAP-like scenarios such effects are more localized and less dependent on the total rapidity gap.

This dichotomic behavior is robust and persists at both 14 TeV and 100 TeV. However, FCC energies offer additional benefits. In all predictions at 100 TeV, uncertainty bands appear less sensitive to MHOUs, remaining relatively flat or even slightly shrinking. This observation reflects the mitigation of soft-threshold logarithms that can affect the high- $\varphi$  tail. Such threshold effects originate from Sudakov-like double logarithms that survive in configurations where the longitudinal momen-

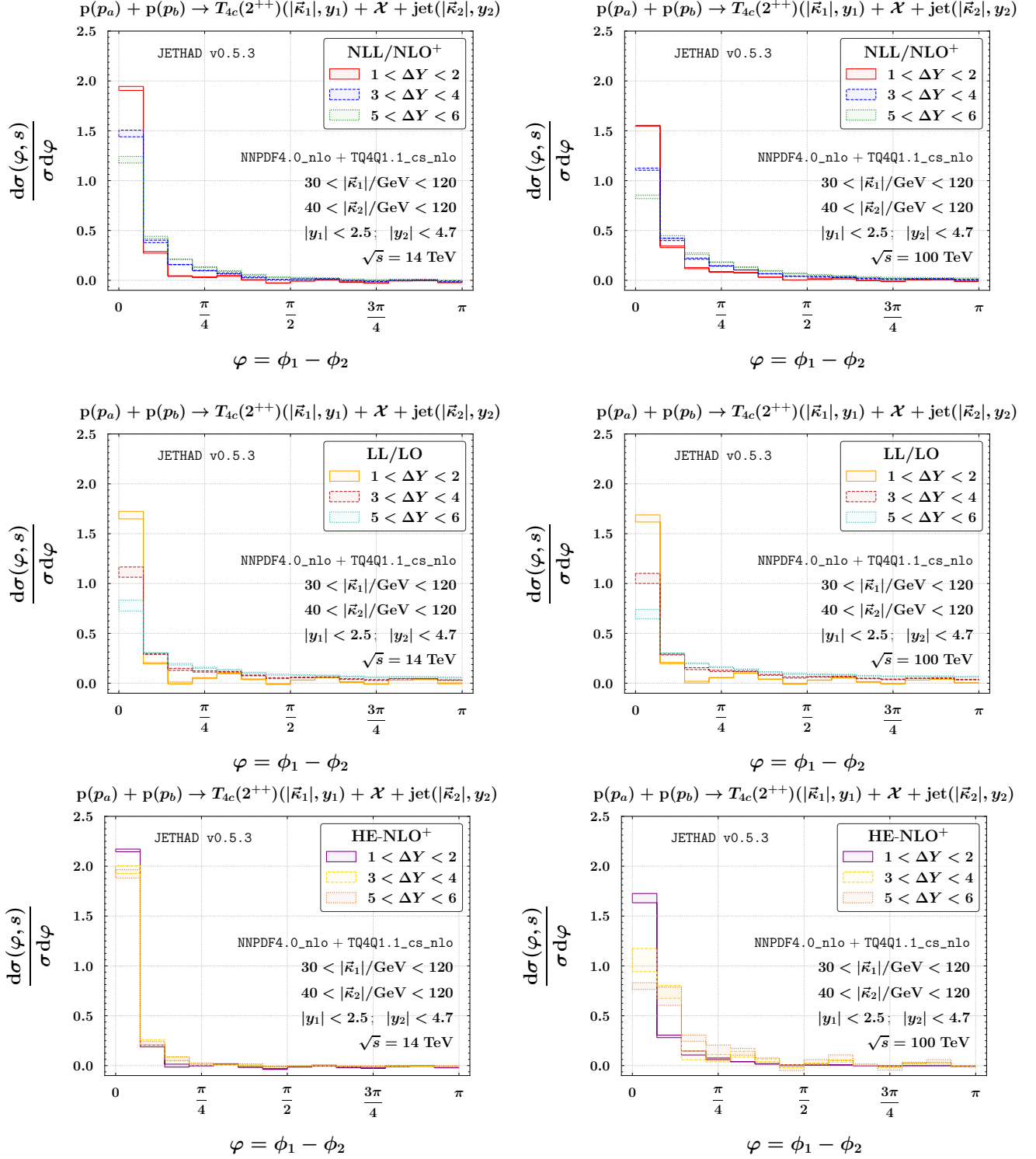


FIG. 9. Angular multiplicities for tensor tetraquarks  $T_{4c}(2^{++})$  produced in association with a jet at  $\sqrt{s} = 14$  TeV (HL-LHC, left) and 100 TeV (nominal FCC, right). Predictions shown in the upper, central, and lower panels are computed at NLL/NLO<sup>+</sup>, LL/LO, and HE-NLO<sup>+</sup> accuracy, respectively, within the HyF framework. Filled bands in the main panels indicate the uncertainty coming from MHOUs.

tum fractions  $x_{1,2} \rightarrow 1$ , a region that is approached at LHC but avoided at FCC. Indeed, at fixed rapidities and transverse momenta, increasing  $\sqrt{s}$  pushes the relevant  $x$  values further from unity (see Eq. (B3)). Therefore, FCC kinematics helps suppress the *threshold* region, leading to better stability and reduced sensitivity to logarithmic contributions not resummed in our HyF formalism.

Finally, we highlight that all our azimuthal multiplicities remain positive over the entire  $\varphi$ -range, within the estimated theoretical uncertainties. This is a nontrivial feature. In previous studies of different final states, such as vector quarkonia [186] and  $B_c$  mesons [187], oscillating behavior and negative bins were occasionally observed at large  $\varphi$ , due to residual *threshold* logarithmic instabilities [259]. In contrast, the fragmentation of the tensor tetraquark exhibits a stabilizing influence that smoothens the distributions, even at the LL/LO level, reinforcing the robustness of the observable. This qualitative difference underscores the beneficial role played by multiple heavy-flavor fragmentation in taming theoretical instabilities, making tetraquark-jet systems a reliable probe for the analysis of BFKL effects in exotic-hadron production.

#### IV. SUMMARY AND NEW DIRECTIONS

Guided by a hadron-structure-oriented vision, we have advanced the exploration of exotic matter production via the derivation and public release of the TQ4Q1.1 set of collinear FFs for a family of fully heavy tetraquarks [325]. Our analysis spans the three accessible channels characterized by quantum numbers  $J^{PC} = 0^{++}$  (scalar),  $1^{+-}$  (axial vector), and  $2^{++}$  (tensor), and targets both charm and bottom flavors. The construction of these FFs relies on the leading-power, single-parton fragmentation picture embedded in a NRQCD framework, which incorporates the contribution of distinct color-spin Fock-state configurations through their associated LDMEs.

SDCs are calculated at the initial scale for both gluon and heavy-quark fragmentation channels. These inputs are then evolved through a DGLAP evolution in the VFNS, implemented via the threshold-matched HF-NRevo scheme [131–133]. The TQ4Q1.1 sets repre-

sent the first release to include a detailed treatment of theoretical uncertainties from the LDMEs, enabling systematic propagation of hadronization-model ambiguities into collider-level predictions.

As a direct phenomenological application, we have employed the (sym)JETHAD multimodular interface [146–150] to evaluate high-energy cross sections for semi-inclusive tetraquark plus jet production at the HL-LHC and the FCC, operating at full NLL/NLO<sup>+</sup> accuracy within the HyF factorization formalism, that consistently combines collinear factorization with BFKL resummation.

We have computed differential distributions in the rapidity interval between the final-state hadrons,  $\Delta Y = y_1 - y_2$ , as well as angular multiplicities in the relative azimuthal angle  $\varphi = \phi_1 - \phi_2 - \pi$ . These observables are known to be highly sensitive to the structure of logarithmic resummation at high energies and to the interplay between perturbative and nonperturbative mechanisms of hadron formation.

Our rapidity-interval analyses revealed characteristic trends across the scalar, axial-vector, and tensor channels, with cross sections that decrease as  $\Delta Y$  increases and uncertainty bands that display a consistent stabilization pattern, especially at FCC energies. We found that the HyF signal becomes increasingly distinguishable from fixed-order backgrounds in the large- $\Delta Y$  regime, particularly in the scalar and tensor channels.

Notably, axial-vector configurations, despite yielding lower absolute cross sections due to fragmentation suppression, exhibit enhanced stability and tightly constrained uncertainty bands, rooted in the strong  $\mu_F$  evolution of the gluon FF and in the reduced propagation of LDME ambiguities. This *natural stability* [235] highlights the potential of this channel as a benchmark for future precision studies.

Angular multiplicities, on the other hand, provide complementary diagnostic power by isolating genuine resummation effects at fixed  $\Delta Y$ . Thanks to their definition as ratios of differential cross sections, these observables are largely insensitive to LDME modeling and phase-space integration effects, allowing for unambiguous comparison and discrimination between NLL resummed and high-energy NLO predictions.

The phenomenological richness arising from this mul-



tichannel investigation endows the TQ4Q1.1 functions with a twofold role. On the one hand, they serve as precision tools to probe high-energy QCD dynamics through stable, infrared-safe observables. On the other hand, they enable an in-depth exploration of exotic matter, providing access to the color-spin composition and hadronization pathways of fully heavy tetraquarks in different quantum states. This synergy between structural and dynamical insights constitutes a cornerstone for future studies at both current and next-generation hadron colliders.

Future developments will aim to consolidate the bridge between exotic hadron structure and the high-energy regime of QCD, building upon the multifaceted potential offered by the new TQ4Q1.1 functions. These tools open promising avenues for investigating not only the fragmentation mechanisms responsible for the emergence of fully heavy tetraquarks, but also the underlying dynamics of hadronization and gluon radiation in the forward domain. Advancing our grasp of exotic matter production will require increasingly accurate modeling of perturbative and nonperturbative effects, calling for a broader and more refined treatment of the many theoretical components involved.

A central priority is the enhancement of uncertainty quantification, in particular, MHOUs. As shown in recent studies [326–331], new methodologies for the propagation and statistical treatment of theoretical uncertainties are increasingly being established as standard practice. These developments should soon be extended to the case of exotic-hadron fragmentation. In our formalism, the explicit role of LDMEs as hadron-specific, nonperturbative parameters allows one to build dedicated strategies for tracing and reducing theoretical errors channel by channel.

Another crucial upgrade will come from the inclusion of color-octet configurations in the NRQCD expansion for tetraquark states. Although the present TQ4Q1.1 release focuses on the color-singlet channels at LO, the inclusion of higher Fock-state components is expected to affect the magnitude and shape of the FFs, especially for the scalar and tensor states. Once reliable LDME estimates for octet configurations become available, we plan to incorporate them into a consistent framework, extending the predictive power of our approach.

In the long term, progress will also involve an ex-

pansion of the HyF framework into a *multilateral* scheme integrating complementary resummation techniques. Specifically, establishing connections with soft-gluon [332–335] and jet-radius [336–340] resummations represents a compelling path forward. The investigation of jet angularities and their interplay with fragmentation [341–343] is equally promising, especially as experimental access to such observables improves. These enhancements will render our hybrid NLL/NLO<sup>+</sup> approach increasingly suitable for precision physics at high energies.

From a phenomenological perspective, the rare and suppressed character of fully bottomed tetraquarks provides an ideal laboratory to test the limits of the fragmentation formalism. Although current predictions of  $T_{4b}$  cross sections remain small, the evolution of bottom-flavored FFs at high scales, as described by TQ4Q1.1, will allow us to probe more exclusive observables and eventually extract structural information even in low-statistics environments.

The upcoming data from the FCC [7–9], as well as from other planned facilities [234, 344–359], will play a decisive role in driving these developments. Complementary programs at future lepton-hadron colliders such as the EIC [1–6] will offer further ways to investigate exotic states in cleaner environments, where gluon-initiated fragmentation may be isolated and studied more directly.

Among the next targets of our program stands the phenomenological investigation of the enigmatic  $Z_c(3900)$  state [360], whose prompt production has not yet been observed. Tetraquark production channels, powered by the high-energy and high-luminosity capabilities of new-generation machines, may help clarify its production mechanisms and reveal its inner composition.

In parallel, a deeper understanding of hadron structure will emerge from a progressive refinement of our knowledge of the underlying dynamics governing quarkonium and exotic-matter formation. This effort will benefit from data collected at future colliders, which will serve as a promising environment for probing the existence of intrinsic heavy-quark components. In particular, the case of intrinsic charm (IC) [361–367] has recently received renewed attention, with compelling evidence for its valence distribution in the proton [368].

This opens the possibility of using exotic-hadron production, including heavy tetraquarks, as indirect probes of IC dynamics. Reciprocally, the modeling of exotic hadrons containing heavy quarks may benefit from improved knowledge of IC, potentially suggesting a two-way portal between proton structure and exotic spectroscopy [369].

An additional frontier involves exploring the sensitivity of tetraquark production to the *dead-cone* effect [370], a unique prediction of QCD for heavy-quark fragmentation. This effect, recently confirmed by ALICE [371], may manifest itself in observables involving fully heavy tetraquarks and their distribution inside jets. Tetraquark-in-jet observables, when analyzed within the HyF factorization formalism, may provide a clean environment to quantify and constrain the dynamics of gluon radiation suppression at small angles, thereby enriching our understanding of the mass-dependent features of QCD radiation.

Finally, we stress the importance of treating individual tetraquark quantum states as distinct diagnostic tools. Each spin configuration examined here, namely scalar, axial-vector, and tensor, exhibit specific features in the behavior of FFs, their evolution, and the resulting production rates. Their differential impact on angular and rapidity observables enriches the phenomenological picture and offers valuable access to both the hadronization mechanisms at work and the core QCD dynamics in high-energy collisions.

In this context, the recent CMS spin-parity determination of fully charmed tetraquarks [90, 92] marks a major step forward in the exploration of exotic hadrons. The TQ4Q1.1 functions serve as a case study for a broader, evolution-consistent fragmentation framework that encompasses different families of fully heavy states. Thanks to its modular structure, our approach lends itself naturally to future extensions toward *multimodal* descriptions, where distinct classes of initial-scale inputs can be systematically included. Such a theoretical in-

frastructure provides versatile support to ongoing experimental efforts and enhances data-driven investigations of exotic multi-quark systems.

The release of TQ4Q1.1, now extended to include scalar, axial-vector, and tensor configurations—and now providing an estimate of uncertainties from the nonperturbative sector—lays the groundwork for a new generation of studies on the formation of exotic matter via collinear fragmentation. This work represents a timely step toward decoding the structure and formation of fully heavy hadrons, connecting state-of-the-art QCD methods to experimental programs at the energy and precision frontiers.

## ACKNOWLEDGMENTS

We acknowledge the use of calculations from Refs. [10, 14], which were independently rederived using (sym)JETHAD [146–150], and employed as proxies for the fragmentation process at the initial scale. We are grateful to Marco Bonvini, Angelo Esposito, Luca Maxia, Alessandro Papa, Fulvio Piccinini, and Alessandro Pilloni for valuable discussions on the physics of exotic hadronic states. This work is supported by the Atracción de Talento Grant No. 2022-T1/TIC-24176 from the Comunidad Autónoma de Madrid, Spain.

## DATA AVAILABILITY

The TQ4Q1.1 fragmentation functions for fully heavy tetraquarks  $T_{4Q}(J^{PC})$  [325] are available at: [https://github.com/FGCeliberto/Collinear\\_FFs/](https://github.com/FGCeliberto/Collinear_FFs/). For convenience, only the central values are provided. As the FFs scale linearly with the LDME (see Eqs. (4)), there is no need to provide separate error sets: users can straightforwardly rescale the FFs by varying the LDME within the uncertainty range specified in Tables I and II.

### Appendix A: Analytic expressions for the SDCs

In this appendix, we provide the functional form of all the nonvanishing dimensionless SDCs for our  $T_{4Q}$  fragmentation channels.

#### Scalar channel ( $0^{++}$ ).

The  $[g \rightarrow T_{4Q}(0^{++})]$  SDCs read [10]

$$\begin{aligned} \tilde{\mathcal{D}}_g^{(0^{++})}(z, [3, 3]) = & \frac{\pi^2 \alpha_s^4(4m_Q)}{497664 d_g^{T_{4Q}}(z)} [186624 - 430272z + 511072z^2 - 425814z^3 \\ & + 217337z^4 - 61915z^5 + 7466z^6 + 42(1-z)(2-z)(3-z)(-144 + 634z \\ & - 385z^2 + 70z^3) \ln(1-z) + 36(2-z)(3-z)(144 - 634z + 749z^2 - 364z^3 \\ & + 74z^4) \ln\left(1 - \frac{z}{2}\right) + 12(2-z)(3-z)(72 - 362z + 361z^2 - 136z^3 + 23z^4) \\ & \times \ln\left(1 - \frac{z}{3}\right)] , \end{aligned} \quad (\text{A1})$$

$$\begin{aligned} \tilde{\mathcal{D}}_g^{(0^{++})}(z, [6, 6]) = & \frac{\pi^2 \alpha_s^4(4m_Q)}{331776 d_g^{T_{4Q}}(z)} [186624 - 430272z + 617824z^2 - 634902z^3 \\ & + 374489z^4 - 115387z^5 + 14378z^6 - 6(1-z)(2-z)(3-z)(-144 - 2166z \\ & + 1015z^2 + 70z^3) \ln(1-z) - 156(2-z)(3-z)(144 - 1242z + 1693z^2 - 876z^3 \\ & + 170z^4) \ln\left(1 - \frac{z}{2}\right) + 300(2-z)(3-z)(72 - 714z + 953z^2 - 472z^3 + 87z^4) \\ & \times \ln\left(1 - \frac{z}{3}\right)] , \end{aligned} \quad (\text{A2})$$

$$\begin{aligned} \tilde{\mathcal{D}}_g^{(0^{++})}(z, [3, 6]) = & \frac{\pi^2 \alpha_s^4(4m_Q)}{165888 d_g^{T_{4Q}}(z)} [186624 - 430272z + 490720z^2 - 394422z^3 \\ & + 199529z^4 - 57547z^5 + 7082z^6 + 6(1-z)(2-z)(3-z)(-432 + 3302z \\ & - 1855z^2 + 210z^3) \ln(1-z) - 12(2-z)(3-z)(720 - 2258z + 2329z^2 - 1052z^3 \\ & + 226z^4) \ln\left(1 - \frac{z}{2}\right) + 12(2-z)(3-z)(936 - 4882z + 4989z^2 - 1936z^3 + 331z^4) \\ & \times \ln\left(1 - \frac{z}{3}\right)] , \end{aligned} \quad (\text{A3})$$

with  $d_g^{T_{4Q}}(z) = z(2-z)^2(3-z)$ . Analogously, the  $[Q \rightarrow T_{4Q}(0^{++})]$  SDCs read [14]

$$\begin{aligned} \tilde{\mathcal{D}}_Q^{(0^{++})}(z, [3, 3]) &= \frac{\pi^2 \alpha_s^4 (5m_Q)}{559872 d_Q^{T_{4Q}}(z)} [-264(z-4)(11z-12)(z^2-16z+16) \\ &\times (13z^4 - 57z^3 - 656z^2 + 1424z - 512)(3z-4)^5 \log(z^2-16z+16) + 6(11z-12)(z^2-16z+16) \\ &\times (1273z^5 - 16764z^4 + 11840z^3 + 247808z^2 - 472320z + 171008)(3z-4)^5 \log(4-3z) \\ &- 3(11z-12)(z^2-16z+16)(129z^5 - 7172z^4 + 49504z^3 - 108416z^2 + 73984z - 9216)(3z-4)^5 \\ &\times \log \left[ \left( 4 - \frac{11z}{3} \right) (4-z) \right] + 16(z-1)(657763z^{12} - 10028192z^{11} + 188677968z^{10} - 2600899712z^9 \\ &+ 18018056448z^8 - 71685000192z^7 + 179414380544z^6 - 294834651136z^5 \\ &+ 321642168320z^4 - 229388845056z^3 + 102018056192z^2 - 25480396800z + 2717908992)] , \end{aligned} \quad (\text{A4})$$

$$\begin{aligned} \tilde{\mathcal{D}}_Q^{(0^{++})}(z, [6, 6]) &= \frac{\pi^2 \alpha_s^4 (5m_Q)}{373248 d_Q^{T_{4Q}}(z)} [-120(z-4)(11z-12)(z^2-16z+16) \\ &\times (35z^4 - 535z^3 + 3472z^2 - 4240z + 512)(3z-4)^5 \log(z^2-16z+16) \\ &- 30(11z-12)(z^2-16z+16)(3395z^5 - 48020z^4 + 126144z^3 \\ &- 75776^2 - 38656z + 62464)(3z-4)^5 \log(4-3z) + 75(11z-12)(z^2-16z+16) \\ &\times (735z^5 - 10684z^4 + 34208z^3 - 44160z^2 + 20224z + 9216)(3z-4)^5 \log \left[ \left( 4 - \frac{11z}{3} \right) (4-z) \right] \\ &+ 16(z-1)(7916587z^{12} - 263987840z^{11} + 3125201872z^{10} - 16993694336z^9 \\ &+ 51814689024z^8 - 99638283264z^7 + 133459423232z^6 - 140136398848z^5 \\ &+ 127161204736z^4 - 96695746560z^3 + 53372518400z^2 - 17930649600z + 2717908992)] , \end{aligned} \quad (\text{A5})$$

$$\begin{aligned} \tilde{\mathcal{D}}_Q^{(0^{++})}(z, [3, 6]) &= \frac{\pi^2 \alpha_s^4 (5m_Q)}{186624\sqrt{6} d_Q^{T_{4Q}}(z)} [24(z-4)(11z-12)(z^2-16z+16) \\ &\times (225z^4 - 3085z^3 + 17456z^2 - 19760z + 1536)(3z-4)^5 \log(z^2-16z+16) \\ &- 6(11z-12)(z^2-16z+16)(555z^5 + 52428z^4 - 363328z^3 + 616448z^2 - 270080z + 70656) \\ &\times (3z-4)^5 \log(4-3z) + 75(11z-12)(z^2-16z+16)(1245z^5 - 84308z^4 \\ &+ 601696z^3 - 1333120z^2 + 914688z - 119808)(3z-4)^5 \log \left[ \left( 4 - \frac{11z}{3} \right) (4-z) \right] \\ &+ 16(z-1)(1829959z^{12} - 44960912z^{11} + 285792656z^{10} - 1090093952z^9 \\ &+ 5123084544z^8 - 24390724608z^7 + 77450817536z^6 - 153897779200z^5 \\ &+ 194102034432z^4 - 155643543552z^3 + 77091307520z^2 - 21705523200z + 2717908992)] , \end{aligned} \quad (\text{A6})$$

with  $d_Q^{T_{4Q}}(z) = (4-3z)^6(z-4)^2z(11z-12)(z^2-16z+16)$ .

**Axial-vector channel  $(1^{+-})$ .**

As discussed in Section II C, Fermi-Dirac statistics, together with the symmetry constraints imposed by the  $S$ -wave configuration, allow only the  $[3, 3]$  color-spin channel to contribute to the axial-vector state. Furthermore, the  $[g \rightarrow T_{4Q}(1^{+-})]$  fragmentation channel is suppressed at LO due to the Landau-Yang selection rule.

$$\begin{aligned}
\tilde{\mathcal{D}}_Q^{(1^{+-})}(z, [3, 3]) = & \frac{\pi^2 [\alpha_s^4(5m_Q)]}{279936 d_Q^{T_{4Q}}(z)} [480(z-4)(11z-12)(z^2-16z+16) \\
& \times (4z^4 + 115z^3 - 316z^2 + 112z + 64)(3z-4)^5 \log(z^2-16z+16) \\
& + 6(11z-12)(z^2-16z+16)(4825z^5 - 56232z^4 + 378480z^3 \\
& - 942528z^2 + 672768z - 60416)(3z-4)^5 \log(4-3z) - 3(11z-12)(z^2-16z+16)(5465z^5 \\
& - 40392z^4 + 254320z^3 - 722368z^2 + 611328z - 101376)(3z-4)^5 \log\left[\left(\frac{11z}{3} - 4\right)(z-4)\right] \\
& + 16(z-1)z(476423z^{11} + 32559240z^{10} - 934590720z^9 + 8015251776z^8 \\
& - 35393754624z^7 + 94265413632z^6 - 160779010048z^5 + 177897046016z^4 \\
& - 124600254464z^3 + 51223461888z^2 - 10217324544z + 490733568)] , \tag{A7}
\end{aligned}$$

### Tensor channel ( $2^{++}$ ).

As noted in Section II C, the combined effect of Fermi-Dirac statistics and the combined effect and the  $S$ -wave structure restricts the surviving SDCs for tensor states to the  $[3, 3]$  structures only. In the  $[g \rightarrow T_{4Q}(2^{++})]$  channel, one finds [10]

$$\begin{aligned}
\tilde{\mathcal{D}}_g^{(2^{++})}(z, [3, 3]) = & \frac{\pi^2 \alpha_s^4(4m_c)}{622080 z d_g^{T_{4Q}}(z)} [(46656 - 490536z + 1162552z^2 - 1156308z^3 \\
& + 595421z^4 - 170578z^5 + 21212z^6) 2z + 3(1-z)(2-z)(3-z)(-20304 - 31788z) \\
& \times (1296 + 1044z + 73036z^2 - 36574z^3 + 7975z^4) \\
& \times \ln(1-z) + 33(2-z)(3-z)(1296 + 25)] \\
& - 9224z^2 + 9598z^3 - 3943z^4 + 725z^5 \ln\left(1 - \frac{z}{3}\right)] . \tag{A8}
\end{aligned}$$



Analogously, the  $[Q \rightarrow T_{4Q}(2^{++})]$  SDC reads [14]

$$\begin{aligned}
\tilde{D}_Q^{(2^{++})}(z, [3, 3]) &= \frac{\pi^2 \alpha_s^4 (5m_Q)}{2799360 z d_Q^{T_{4Q}}(z)} [672(z-4)(11z-12)(z^2-16z+16) \\
&\times (47z^5 + 12186z^4 - 44608z^3 + 40000z^2 - 7936z + 4608) \\
&\times (3z-4)^5 \log(z^2-16z+16) + 6(11z-12)(z^2-16z+16) \\
&\times (107645z^6 - 1088988z^5 + 7805536z^4 - 20734976z^3 + 8933504z^2 - 6013952z + 1695744) \\
&\times (3z-4)^5 \log(4-3z) - 33(11z-12)(z^2-16z+16)(3581z^5 - 53216z^4 - 326176z^3 + 419456z^2 \\
&- 6912z + 55296)(3z-4)^6 \log\left[\left(4 - \frac{11z}{3}\right)(4-z)\right] \\
&+ 16(z-1)(96449507z^{12} - 158520388z^{11} - 26228206896z^{10} + 281743037888z^9 \\
&- 1355257362432z^8 + 1355257362432z^7 - 6637452959744z^6 + 7595797282816z^5 \\
&- 5643951472640z^4 + 2662988513280z^3 - 788934950912z^2 + 161828831232z - 24461180928)] .
\end{aligned} \tag{A9}$$

## Appendix B: Tetraquark-jet systems in NLL/NLO<sup>+</sup> HyF

We consider the following reaction (Fig. 10)

$$p(p_a) + p(p_b) \rightarrow T_{4Q}(\kappa_1, y_1) + \mathcal{X} + \text{jet}(\kappa_2, y_2) , \tag{B1}$$

where a fully heavy tetraquark,  $T_{4c}$  or  $T_{4b}$ , is semi-inclusively identified together with a light jet, and an undetected gluon radiation cascade,  $\mathcal{X}$ . The outgoing particles carry transverse momenta that fulfill the condition  $|\vec{\kappa}_{1,2}| \gg \Lambda_{\text{QCD}}$ , where  $\Lambda_{\text{QCD}}$  denotes the QCD hadronization scale. These objects are also separated by a large rapidity interval,  $\Delta Y = y_1 - y_2$ . We apply a Sudakov decomposition of the four-momenta  $\kappa_{1,2}$  using the momenta of the incoming protons,  $p_{a,b}$ , which yields

$$\kappa_{1,2} = x_{1,2} p_{a,b} + \frac{\vec{\kappa}_{1,2}^2}{x_{1,2} s} p_{b,a} + \kappa_{1,2\perp} \quad \kappa_{1,2\perp}^2 = -\vec{\kappa}_{1,2}^2 , \tag{B2}$$

In the center-of-mass frame, the following relations hold between rapidities  $y_{1,2}$  and longitudinal momentum fractions of the final-state particles

$$y_{1,2} = \pm \ln \frac{x_{1,2} \sqrt{s}}{|\vec{\kappa}_{1,2}|} . \tag{B3}$$

In a purely collinear factorization framework, the LO differential cross section for our processes would be expressed as a one-dimensional convolution involving the on-shell hard scattering kernel, the proton PDFs, and the  $T_{4Q}$  FF

$$\frac{d\sigma_{[\text{collinear}]}^{\text{LO}}}{dx_1 dx_2 d^2 \vec{\kappa}_1 d^2 \vec{\kappa}_2} = \sum_{i,j=q,\bar{q},g} \int_0^1 dx_a \int_0^1 dx_b f_i(x_a) f_j(x_b) \int_{x_1}^1 \frac{d\zeta}{\zeta} D_i^{T_{4Q}}\left(\frac{x_1}{\zeta}\right) \frac{d\hat{\sigma}_{i,j}(\hat{s})}{dx_1 dx_2 d^2 \vec{\kappa}_1 d^2 \vec{\kappa}_2} . \tag{B4}$$

Here, the indices  $i, j$  run over all partons except for the top quark, which does not hadronize. For compactness, the explicit dependence on the factorization scale  $\mu_F$  is omitted in Eq. (B4). The functions  $f_{i,j}(x_{a,b}, \mu_F)$  denote

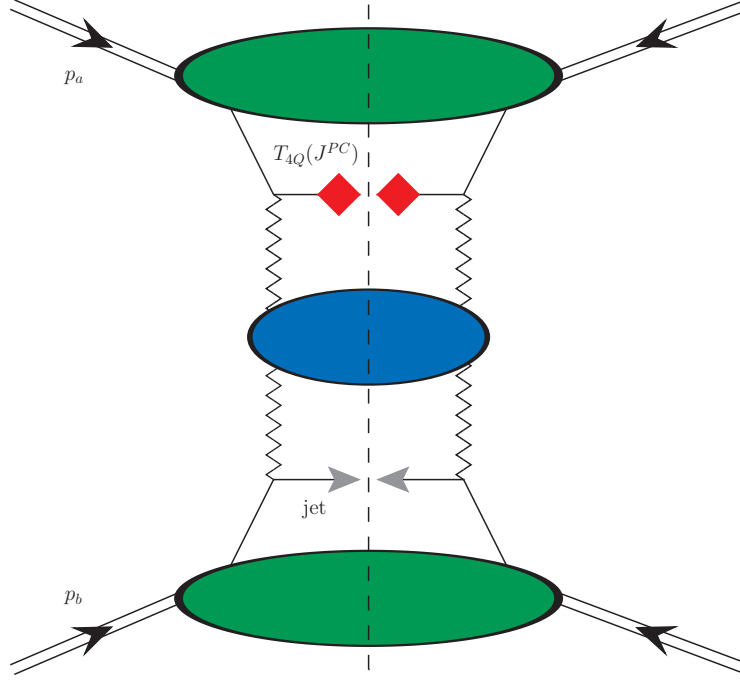


FIG. 10. Pictorial representation of the semi-inclusive hadroproduction of a tetraquark-jet system within the hybrid collinear and high-energy factorization (HyF) framework. Red rhombi indicate the collinear FFs of the fully heavy  $T_{4Q}(J^{PC})$  tetraquark. Black arrows represent the final-state jet, while green ovals correspond to proton collinear PDFs. Blue blobs denote the exponentiated resummation kernel, which is connected to the two off-shell gluon emission functions via zigzag Reggeon lines.

the proton PDFs, while  $D_i^{T_{4Q}}(x_1/\zeta, \mu_F)$  represent the tetraquark FFs. Here,  $x_a, b$  are the longitudinal momentum fractions of the incoming partons, and  $\zeta$  is the momentum fraction carried by the outgoing parton that fragments into the  $T_{4Q}$  hadron. Finally,  $d\hat{\sigma}_{i,j}(\hat{s})$  refers to the partonic cross section, with  $\hat{s} = x_a x_b s$  the partonic center-of-mass energy squared.

The differential cross section can be recast as a Fourier sum of angular coefficients,  $C_{n \geq 0}$ . We write

$$\frac{d\sigma}{d\Delta Y d\varphi d|\vec{\kappa}_1| d|\vec{\kappa}_2|} = \frac{1}{\pi} \left[ \frac{1}{2} C_0 + \sum_{n=1}^{\infty} \cos(n\varphi) C_n \right], \quad (\text{B5})$$

with  $\varphi = \phi_1 - \phi_2 - \pi$  and  $\phi_{1,2}$  standing for the azimuthal angles of the two outgoing particles. Within the HyF framework, employing the  $\overline{\text{MS}}$  renormalization scheme [372], we derive a master formula for the  $C_n$  coefficients. This formulation is valid at NLO accuracy and includes the NLL resummation of high-energy logarithms. Explicitly,

one obtains

$$C_n^{\text{NLL/NLO}^+} = \int_{\kappa_1^{\min}}^{\kappa_1^{\max}} d|\vec{\kappa}_1| \int_{\kappa_2^{\min}}^{\kappa_2^{\max}} d|\vec{\kappa}_2| \int_{y_1^{\min}}^{y_1^{\max}} dy_1 \int_{y_2^{\min}}^{y_2^{\max}} dy_2 \delta(y_1 - y_2 - \Delta Y) \int_{-\infty}^{+\infty} d\nu e^{\bar{\alpha}_s \Delta Y \chi^{\text{NLL}}(n, \nu)} \times \frac{e^{\Delta Y}}{s} \alpha_s^2(\mu_R) \left\{ \mathcal{F}_1^{\text{NLO}}(n, \nu, |\vec{\kappa}_1|, x_1) [\mathcal{F}_2^{\text{NLO}}(n, \nu, |\vec{\kappa}_2|, x_2)]^* + \bar{\alpha}_s^2 \frac{\beta_0 \Delta Y}{4N_c} \chi(n, \nu) v(\nu) \right\}, \quad (\text{B6})$$

Here,  $\bar{\alpha}_s(\mu_R) = \alpha_s(\mu_R) N_c / \pi$ , where  $N_c$  is the number of colors, and  $\beta_0 = 11N_c/3 - 2n_f/3$  is the leading coefficient of the QCD  $\beta$ -function. We employ a two-loop running coupling with  $\alpha_s(M_Z) = 0.118$  and a dynamic flavor number,  $n_f$ . The  $\chi(n, \nu)$  function appearing in the exponent of Eq. (B6) denotes the BFKL kernel [236–238], responsible for resumming NLL energy logarithms

$$\chi^{\text{NLL}}(n, \nu) = \chi(n, \nu) + \bar{\alpha}_s \hat{\chi}(n, \nu), \quad (\text{B7})$$

where

$$\chi(n, \nu) = -2 \{ \gamma_E + \text{Re} [\psi((n+1)/2 + i\nu)] \} \quad (\text{B8})$$

are the LO BFKL eigenvalues. Moreover,  $\psi(z) = \Gamma'(z)/\Gamma(z)$  represents the logarithmic derivative of the Gamma function, while  $\gamma_E$  denotes the Euler-Mascheroni constant. The  $\hat{\chi}(n, \nu)$  function stands for the NLO kernel correction

$$\hat{\chi}(n, \nu) = \bar{\chi}(n, \nu) + \frac{\beta_0}{8N_c} \chi(n, \nu) \left\{ -\chi(n, \nu) + 2 \ln(\mu_R^2/\hat{\mu}^2) + \frac{10}{3} \right\}, \quad (\text{B9})$$

with  $\hat{\mu} = \sqrt{|\vec{\kappa}_1| |\vec{\kappa}_2|}$ . The complete formula for the characteristic  $\bar{\chi}(n, \nu)$  function is given, *e.g.* in Sec. 2.1.1 of Ref. [146]. The two quantities

$$\mathcal{F}_{1,2}^{\text{NLO}}(n, \nu, |\vec{\kappa}|, x) = \mathcal{F}_{1,2}(n, \nu, |\vec{\kappa}|, x) + \alpha_s(\mu_R) \hat{\mathcal{F}}_{1,2}(n, \nu, |\vec{\kappa}|, x) \quad (\text{B10})$$

portray the NLO singly off-shell, transverse-momentum-dependent emission functions, commonly referred to in the BFKL context as forward-production impact factors. Tetraquark emissions are captured by the NLO forward-hadron impact factor [373]. Although originally derived for light hadrons, this object remains valid within our VFNS-based framework [143, 144], provided that the relevant transverse-momentum regimes lie well above the DGLAP evolution thresholds associated with heavy-quark production. At LO, we have

$$\mathcal{F}_{T_{4Q}}(n, \nu, |\vec{\kappa}|, x) = 2 \sqrt{\frac{C_F}{C_A}} |\vec{\kappa}|^{2i\nu-1} \int_x^1 \frac{d\zeta}{\zeta} \left( \frac{x}{\zeta} \right)^{1-2i\nu} \times \left[ \frac{C_A}{C_F} f_g(\zeta, \mu_F) D_g^{T_{4Q}} \left( \frac{x}{\zeta}, \mu_F \right) + \sum_{i=q, \bar{q}} f_i(\zeta, \mu_F) D_i^{T_{4Q}} \left( \frac{x}{\zeta}, \mu_F \right) \right], \quad (\text{B11})$$

with  $C_F = (N_c^2 - 1)/(2N_c)$  and  $C_A \equiv N_c$  being the Casimir invariants associated with gluon emissions from a quark and a gluon, respectively. Here,  $f_i(x, \mu_F)$  denotes the PDF of parton  $i$  inside the parent proton, while  $D_i^{T_{4Q}}(x/\zeta, \mu_F)$  is the FF describing the fragmentation of parton  $i$  into the detected tetraquark,  $T_{4Q}$ . The full NLO correction is detailed in [373]. At LO, the jet emission function is given by

$$\mathcal{F}_J(n, \nu, |\vec{\kappa}|, x) = 2 \sqrt{\frac{C_F}{C_A}} |\vec{\kappa}|^{2i\nu-1} \left[ \frac{C_A}{C_F} f_g(x, \mu_F) + \sum_{j=q, \bar{q}} f_j(x, \mu_F) \right]. \quad (\text{B12})$$

while its NLO correction is derived from [246]. It bases on small-cone selection functions with the jet cone radius fixed to  $R_J = 0.5$ , in accordance with recent analyses at CMS [319, 320, 374]. The remaining element in Eq. (B6) is the function  $v(\nu)$ , which reads

$$v(\nu) = \frac{1}{2} \left[ 4 \ln \hat{\mu} + i \frac{d}{d\nu} \ln \frac{\mathcal{F}_1(n, \nu, |\vec{\kappa}_1|, x_1)}{\mathcal{F}_2[(n, \nu, |\vec{\kappa}_1|, x_1)]^*} \right]. \quad (\text{B13})$$

Equations (B6) to (B12) provide a detailed characterization of our hybrid-factorization framework. In line with the BFKL approach, the cross section exhibits high-energy factorization, represented as a convolution of the BFKL Green's function with two singly off-shell emission functions. These emission functions incorporate collinear inputs, namely the convolutions of the initial-state proton PDFs with the final-state hadron FFs. The NLL/NLO<sup>+</sup> label denotes a fully resummed next-to-leading logarithmic treatment of energy logarithms within a next-to-leading order perturbative expansion. The '+' superscript indicates the inclusion of subleading terms beyond NLL accuracy, arising from the product of NLO corrections to the emission functions in our computation of azimuthal coefficients.

For the sake of comparison, we also consider the pure LL limit within the  $\overline{\text{MS}}$  scheme, which is obtained by neglecting NLO corrections in both the resummation kernel (Eq.(B7)) and the impact factors (Eq.(B10)). This yields

$$C_n^{\text{LL/LO}} \propto \frac{e^{\Delta Y}}{s} \int_{-\infty}^{+\infty} d\nu e^{\bar{\alpha}_s \Delta Y \chi(n, \nu)} \alpha_s^2(\mu_R) \mathcal{F}_{T_{4Q}}(n, \nu, |\vec{\kappa}_1|, x_1) [\mathcal{F}_J(n, \nu, |\vec{\kappa}_2|, x_2)]^*. \quad (\text{B14})$$

We note that integration over transverse momenta and rapidities of the final-state objects, explicitly displayed in the first line of Eq. (B6), is omitted in Eq. (B14) but remains implicitly understood.

A detailed comparison between high-energy resummation and fixed-order methods hinges on contrasting NLL-resummed predictions with purely fixed-order calculations. However, to the best of our knowledge, no numerical framework currently allows for full NLO evaluations of observables sensitive to two-particle hadroproduction. To provide a fixed-order baseline, we truncate the perturbative expansion of the  $C_n$  coefficients in Eq. (B6) at  $\mathcal{O}(\alpha_s^3)$ . This procedure yields an effective high-energy fixed-order (HE-NLO<sup>+</sup>) representation, suitable for phenomenological applications. It retains the dominant high-energy logarithmic contributions found in a full NLO result, while systematically neglecting subleading terms suppressed by inverse powers of the partonic center-of-mass energy. The resulting  $\overline{\text{MS}}$ -scheme expression for the HE-NLO<sup>+</sup> angular coefficients reads

$$C_n^{\text{HE-NLO}^+} \propto \frac{e^{\Delta Y}}{s} \int_{-\infty}^{+\infty} d\nu \alpha_s^2(\mu_R) [1 + \bar{\alpha}_s(\mu_R) \Delta Y \chi(n, \nu)] \mathcal{F}_{T_{4Q}}^{\text{NLO}}(n, \nu, |\vec{\kappa}_1|, x_1) [\mathcal{F}_J^{\text{NLO}}(n, \nu, |\vec{\kappa}_2|, x_2)]^*. \quad (\text{B15})$$

Here, the exponentiated kernel is expanded up to  $\mathcal{O}(\alpha_s)$ . As before, for the sake of brevity, the integration over the transverse momenta and rapidities of the final-state objects is left implicit.

- 
- |  |  |
|--|--|
| <p>[1] R. Abdul Khalek <i>et al.</i>, <i>Nucl. Phys. A</i> <b>1026</b>, 122447 (2022), <a href="#">arXiv:2103.05419 [physics.ins-det]</a>.</p> <p>[2] R. Abdul Khalek <i>et al.</i>, in <i>2022 Snowmass Summer Study</i> (2022) <a href="#">arXiv:2203.13199 [hep-ph]</a>.</p> <p>[3] M. Hentschinski <i>et al.</i>, <i>Acta Phys. Polon. B</i> <b>54</b>, 2 (2023), <a href="#">arXiv:2203.08129 [hep-ph]</a>.</p> | <p>[4] S. Amoroso <i>et al.</i>, <i>Acta Phys. Polon. B</i> <b>53</b>, A1 (2022), <a href="#">arXiv:2203.13923 [hep-ph]</a>.</p> <p>[5] R. Abir <i>et al.</i>, (2023), <a href="#">arXiv:2305.14572 [hep-ph]</a>.</p> <p>[6] C. Allaire <i>et al.</i>, <i>Comput. Softw. Big Sci.</i> <b>8</b>, 5 (2024), <a href="#">arXiv:2307.08593 [physics.acc-ph]</a>.</p> <p>[7] M. Benedikt <i>et al.</i> (FCC), (2025),</p> |
|--|--|

- 10.17181/CERN.9DKX.TDH9, [arXiv:2505.00272 \[hep-ex\]](#).
- [8] M. Benedikt *et al.* (FCC), (2025), [10.17181/CERN.EBAY.7W4X](#), [arXiv:2505.00274 \[physics.acc-ph\]](#).
- [9] M. Benedikt *et al.* (FCC), (2025), [10.17181/CERN.I26X.V4VF](#), [arXiv:2505.00273 \[physics.acc-ph\]](#).
- [10] F. Feng, Y. Huang, Y. Jia, W.-L. Sang, X. Xiong, and J.-Y. Zhang, *Phys. Rev. D* **106**, 114029 (2022), [arXiv:2009.08450 \[hep-ph\]](#).
- [11] F. Feng, Y. Huang, Y. Jia, W.-L. Sang, and J.-Y. Zhang, *Phys. Lett. B* **818**, 136368 (2021), [arXiv:2011.03039 \[hep-ph\]](#).
- [12] F. Feng, Y. Huang, Y. Jia, W.-L. Sang, D.-S. Yang, and J.-Y. Zhang, *Phys. Rev. D* **108**, L051501 (2023), [arXiv:2304.11142 \[hep-ph\]](#).
- [13] F. Feng, Y. Huang, Y. Jia, W.-L. Sang, D.-S. Yang, and J.-Y. Zhang, *Phys. Rev. D* **110**, 054007 (2024), [arXiv:2311.08292 \[hep-ph\]](#).
- [14] X.-W. Bai, F. Feng, C.-M. Gan, Y. Huang, W.-L. Sang, and H.-F. Zhang, *JHEP* **09**, 002 (2024), [arXiv:2404.13889 \[hep-ph\]](#).
- [15] X.-W. Bai, Y. Huang, and W.-L. Sang, *Phys. Rev. D* **111**, 054006 (2025), [arXiv:2411.19296 \[hep-ph\]](#).
- [16] S. M. Moosavi Nejad and N. Amiri, *Phys. Rev. D* **105**, 034001 (2022), [arXiv:2110.15251 \[hep-ph\]](#).
- [17] F. G. Celiberto and A. Papa, *Phys. Lett. B* **848**, 138406 (2024), [arXiv:2308.00809 \[hep-ph\]](#).
- [18] F. G. Celiberto, G. Gatto, and A. Papa, *Eur. Phys. J. C* **84**, 1071 (2024), [arXiv:2405.14773 \[hep-ph\]](#).
- [19] F. G. Celiberto and G. Gatto, *Phys. Rev. D* **111**, 034037 (2025), [arXiv:2412.10549 \[hep-ph\]](#).
- [20] F. G. Celiberto, *Phys. Rev. D* **111**, L111501 (2025), [arXiv:2504.03949 \[hep-ph\]](#).
- [21] F. G. Celiberto, (2025), [arXiv:2502.11136 \[hep-ph\]](#).
- [22] E. Kou and O. Pene, *Phys. Lett. B* **631**, 164 (2005), [arXiv:hep-ph/0507119](#).
- [23] E. Braaten, *Phys. Rev. Lett.* **111**, 162003 (2013), [arXiv:1305.6905 \[hep-ph\]](#).
- [24] M. Berwein, N. Brambilla, J. Tarrús Castellà, and A. Vairo, *Phys. Rev. D* **92**, 114019 (2015), [arXiv:1510.04299 \[hep-ph\]](#).
- [25] P. Minkowski and W. Ochs, *Eur. Phys. J. C* **9**, 283 (1999), [arXiv:hep-ph/9811518](#).
- [26] V. Mathieu, N. Kochelev, and V. Vento, *Int. J. Mod. Phys. E* **18**, 1 (2009), [arXiv:0810.4453 \[hep-ph\]](#).
- [27] H.-X. Chen, W. Chen, and S.-L. Zhu, *Phys. Rev. D* **103**, L091503 (2021), [arXiv:2103.17201 \[hep-ph\]](#).
- [28] T. Csörgő, T. Novak, R. Pasechnik, A. Ster, and I. Szanyi, *Eur. Phys. J. C* **81**, 180 (2021), [arXiv:1912.11968 \[hep-ph\]](#).
- [29] V. M. Abazov *et al.* (D0, TOTEM), *Phys. Rev. Lett.* **127**, 062003 (2021), [arXiv:2012.03981 \[hep-ex\]](#).
- [30] M. Gell-Mann, *Phys. Lett.* **8**, 214 (1964).
- [31] R. L. Jaffe, *Phys. Rev. D* **15**, 267 (1977).
- [32] R. L. Jaffe, *Phys. Rev. D* **15**, 281 (1977).
- [33] R. L. Jaffe, *Phys. Rev. Lett.* **38**, 195 (1977), [Erratum: *Phys. Rev. Lett.* **38**, 617 (1977)].
- [34] J. P. Ader, J. M. Richard, and P. Taxil, *Phys. Rev. D* **25**, 2370 (1982).
- [35] J. L. Rosner, *Phys. Rev. D* **33**, 2043 (1986).
- [36] S. Pepin and F. Stancu, *Phys. Rev. D* **57**, 4475 (1998), [arXiv:hep-ph/9710528](#).
- [37] J. Vijande, A. Valcarce, and J. M. Richard, *Phys. Rev. D* **85**, 014019 (2012), [arXiv:1111.5921 \[hep-ph\]](#).
- [38] A. Esposito, A. Pilloni, and A. D. Polosa, *Phys. Rept.* **668**, 1 (2017), [arXiv:1611.07920 \[hep-ph\]](#).
- [39] R. F. Lebed, R. E. Mitchell, and E. S. Swanson, *Prog. Part. Nucl. Phys.* **93**, 143 (2017), [arXiv:1610.04528 \[hep-ph\]](#).
- [40] F.-K. Guo, C. Hanhart, U.-G. Meißner, Q. Wang, Q. Zhao, and B.-S. Zou, *Rev. Mod. Phys.* **90**, 015004 (2018), [Erratum: *Rev. Mod. Phys.* **94**, 029901 (2022)], [arXiv:1705.00141 \[hep-ph\]](#).
- [41] W. Lucha, D. Melikhov, and H. Sazdjian, *Phys. Rev. D* **96**, 014022 (2017), [arXiv:1706.06003 \[hep-ph\]](#).
- [42] A. Ali, L. Maiani, and A. D. Polosa, *Multiquark Hadrons* (Cambridge University Press, 2019).
- [43] S. K. Choi *et al.* (Belle), *Phys. Rev. Lett.* **91**, 262001 (2003), [arXiv:hep-ex/0309032](#).
- [44] D. Acosta *et al.* (CDF), *Phys. Rev. Lett.* **93**, 072001 (2004), [arXiv:hep-ex/0312021](#).
- [45] R. Aaij *et al.* (LHCb), *Phys. Rev. Lett.* **110**, 222001 (2013), [arXiv:1302.6269 \[hep-ex\]](#).
- [46] A. M. Sirunyan *et al.* (CMS), *Phys. Rev. Lett.* **128**, 032001 (2022), [arXiv:2102.13048 \[hep-ex\]](#).
- [47] E. S. Swanson, *Phys. Rept.* **429**, 243 (2006), [arXiv:hep-ph/0601110](#).



- 
- [48] J. E. Augustin *et al.* (SLAC-SP-017), *Phys. Rev. Lett.* **33**, 1406 (1974).
- [49] J. J. Aubert *et al.* (E598), *Phys. Rev. Lett.* **33**, 1404 (1974).
- [50] C. Bacci *et al.*, *Phys. Rev. Lett.* **33**, 1408 (1974), [Erratum: *Phys. Rev. Lett.* **33**, 1649 (1974)].
- [51] H.-X. Chen, W. Chen, X. Liu, and S.-L. Zhu, *Phys. Rept.* **639**, 1 (2016), arXiv:1601.02092 [hep-ph].
- [52] Y.-R. Liu, H.-X. Chen, W. Chen, X. Liu, and S.-L. Zhu, *Prog. Part. Nucl. Phys.* **107**, 237 (2019), arXiv:1903.11976 [hep-ph].
- [53] R. Aaij *et al.* (LHCb), *Phys. Rev. Lett.* **125**, 242001 (2020), arXiv:2009.00025 [hep-ex].
- [54] L. Maiani, F. Piccinini, A. D. Polosa, and V. Riquer, *Phys. Rev. D* **71**, 014028 (2005), arXiv:hep-ph/0412098.
- [55] G. 't Hooft, G. Isidori, L. Maiani, A. D. Polosa, and V. Riquer, *Phys. Lett. B* **662**, 424 (2008), arXiv:0801.2288 [hep-ph].
- [56] L. Maiani, V. Riquer, R. Faccini, F. Piccinini, A. Pilloni, and A. D. Polosa, *Phys. Rev. D* **87**, 111102 (2013), arXiv:1303.6857 [hep-ph].
- [57] L. Maiani, F. Piccinini, A. D. Polosa, and V. Riquer, *Phys. Rev. D* **89**, 114010 (2014), arXiv:1405.1551 [hep-ph].
- [58] L. Maiani, A. D. Polosa, and V. Riquer, *Phys. Lett. B* **778**, 247 (2018), arXiv:1712.05296 [hep-ph].
- [59] H. Mutuk, *Eur. Phys. J. C* **81**, 367 (2021), arXiv:2104.11823 [hep-ph].
- [60] Z.-G. Wang and T. Huang, *Phys. Rev. D* **89**, 054019 (2014), arXiv:1310.2422 [hep-ph].
- [61] Z.-G. Wang, *Eur. Phys. J. C* **74**, 2874 (2014), arXiv:1311.1046 [hep-ph].
- [62] B. Grinstein, L. Maiani, and A. D. Polosa, *Phys. Rev. D* **109**, 074009 (2024), arXiv:2401.11623 [hep-ph].
- [63] N. A. Tornqvist, *Z. Phys. C* **61**, 525 (1994), arXiv:hep-ph/9310247.
- [64] E. Braaten and M. Kusunoki, *Phys. Rev. D* **69**, 074005 (2004), arXiv:hep-ph/0311147.
- [65] F.-K. Guo, C. Hidalgo-Duque, J. Nieves, and M. P. Valderrama, *Phys. Rev. D* **88**, 054007 (2013), arXiv:1303.6608 [hep-ph].
- [66] H. Mutuk, *Eur. Phys. J. C* **82**, 1142 (2022), arXiv:2211.14836 [hep-ph].
- [67] Z.-G. Wang and T. Huang, *Eur. Phys. J. C* **74**, 2891 (2014), arXiv:1312.7489 [hep-ph].
- [68] Z.-G. Wang, *Eur. Phys. J. C* **74**, 2963 (2014), arXiv:1403.0810 [hep-ph].
- [69] A. Esposito, D. Germani, A. Glioti, A. D. Polosa, R. Rattazzi, and M. Tarquini, *Phys. Lett. B* **847**, 138285 (2023), arXiv:2307.11400 [hep-ph].
- [70] S. Dubynskiy and M. B. Voloshin, *Phys. Lett. B* **666**, 344 (2008), arXiv:0803.2224 [hep-ph].
- [71] M. B. Voloshin, *Phys. Rev. D* **87**, 091501 (2013), arXiv:1304.0380 [hep-ph].
- [72] J. Ferretti, E. Santopinto, M. Naeem Anwar, and M. A. Bedolla, *Phys. Lett. B* **789**, 562 (2019), arXiv:1807.01207 [hep-ph].
- [73] J. Ferretti and E. Santopinto, *Phys. Lett. B* **789**, 550 (2019), arXiv:1806.02489 [hep-ph].
- [74] J. Ferretti and E. Santopinto, *JHEP* **04**, 119 (2020), arXiv:2001.01067 [hep-ph].
- [75] A. Esposito, E. G. Ferreira, A. Pilloni, A. D. Polosa, and C. A. Salgado, *Eur. Phys. J. C* **81**, 669 (2021), arXiv:2006.15044 [hep-ph].
- [76] N. Armesto, E. G. Ferreira, M. A. Escobedo, and V. López-Pardo, *Phys. Lett. B* **854**, 138760 (2024), arXiv:2401.10125 [hep-ph].
- [77] R. Aaij *et al.* (LHCb), *Nature Phys.* **18**, 751 (2022), arXiv:2109.01038 [hep-ex].
- [78] R. Aaij *et al.* (LHCb), *Nature Commun.* **13**, 3351 (2022), arXiv:2109.01056 [hep-ex].
- [79] S. Fleming, R. Hodges, and T. Mehen, *Phys. Rev. D* **104**, 116010 (2021), arXiv:2109.02188 [hep-ph].
- [80] L. Dai, S. Fleming, R. Hodges, and T. Mehen, *Phys. Rev. D* **107**, 076001 (2023), arXiv:2301.11950 [hep-ph].
- [81] R. Hodges, *Studies of  $T_{cc}^+$  Decays and Transverse-Momentum-Dependent  $J/\psi$  Production Using Effective Field Theory*, Phd thesis (2024), arXiv:2404.18907 [hep-ph].
- [82] S. Fleming, M. Kusunoki, T. Mehen, and U. van Kolck, *Phys. Rev. D* **76**, 034006 (2007), arXiv:hep-ph/0703168.
- [83] S. Fleming and T. Mehen, *Phys. Rev. D* **78**, 094019 (2008), arXiv:0807.2674 [hep-ph].
- [84] E. Braaten, H.-W. Hammer, and T. Mehen, *Phys. Rev. D* **82**, 034018 (2010), arXiv:1005.1688 [hep-ph].
- [85] S. Fleming and T. Mehen, *Phys. Rev. D* **85**, 014016 (2012), arXiv:1110.0265 [hep-ph].
- [86] T. Mehen, *Phys. Rev. D* **92**, 034019 (2015),

- arXiv:1503.02719 [hep-ph].
- [87] E. Braaten, L.-P. He, K. Ingles, and J. Jiang, *Phys. Rev. D* **101**, 096020 (2020), arXiv:2004.12841 [hep-ph].
  - [88] R. Aaij *et al.* (LHCb), *Sci. Bull.* **65**, 1983 (2020), arXiv:2006.16957 [hep-ex].
  - [89] H.-X. Chen, W. Chen, X. Liu, Y.-R. Liu, and S.-L. Zhu, *Rept. Prog. Phys.* **86**, 026201 (2023), arXiv:2204.02649 [hep-ph].
  - [90] A. Hayrapetyan *et al.* (CMS), *Phys. Rev. Lett.* **132**, 111901 (2024), arXiv:2306.07164 [hep-ex].
  - [91] F. Zhu, G. Bauer, and K. Yi, *Chin. Phys. Lett.* **41**, 111201 (2024), arXiv:2410.11210 [hep-ph].
  - [92] A. Hayrapetyan *et al.* (CMS), (2025), arXiv:2506.07944 [hep-ex].
  - [93] G.-J. Ding and M.-L. Yan, *Phys. Lett. B* **650**, 390 (2007), arXiv:hep-ph/0611319.
  - [94] J. Ho, R. Berg, T. G. Steele, W. Chen, and D. Harnett, *Phys. Rev. D* **100**, 034012 (2019), arXiv:1905.12779 [hep-ph].
  - [95] N. Su and H.-X. Chen, *Phys. Rev. D* **106**, 014023 (2022), arXiv:2204.13959 [hep-ph].
  - [96] F.-X. Liu, M.-S. Liu, X.-H. Zhong, and Q. Zhao, *Phys. Rev. D* **103**, 016016 (2021), arXiv:2008.01372 [hep-ph].
  - [97] R.-R. Dong, N. Su, and H.-X. Chen, *Eur. Phys. J. C* **82**, 983 (2022), arXiv:2206.09517 [hep-ph].
  - [98] H.-Z. Xi, Y.-W. Jiang, H.-X. Chen, A. Hosaka, and N. Su, *Phys. Rev. D* **108**, 094019 (2023), arXiv:2307.07819 [hep-ph].
  - [99] Y. Ma, W.-L. Wu, L. Meng, Y.-K. Chen, and S.-L. Zhu, *Phys. Rev. D* **110**, 074026 (2024), arXiv:2408.00503 [hep-ph].
  - [100] A. Pineda, *Prog. Part. Nucl. Phys.* **67**, 735 (2012), arXiv:1111.0165 [hep-ph].
  - [101] L. Maiani, A. D. Polosa, and V. Riquer, *Phys. Rev. D* **100**, 014002 (2019), arXiv:1903.10253 [hep-ph].
  - [102] R. Maciula, W. Schäfer, and A. Szczurek, *Phys. Lett. B* **812**, 136010 (2021), arXiv:2009.02100 [hep-ph].
  - [103] A. V. Berezhnoy, A. K. Likhoded, A. V. Luchinsky, and A. A. Novoselov, *Phys. Rev. D* **84**, 094023 (2011), arXiv:1101.5881 [hep-ph].
  - [104] M. Karliner, S. Nussinov, and J. L. Rosner, *Phys. Rev. D* **95**, 034011 (2017), arXiv:1611.00348 [hep-ph].
  - [105] C. Becchi, A. Giachino, L. Maiani, and E. Santopinto, *Phys. Lett. B* **806**, 135495 (2020), arXiv:2002.11077 [hep-ph].
  - [106] F. Carvalho, E. R. Cazaroto, V. P. Gonçalves, and F. S. Navarra, *Phys. Rev. D* **93**, 034004 (2016), arXiv:1511.05209 [hep-ph].
  - [107] L. M. Abreu, F. Carvalho, J. V. C. Oliveira, and V. P. Gonçalves, *Eur. Phys. J. C* **84**, 470 (2024), arXiv:2306.12731 [hep-ph].
  - [108] A. Cisek, W. Schäfer, and A. Szczurek, *Eur. Phys. J. C* **82**, 1062 (2022), arXiv:2203.07827 [hep-ph].
  - [109] W.-L. Wu, L. Meng, and S.-L. Zhu, (2025), arXiv:2506.20555 [hep-ph].
  - [110] A. Bondar *et al.* (Belle), *Phys. Rev. Lett.* **108**, 122001 (2012), arXiv:1110.2251 [hep-ex].
  - [111] L. C. Bland *et al.* (ANDY), (2019), arXiv:1909.03124 [nucl-ex].
  - [112] R. Vogt and A. Angerami, *Phys. Rev. D* **104**, 094025 (2021), arXiv:2109.00706 [hep-ph].
  - [113] A. Francis, R. J. Hudspith, R. Lewis, and K. Maltman, “Evidence for charm-bottom tetraquarks and the mass dependence of heavy-light tetraquark states from lattice QCD,” (2019), arXiv:1810.10550 [hep-lat].
  - [114] M. Padmanath, A. Radhakrishnan, and N. Mathur, *Phys. Rev. Lett.* **132**, 201902 (2024), arXiv:2307.14128 [hep-lat].
  - [115] P. Bicudo, K. Cichy, A. Peters, B. Wagenbach, and M. Wagner, *Phys. Rev. D* **92**, 014507 (2015), arXiv:1505.00613 [hep-lat].
  - [116] L. Leskovec, S. Meinel, M. Pflaumer, and M. Wagner, *Phys. Rev. D* **100**, 014503 (2019), arXiv:1904.04197 [hep-lat].
  - [117] C. Alexandrou, J. Finkenrath, T. Leontiou, S. Meinel, M. Pflaumer, and M. Wagner, *Phys. Rev. D* **110**, 054510 (2024), arXiv:2404.03588 [hep-lat].
  - [118] S. Chatrchyan *et al.* (CMS), *JHEP* **04**, 154 (2013), arXiv:1302.3968 [hep-ex].
  - [119] M. Aaboud *et al.* (ATLAS), *JHEP* **01**, 117 (2017), arXiv:1610.09303 [hep-ex].
  - [120] R. Aaij *et al.* (LHCb), *JHEP* **01**, 131 (2022), arXiv:2109.07360 [hep-ex].
  - [121] W. E. Caswell and G. P. Lepage, *Phys. Lett. B* **167**, 437 (1986).
  - [122] B. A. Thacker and G. P. Lepage, *Phys. Rev. D* **43**, 196 (1991).
  - [123] G. T. Bodwin, E. Braaten, and G. P. Lepage, *Phys. Rev. D* **51**, 1125 (1995), [Erratum: *Phys. Rev. D* **55**, 5853 (1997)], arXiv:hep-ph/9407339.

- 
- [124] P. L. Cho and A. K. Leibovich, *Phys. Rev. D* **53**, 150 (1996), [arXiv:hep-ph/9505329](#).
- [125] P. L. Cho and A. K. Leibovich, *Phys. Rev. D* **53**, 6203 (1996), [arXiv:hep-ph/9511315](#).
- [126] A. K. Leibovich, *Phys. Rev. D* **56**, 4412 (1997), [arXiv:hep-ph/9610381](#).
- [127] G. T. Bodwin, E. Braaten, and J. Lee, *Phys. Rev. D* **72**, 014004 (2005), [arXiv:hep-ph/0504014](#).
- [128] M. Suzuki, *Phys. Lett. B* **71**, 139 (1977).
- [129] M. Suzuki, *Phys. Rev. D* **33**, 676 (1986).
- [130] F. Amiri and C.-R. Ji, *Phys. Lett. B* **195**, 593 (1987).
- [131] F. G. Celiberto, in *58th Rencontres de Moriond on QCD and High Energy Interactions* (2024) [arXiv:2405.08221 \[hep-ph\]](#).
- [132] F. G. Celiberto, *PoS DIS2024*, 168 (2025), [arXiv:2406.10779 \[hep-ph\]](#).
- [133] F. G. Celiberto, *Acta Phys. Polon. Supp.* **18**, 1 (2025), [arXiv:2412.05661 \[hep-ph\]](#).
- [134] H. Kim, K. S. Kim, M.-K. Cheoun, and M. Oka, *Phys. Rev. D* **97**, 094005 (2018), [arXiv:1711.08213 \[hep-ph\]](#).
- [135] H. Kim, K. S. Kim, M.-K. Cheoun, D. Jido, and M. Oka, *Phys. Rev. D* **99**, 014005 (2019), [arXiv:1811.00187 \[hep-ph\]](#).
- [136] N. Isgur and M. B. Wise, *Phys. Rev. Lett.* **66**, 1130 (1991).
- [137] M. Neubert, *Phys. Rept.* **245**, 259 (1994), [arXiv:hep-ph/9306320](#).
- [138] X.-Z. Weng, X.-L. Chen, W.-Z. Deng, and S.-L. Zhu, *Phys. Rev. D* **103**, 034001 (2021), [arXiv:2010.05163 \[hep-ph\]](#).
- [139] H.-T. An, S.-Q. Luo, Z.-W. Liu, and X. Liu, *Eur. Phys. J. C* **83**, 740 (2023), [arXiv:2208.03899 \[hep-ph\]](#).
- [140] L. D. Landau, *Dokl. Akad. Nauk SSSR* **60**, 207 (1948).
- [141] C.-N. Yang, *Phys. Rev.* **77**, 242 (1950).
- [142] M. Karliner and J. L. Rosner, *Phys. Rev. D* **102**, 114039 (2020), [arXiv:2009.04429 \[hep-ph\]](#).
- [143] B. Mele and P. Nason, *Nucl. Phys. B* **361**, 626 (1991), [Erratum: *Nucl. Phys. B* 921, 841–842 (2017)].
- [144] M. Cacciari and M. Greco, *Nucl. Phys. B* **421**, 530 (1994), [arXiv:hep-ph/9311260](#).
- [145] M. Buza, Y. Matiounine, J. Smith, and W. L. van Neerven, *Eur. Phys. J. C* **1**, 301 (1998), [arXiv:hep-ph/9612398](#).
- [146] F. G. Celiberto, *Eur. Phys. J. C* **81**, 691 (2021), [arXiv:2008.07378 \[hep-ph\]](#).
- [147] F. G. Celiberto, *Phys. Rev. D* **105**, 114008 (2022), [arXiv:2204.06497 \[hep-ph\]](#).
- [148] F. G. Celiberto, *Universe* **9**, 324 (2023), [arXiv:2305.14295 \[hep-ph\]](#).
- [149] F. G. Celiberto, *Symmetry* **16**, 550 (2024), [arXiv:2403.15639 \[hep-ph\]](#).
- [150] F. G. Celiberto, *Particles* **7**, 502 (2024), [arXiv:2405.09526 \[hep-ph\]](#).
- [151] M. Cacciari, M. Greco, S. Rolli, and A. Tanzini, *Phys. Rev. D* **55**, 2736 (1997), [arXiv:hep-ph/9608213](#).
- [152] R. L. Jaffe and L. Randall, *Nucl. Phys. B* **412**, 79 (1994), [arXiv:hep-ph/9306201](#).
- [153] B. A. Kniehl, G. Kramer, I. Schienbein, and H. Spiesberger, *Eur. Phys. J. C* **41**, 199 (2005), [arXiv:hep-ph/0502194](#).
- [154] I. Helenius and H. Paukkunen, *JHEP* **05**, 196 (2018), [arXiv:1804.03557 \[hep-ph\]](#).
- [155] I. Helenius and H. Paukkunen, *JHEP* **07**, 054 (2023), [arXiv:2303.17864 \[hep-ph\]](#).
- [156] B. Mele and P. Nason, *Phys. Lett. B* **245**, 635 (1990).
- [157] P. J. Rijken and W. L. van Neerven, *Phys. Lett. B* **386**, 422 (1996), [arXiv:hep-ph/9604436](#).
- [158] A. Mitov and S.-O. Moch, *Nucl. Phys. B* **751**, 18 (2006), [arXiv:hep-ph/0604160](#).
- [159] J. Blumlein and V. Ravindran, *Nucl. Phys. B* **749**, 1 (2006), [arXiv:hep-ph/0604019](#).
- [160] K. Melnikov and A. Mitov, *Phys. Rev. D* **70**, 034027 (2004), [arXiv:hep-ph/0404143](#).
- [161] A. Mitov, *Phys. Rev. D* **71**, 054021 (2005), [arXiv:hep-ph/0410205](#).
- [162] C. Biello and L. Bonino, *Eur. Phys. J. C* **84**, 1192 (2024), [arXiv:2407.07623 \[hep-ph\]](#).
- [163] V. Kartvelishvili, A. Likhoded, and V. Petrov, *Phys. Lett. B* **78**, 615 (1978).
- [164] M. G. Bowler, *Z. Phys. C* **11**, 169 (1981).
- [165] C. Peterson, D. Schlatter, I. Schmitt, and P. M. Zerwas, *Phys. Rev. D* **27**, 105 (1983).
- [166] B. Andersson, G. Gustafson, and B. Soderberg, *Z. Phys. C* **20**, 317 (1983).
- [167] P. D. B. Collins and T. P. Spiller, *J. Phys. G* **11**, 1289 (1985).
- [168] G. Colangelo and P. Nason, *Phys. Lett. B* **285**, 167 (1992).

- 
- [169] H. Georgi, *Phys. Lett. B* **240**, 447 (1990).
- [170] E. Eichten and B. R. Hill, *Phys. Lett. B* **234**, 511 (1990).
- [171] B. Grinstein, *Ann. Rev. Nucl. Part. Sci.* **42**, 101 (1992).
- [172] B. Grinstein, *Int. J. Mod. Phys. A* **15**, 461 (2000), [arXiv:hep-ph/9811264](#).
- [173] M. Krämer, *Prog. Part. Nucl. Phys.* **47**, 141 (2001), [arXiv:hep-ph/0106120](#).
- [174] N. Brambilla *et al.* (Quarkonium Working Group), (2004), 10.5170/CERN-2005-005, [arXiv:hep-ph/0412158](#).
- [175] J.-P. Lansberg, *Quarkonium production at high-energy hadron colliders: A Systematic gauge-invariant approach to relativistic effects of  $J/\psi$ ,  $\psi'$  and  $\nu$  production*, Phd thesis (2005), [arXiv:hep-ph/0507175](#).
- [176] J.-P. Lansberg, *Phys. Rept.* **889**, 1 (2020), [arXiv:1903.09185 \[hep-ph\]](#).
- [177] S. Alekhin, J. Blumlein, S. Klein, and S. Moch, *Phys. Rev. D* **81**, 014032 (2010), [arXiv:0908.2766 \[hep-ph\]](#).
- [178] S. Fleming, A. K. Leibovich, T. Mehen, and I. Z. Rothstein, *Phys. Rev. D* **86**, 094012 (2012), [arXiv:1207.2578 \[hep-ph\]](#).
- [179] Z.-B. Kang, Y.-Q. Ma, J.-W. Qiu, and G. Sterman, *Phys. Rev. D* **90**, 034006 (2014), [arXiv:1401.0923 \[hep-ph\]](#).
- [180] M. G. Echevarria, *JHEP* **10**, 144 (2019), [arXiv:1907.06494 \[hep-ph\]](#).
- [181] D. Boer, J. Bor, L. Maxia, C. Pisano, and F. Yuan, *JHEP* **08**, 105 (2023), [arXiv:2304.09473 \[hep-ph\]](#).
- [182] E. Braaten and T. C. Yuan, *Phys. Rev. Lett.* **71**, 1673 (1993), [arXiv:hep-ph/9303205](#).
- [183] E. Braaten, K.-m. Cheung, and T. C. Yuan, *Phys. Rev. D* **48**, 4230 (1993), [arXiv:hep-ph/9302307](#).
- [184] X.-C. Zheng, C.-H. Chang, T.-F. Feng, and X.-G. Wu, *Phys. Rev. D* **100**, 034004 (2019), [arXiv:1901.03477 \[hep-ph\]](#).
- [185] X.-C. Zheng, C.-H. Chang, and X.-G. Wu, *JHEP* **05**, 036 (2022), [arXiv:2112.10520 \[hep-ph\]](#).
- [186] F. G. Celiberto and M. Fucilla, *Eur. Phys. J. C* **82**, 929 (2022), [arXiv:2202.12227 \[hep-ph\]](#).
- [187] F. G. Celiberto, *Phys. Lett. B* **835**, 137554 (2022), [arXiv:2206.09413 \[hep-ph\]](#).
- [188] F. G. Celiberto, *Eur. Phys. J. C* **84**, 384 (2024), [arXiv:2401.01410 \[hep-ph\]](#).
- [189] R. Aaij *et al.* (LHCb), *Phys. Rev. Lett.* **114**, 041801 (2015), [arXiv:1411.3104 \[hep-ex\]](#).
- [190] R. Aaij *et al.* (LHCb), *Phys. Rev. Lett.* **118**, 052002 (2017), [Erratum: *Phys. Rev. Lett.* **119**, 169901 (2017)], [arXiv:1612.05140 \[hep-ex\]](#).
- [191] G. Aad *et al.* (ATLAS), *Phys. Rev. Lett.* **131**, 151902 (2023), [arXiv:2304.08962 \[hep-ex\]](#).
- [192] H.-F. Zhang and Y.-Q. Ma, (2020), [arXiv:2009.08376 \[hep-ph\]](#).
- [193] R. Zhu, *Nucl. Phys. B* **966**, 115393 (2021), [arXiv:2010.09082 \[hep-ph\]](#).
- [194] F. G. Celiberto, (2025), [arXiv:2506.00776 \[hep-ph\]](#).
- [195] M. A. Shifman, A. I. Vainshtein, and V. I. Zakharov, *Nucl. Phys. B* **147**, 385 (1979).
- [196] F. J. Gilman and M. B. Wise, *Phys. Rev. D* **20**, 2392 (1979).
- [197] A. Petrelli, M. Cacciari, M. Greco, F. Maltoni, and M. L. Mangano, *Nucl. Phys. B* **514**, 245 (1998), [arXiv:hep-ph/9707223](#).
- [198] N. Brambilla *et al.*, *Eur. Phys. J. C* **71**, 1534 (2011), [arXiv:1010.5827 \[hep-ph\]](#).
- [199] A. Andronic *et al.*, *Eur. Phys. J. C* **76**, 107 (2016), [arXiv:1506.03981 \[nucl-ex\]](#).
- [200] M. Beneke and I. Z. Rothstein, *Phys. Rev. D* **54**, 2005 (1996).
- [201] M. Butenschoen and B. A. Kniehl, *Phys. Rev. Lett.* **106**, 022003 (2011).
- [202] K.-T. Chao, Y.-Q. Ma, H.-S. Shao, K. Wang, and Y.-J. Zhang, *Phys. Rev. Lett.* **108**, 242004 (2012), [arXiv:1201.2675 \[hep-ph\]](#).
- [203] B. Gong, L.-P. Wan, J.-X. Wang, and H.-F. Zhang, *Phys. Rev. Lett.* **110**, 042002 (2013).
- [204] H. Han, Y.-Q. Ma, C. Meng, H.-S. Shao, and K.-T. Chao, *Phys. Rev. Lett.* **114**, 092005 (2015), [arXiv:1411.7350 \[hep-ph\]](#).
- [205] R. Aaij *et al.* (LHCb), *Eur. Phys. J. C* **75**, 311 (2015), [arXiv:1409.3612 \[hep-ex\]](#).
- [206] R. Aaij *et al.* (LHCb), *Eur. Phys. J. C* **80**, 191 (2020), [arXiv:1911.03326 \[hep-ex\]](#).
- [207] R. Aaij *et al.* (LHCb), *JHEP* **07**, 069 (2023), [arXiv:2212.12664 \[hep-ex\]](#).
- [208] P. Artoisenet, J. M. Campbell, J. P. Lansberg, F. Maltoni, and F. Tramontano, *Phys. Rev. Lett.* **101**, 152001 (2008), [arXiv:0806.3282 \[hep-ph\]](#).

- 
- [209] B. Gong, J.-X. Wang, and H.-F. Zhang, *Phys. Rev. D* **83**, 114021 (2011), [arXiv:1009.3839 \[hep-ph\]](#).
- [210] E. Eichten, K. Gottfried, T. Kinoshita, J. B. Kogut, K. D. Lane, and T.-M. Yan, *Phys. Rev. Lett.* **34**, 369 (1975), [Erratum: *Phys.Rev.Lett.* 36, 1276 (1976)].
- [211] E. Eichten, K. Gottfried, T. Kinoshita, K. D. Lane, and T.-M. Yan, *Phys. Rev. D* **17**, 3090 (1978), [Erratum: *Phys.Rev.D* 21, 313 (1980)].
- [212] J. Zhao, S. Shi, and P. Zhuang, *Phys. Rev. D* **102**, 114001 (2020), [arXiv:2009.10319 \[hep-ph\]](#).
- [213] Q.-F. Lü, D.-Y. Chen, and Y.-B. Dong, *Eur. Phys. J. C* **80**, 871 (2020), [arXiv:2006.14445 \[hep-ph\]](#).
- [214] M.-S. Liu, F.-X. Liu, X.-H. Zhong, and Q. Zhao, *Phys. Rev. D* **109**, 076017 (2024), [arXiv:2006.11952 \[hep-ph\]](#).
- [215] A. M. Sirunyan *et al.* (CMS), *Phys. Lett. B* **780**, 251 (2018), [arXiv:1710.11002 \[hep-ex\]](#).
- [216] G.-L. Yu, Z.-Y. Li, Z.-G. Wang, J. Lu, and M. Yan, *Eur. Phys. J. C* **83**, 416 (2023), [arXiv:2212.14339 \[hep-ph\]](#).
- [217] G.-J. Wang, L. Meng, and S.-L. Zhu, *Phys. Rev. D* **100**, 096013 (2019), [arXiv:1907.05177 \[hep-ph\]](#).
- [218] V. Bertone, S. Carrazza, and J. Rojo, *Comput. Phys. Commun.* **185**, 1647 (2014), [arXiv:1310.1394 \[hep-ph\]](#).
- [219] S. Carrazza, A. Ferrara, D. Palazzo, and J. Rojo, *J. Phys. G* **42**, 057001 (2015), [arXiv:1410.5456 \[hep-ph\]](#).
- [220] V. Bertone, *PoS DIS2017*, 201 (2018), [arXiv:1708.00911 \[hep-ph\]](#).
- [221] A. Candido, F. Hekhorn, and G. Magni, *Eur. Phys. J. C* **82**, 976 (2022), [arXiv:2202.02338 \[hep-ph\]](#).
- [222] F. Hekhorn and G. Magni, (2023), [arXiv:2306.15294 \[hep-ph\]](#).
- [223] P. Artoisenet and E. Braaten, *JHEP* **04**, 121 (2015), [arXiv:1412.3834 \[hep-ph\]](#).
- [224] P. Zhang, C.-Y. Wang, X. Liu, Y.-Q. Ma, C. Meng, and K.-T. Chao, *JHEP* **04**, 116 (2019), [arXiv:1810.07656 \[hep-ph\]](#).
- [225] X.-C. Zheng, Z.-Y. Zhang, and X.-G. Wu, *Phys. Rev. D* **103**, 074004 (2021), [arXiv:2101.01527 \[hep-ph\]](#).
- [226] X.-C. Zheng, X.-G. Wu, and X.-D. Huang, *JHEP* **07**, 014 (2021), [arXiv:2105.14580 \[hep-ph\]](#).
- [227] X.-C. Zheng, C.-H. Chang, and X.-G. Wu, *Phys. Rev. D* **100**, 014005 (2019), [arXiv:1905.09171 \[hep-ph\]](#).
- [228] J. D. Bjorken, *Phys. Rev. D* **17**, 171 (1978).
- [229] G. T. Bodwin and A. Petrelli, *Phys. Rev. D* **66**, 094011 (2002), [Erratum: *Phys.Rev.D* 87, 039902 (2013)], [arXiv:hep-ph/0205210](#).
- [230] Y.-Q. Ma, J.-W. Qiu, and H. Zhang, *JHEP* **06**, 021 (2015), [arXiv:1501.04556 \[hep-ph\]](#).
- [231] Y.-Z. Xu, S. Chen, Z.-Q. Yao, D. Binosi, Z.-F. Cui, and C. D. Roberts, *Eur. Phys. J. C* **81**, 895 (2021), [arXiv:2107.03488 \[hep-ph\]](#).
- [232] F. G. Celiberto, M. Fucilla, D. Yu. Ivanov, and A. Papa, *Eur. Phys. J. C* **81**, 780 (2021), [arXiv:2105.06432 \[hep-ph\]](#).
- [233] F. G. Celiberto, M. Fucilla, D. Yu. Ivanov, M. M. A. Mohammed, and A. Papa, *Phys. Rev. D* **104**, 114007 (2021), [arXiv:2109.11875 \[hep-ph\]](#).
- [234] J. L. Feng *et al.*, *J. Phys. G* **50**, 030501 (2023), [arXiv:2203.05090 \[hep-ex\]](#).
- [235] F. G. Celiberto, *Acta Phys. Polon. Supp.* **16**, 41 (2023), [arXiv:2211.11780 \[hep-ph\]](#).
- [236] V. S. Fadin, E. Kuraev, and L. Lipatov, *Phys. Lett. B* **60**, 50 (1975).
- [237] E. Kuraev, L. Lipatov, and V. S. Fadin, *Sov. Phys. JETP* **45**, 199 (1977).
- [238] I. Balitsky and L. Lipatov, *Sov. J. Nucl. Phys.* **28**, 822 (1978).
- [239] V. S. Fadin and L. N. Lipatov, *Phys. Lett. B* **429**, 127 (1998), [arXiv:hep-ph/9802290](#).
- [240] M. Ciafaloni and G. Camici, *Phys. Lett. B* **430**, 349 (1998), [arXiv:hep-ph/9803389](#).
- [241] D. Colferai, F. Schwennsen, L. Szymanowski, and S. Wallon, *JHEP* **12**, 026 (2010), [arXiv:1002.1365 \[hep-ph\]](#).
- [242] F. G. Celiberto, D. Yu. Ivanov, B. Murdaca, and A. Papa, *Eur. Phys. J. C* **75**, 292 (2015), [arXiv:1504.08233 \[hep-ph\]](#).
- [243] F. G. Celiberto, D. Yu. Ivanov, B. Murdaca, and A. Papa, *Eur. Phys. J. C* **77**, 382 (2017), [arXiv:1701.05077 \[hep-ph\]](#).
- [244] A. H. Mueller and H. Navelet, *Nucl. Phys. B* **282**, 727 (1987).
- [245] B. Ducloué, L. Szymanowski, and S. Wallon, *JHEP* **05**, 096 (2013), [arXiv:1302.7012 \[hep-ph\]](#).
- [246] D. Colferai and A. Niccoli, *JHEP* **04**, 071 (2015), [arXiv:1501.07442 \[hep-ph\]](#).
- [247] F. G. Celiberto, D. Yu. Ivanov, B. Murdaca, and A. Papa, *Acta Phys. Polon. Supp.* **8**, 935 (2015), [arXiv:1510.01626 \[hep-ph\]](#).



- 
- [248] F. G. Celiberto, D. Yu. Ivanov, B. Murdaca, and A. Papa, *Eur. Phys. J. C* **76**, 224 (2016), [arXiv:1601.07847 \[hep-ph\]](#).
- [249] F. G. Celiberto, *High-energy resummation in semi-hard processes at the LHC*, Phd thesis, Università della Calabria and INFN-Cosenza (2017), [arXiv:1707.04315 \[hep-ph\]](#).
- [250] F. Caporale, F. G. Celiberto, G. Chachamis, D. Gordo Gómez, and A. Sabio Vera, *Nucl. Phys. B* **935**, 412 (2018), [arXiv:1806.06309 \[hep-ph\]](#).
- [251] N. B. de León, G. Chachamis, and A. Sabio Vera, *Eur. Phys. J. C* **81**, 1019 (2021), [arXiv:2106.11255 \[hep-ph\]](#).
- [252] F. G. Celiberto and A. Papa, *Phys. Rev. D* **106**, 114004 (2022), [arXiv:2207.05015 \[hep-ph\]](#).
- [253] C. Baldenegro, G. Chachamis, M. Kampshoff, M. Klasen, G. J. Milhano, C. Royon, and A. Sabio Vera, *Phys. Rev. D* **110**, 114027 (2024), [arXiv:2406.10681 \[hep-ph\]](#).
- [254] F. G. Celiberto, D. Yu. Ivanov, B. Murdaca, and A. Papa, *Phys. Rev. D* **94**, 034013 (2016), [arXiv:1604.08013 \[hep-ph\]](#).
- [255] F. G. Celiberto, D. Yu. Ivanov, and A. Papa, *Phys. Rev. D* **102**, 094019 (2020), [arXiv:2008.10513 \[hep-ph\]](#).
- [256] A. D. Bolognino, F. G. Celiberto, D. Yu. Ivanov, M. M. A. Mohammed, and A. Papa, *Eur. Phys. J. C* **78**, 772 (2018), [arXiv:1808.05483 \[hep-ph\]](#).
- [257] A. D. Bolognino, F. G. Celiberto, D. Yu. Ivanov, M. M. A. Mohammed, and A. Papa, *PoS DIS2019*, 049 (2019), [arXiv:1906.11800 \[hep-ph\]](#).
- [258] A. D. Bolognino, F. G. Celiberto, D. Yu. Ivanov, M. M. A. Mohammed, and A. Papa, *Acta Phys. Polon. Supp.* **12**, 773 (2019), [arXiv:1902.04511 \[hep-ph\]](#).
- [259] F. G. Celiberto, *Eur. Phys. J. C* **83**, 332 (2023), [arXiv:2208.14577 \[hep-ph\]](#).
- [260] F. Caporale, F. G. Celiberto, G. Chachamis, D. Gordo Gómez, and A. Sabio Vera, *Nucl. Phys. B* **910**, 374 (2016), [arXiv:1603.07785 \[hep-ph\]](#).
- [261] F. Caporale, F. G. Celiberto, G. Chachamis, D. Gordo Gómez, and A. Sabio Vera, *Eur. Phys. J. C* **77**, 5 (2017), [arXiv:1606.00574 \[hep-ph\]](#).
- [262] F. G. Celiberto, *Frascati Phys. Ser.* **63**, 43 (2016), [arXiv:1606.07327 \[hep-ph\]](#).
- [263] F. Caporale, F. G. Celiberto, G. Chachamis, D. Gordo Gómez, and A. Sabio Vera, *Phys. Rev. D* **95**, 074007 (2017), [arXiv:1612.05428 \[hep-ph\]](#).
- [264] M. Hentschinski, K. Kutak, and A. van Hameren, *Eur. Phys. J. C* **81**, 112 (2021), [Erratum: *Eur. Phys. J. C* **81**, 262 (2021)], [arXiv:2011.03193 \[hep-ph\]](#).
- [265] F. G. Celiberto, M. Fucilla, D. Yu. Ivanov, M. M. A. Mohammed, and A. Papa, *JHEP* **08**, 092 (2022), [arXiv:2205.02681 \[hep-ph\]](#).
- [266] F. G. Celiberto, D. Yu. Ivanov, M. M. A. Mohammed, and A. Papa, *Eur. Phys. J. C* **81**, 293 (2021), [arXiv:2008.00501 \[hep-ph\]](#).
- [267] M. M. A. Mohammed, *Hunting stabilization effects of the high-energy resummation at the LHC*, Phd thesis, Università della Calabria and INFN-Cosenza (2022), [arXiv:2204.11606 \[hep-ph\]](#).
- [268] F. G. Celiberto and A. Papa, (2023), [arXiv:2305.00962 \[hep-ph\]](#).
- [269] F. G. Celiberto, L. Delle Rose, M. Fucilla, G. Gatto, and A. Papa, in *57th Rencontres de Moriond on QCD and High Energy Interactions* (2023) [arXiv:2305.05052 \[hep-ph\]](#).
- [270] F. G. Celiberto, L. Delle Rose, M. Fucilla, G. Gatto, and A. Papa, *PoS RADCOR2023*, 069 (2024), [arXiv:2309.11573 \[hep-ph\]](#).
- [271] F. G. Celiberto, L. Delle Rose, M. Fucilla, G. Gatto, and A. Papa, *PoS EPS-HEP2023*, 390 (2024), [arXiv:2310.16967 \[hep-ph\]](#).
- [272] F. G. Celiberto, M. Fucilla, M. M. A. Mohammed, D. Yu. Ivanov, and A. Papa, *PoS RADCOR2023*, 091 (2024), [arXiv:2309.07570 \[hep-ph\]](#).
- [273] F. G. Celiberto, M. Fucilla, M. M. A. Mohammed, and A. Papa, *Phys. Rev. D* **105**, 114056 (2022), [arXiv:2205.13429 \[hep-ph\]](#).
- [274] F. G. Celiberto, L. Delle Rose, M. Fucilla, G. Gatto, and A. Papa, *JHEP* **12**, 061 (2024), [arXiv:2409.20354 \[hep-ph\]](#).
- [275] F. G. Celiberto, D. Gordo Gómez, and A. Sabio Vera, *Phys. Lett. B* **786**, 201 (2018), [arXiv:1808.09511 \[hep-ph\]](#).
- [276] K. Golec-Biernat, L. Motyka, and T. Stebel, *JHEP* **12**, 091 (2018), [arXiv:1811.04361 \[hep-ph\]](#).
- [277] F. G. Celiberto, D. Yu. Ivanov, B. Murdaca, and A. Papa, *Phys. Lett. B* **777**, 141 (2018), [arXiv:1709.10032 \[hep-ph\]](#).
- [278] R. Boussarie, B. Ducloué, L. Szymanowski, and S. Wallon, *Phys. Rev. D* **97**, 014008 (2018), [arXiv:1709.01380 \[hep-ph\]](#).
- [279] A. D. Bolognino, F. G. Celiberto, M. Fucilla, D. Yu. Ivanov, B. Murdaca, and A. Papa, *PoS DIS2019*, 067

- (2019), [arXiv:1906.05940 \[hep-ph\]](#).
- [280] A. D. Bolognino, F. G. Celiberto, M. Fucilla, D. Yu. Ivanov, and A. Papa, *Eur. Phys. J. C* **79**, 939 (2019), [arXiv:1909.03068 \[hep-ph\]](#).
  - [281] A. D. Bolognino, F. G. Celiberto, M. Fucilla, D. Yu. Ivanov, M. M. A. Mohammed, and A. Papa, *Acta Phys. Polon. Supp.* **16**, 17 (2023), [arXiv:2211.16818 \[hep-ph\]](#).
  - [282] F. G. Celiberto and M. Fucilla, in *29th International Workshop on Deep-Inelastic Scattering and Related Subjects* (2022) [arXiv:2208.07206 \[hep-ph\]](#).
  - [283] G. Gatto, *High-energy dynamics of QCD: Theoretical and phenomenological results*, Phd thesis, Università della Calabria and INFN-Cosenza (2025), [arXiv:2506.03222 \[hep-ph\]](#).
  - [284] I. Anikin, A. Besse, D. Yu. Ivanov, B. Pire, L. Szymanowski, and S. Wallon, *Phys. Rev. D* **84**, 054004 (2011), [arXiv:1105.1761 \[hep-ph\]](#).
  - [285] A. Besse, L. Szymanowski, and S. Wallon, *JHEP* **11**, 062 (2013), [arXiv:1302.1766 \[hep-ph\]](#).
  - [286] A. D. Bolognino, F. G. Celiberto, D. Yu. Ivanov, and A. Papa, *Eur. Phys. J.* **C78**, 1023 (2018), [arXiv:1808.02395 \[hep-ph\]](#).
  - [287] A. D. Bolognino, F. G. Celiberto, D. Yu. Ivanov, and A. Papa, *Frascati Phys. Ser.* **67**, 76 (2018), [arXiv:1808.02958 \[hep-ph\]](#).
  - [288] A. D. Bolognino, F. G. Celiberto, D. Yu. Ivanov, and A. Papa, *Acta Phys. Polon. Supp.* **12**, 891 (2019), [arXiv:1902.04520 \[hep-ph\]](#).
  - [289] A. D. Bolognino, A. Szczurek, and W. Schäfer, *Phys. Rev. D* **101**, 054041 (2020), [arXiv:1912.06507 \[hep-ph\]](#).
  - [290] F. G. Celiberto, *Nuovo Cim.* **C42**, 220 (2019), [arXiv:1912.11313 \[hep-ph\]](#).
  - [291] A. D. Bolognino, *From semi-hard processes to the un-integrated gluon distribution: a phenomenological path in the high-energy framework*, Phd thesis, Calabria U. (2021), [arXiv:2109.03033 \[hep-ph\]](#).
  - [292] A. Łuszczak, M. Łuszczak, and W. Schäfer, *Phys. Lett. B* **835**, 137582 (2022), [arXiv:2210.02877 \[hep-ph\]](#).
  - [293] A. D. Bolognino, F. G. Celiberto, D. Yu. Ivanov, A. Papa, W. Schäfer, and A. Szczurek, *Eur. Phys. J. C* **81**, 846 (2021), [arXiv:2107.13415 \[hep-ph\]](#).
  - [294] A. D. Bolognino, F. G. Celiberto, D. Yu. Ivanov, and A. Papa, *SciPost Phys. Proc.* **8**, 089 (2022), [arXiv:2107.12725 \[hep-ph\]](#).
  - [295] A. D. Bolognino, F. G. Celiberto, M. Fucilla, D. Yu. Ivanov, A. Papa, W. Schäfer, and A. Szczurek, *Rev. Mex. Fis. Suppl.* **3**, 0308109 (2022), [arXiv:2202.02513 \[hep-ph\]](#).
  - [296] A. D. Bolognino, F. G. Celiberto, D. Yu. Ivanov, A. Papa, W. Schäfer, and A. Szczurek, in *29th International Workshop on Deep-Inelastic Scattering and Related Subjects* (2022) [arXiv:2207.05726 \[hep-ph\]](#).
  - [297] R. D. Ball, V. Bertone, M. Bonvini, S. Marzani, J. Rojo, and L. Rottoli, *Eur. Phys. J.* **C78**, 321 (2018), [arXiv:1710.05935 \[hep-ph\]](#).
  - [298] H. Abdolmaleki *et al.* (xFitter Developers' Team), *Eur. Phys. J. C* **78**, 621 (2018), [arXiv:1802.00064 \[hep-ph\]](#).
  - [299] M. Bonvini and F. Giuli, *Eur. Phys. J. Plus* **134**, 531 (2019), [arXiv:1902.11125 \[hep-ph\]](#).
  - [300] F. Silveti and M. Bonvini, *Eur. Phys. J. C* **83**, 267 (2023), [arXiv:2211.10142 \[hep-ph\]](#).
  - [301] F. Silveti, *Resummation phenomenology and PDF determination for precision QCD at the LHC*, Phd thesis, Rome U. (2023), [arXiv:2403.20315 \[hep-ph\]](#).
  - [302] A. Rinaudo, *Towards the resummation of high-energy next-to-leading logarithms in QCD*, Phd thesis, Genoa U. (2024).
  - [303] A. Bacchetta, F. G. Celiberto, M. Radici, and P. Tael, *Eur. Phys. J. C* **80**, 733 (2020), [arXiv:2005.02288 \[hep-ph\]](#).
  - [304] A. Bacchetta, F. G. Celiberto, and M. Radici, *Eur. Phys. J. C* **84**, 576 (2024), [arXiv:2402.17556 \[hep-ph\]](#).
  - [305] F. G. Celiberto, *Nuovo Cim.* **C44**, 36 (2021), [arXiv:2101.04630 \[hep-ph\]](#).
  - [306] A. Bacchetta, F. G. Celiberto, M. Radici, and P. Tael, *SciPost Phys. Proc.* **8**, 040 (2022), [arXiv:2107.13446 \[hep-ph\]](#).
  - [307] A. Bacchetta, F. G. Celiberto, and M. Radici, *PoS EPS-HEP2021*, 376 (2022), [arXiv:2111.01686 \[hep-ph\]](#).
  - [308] A. Bacchetta, F. G. Celiberto, and M. Radici, *PoS PANIC2021*, 378 (2022), [arXiv:2111.03567 \[hep-ph\]](#).
  - [309] A. Bacchetta, F. G. Celiberto, and M. Radici, *JPS Conf. Proc.* **37**, 020124 (2022), [arXiv:2201.10508 \[hep-ph\]](#).
  - [310] A. Bacchetta, F. G. Celiberto, and M. Radici, *Rev. Mex. Fis. Suppl.* **3**, 0308108 (2022), [arXiv:2206.07815 \[hep-ph\]](#).
  - [311] A. Bacchetta, F. G. Celiberto, M. Radici, and A. Signori, in *29th International Workshop on Deep-Inelastic Scattering and Related Subjects* (2022)

- arXiv:2208.06252 [hep-ph].
- [312] F. G. Celiberto, *Universe* **8**, 661 (2022), arXiv:2210.08322 [hep-ph].
  - [313] A. Bacchetta, F. G. Celiberto, and M. Radici, *PoS EPS-HEP2023*, 247 (2024), arXiv:2310.19916 [hep-ph].
  - [314] C.-H. Chang and Y.-Q. Chen, *Phys. Rev. D* **46**, 3845 (1992), [Erratum: *Phys.Rev.D* 50, 6013 (1994)].
  - [315] E. Braaten, K.-m. Cheung, and T. C. Yuan, *Phys. Rev. D* **48**, R5049 (1993), arXiv:hep-ph/9305206.
  - [316] J. P. Ma, *Phys. Lett. B* **332**, 398 (1994), arXiv:hep-ph/9401249.
  - [317] F. Feng, Y. Jia, and D. Yang, *Phys. Rev. D* **106**, 054030 (2022), arXiv:2112.15569 [hep-ph].
  - [318] F. Feng and Y. Jia, *Chin. Phys. C* **47**, 033103 (2023), arXiv:1810.04138 [hep-ph].
  - [319] V. Khachatryan *et al.* (CMS), *JHEP* **08**, 139 (2016), arXiv:1601.06713 [hep-ex].
  - [320] V. Khachatryan *et al.* (CMS), *JINST* **16**, P02010 (2021), arXiv:2011.01185 [physics.ins-det].
  - [321] S. Chatrchyan *et al.* (CMS), *Phys. Lett. B* **714**, 136 (2012), arXiv:1205.0594 [hep-ex].
  - [322] M. Bonvini and S. Marzani, *Phys. Rev. Lett.* **120**, 202003 (2018), arXiv:1802.07758 [hep-ph].
  - [323] M. Bonvini, *Eur. Phys. J. C* **78**, 834 (2018), arXiv:1805.08785 [hep-ph].
  - [324] C. Marquet and C. Royon, *Phys. Rev. D* **79**, 034028 (2009), arXiv:0704.3409 [hep-ph].
  - [325] F. G. Celiberto and G. Gatto, *TQ4Q1.1: HF-NRevo FFs for scalar, axial-vector, and tensor fully heavy  $T_{4Q}(J^{PC})$  tetraquarks* (2025).
  - [326] Z. Kassabov, M. Ubiali, and C. Voisey, *JHEP* **03**, 148 (2023), arXiv:2207.07616 [hep-ph].
  - [327] L. A. Harland-Lang and R. S. Thorne, *Eur. Phys. J. C* **79**, 225 (2019), arXiv:1811.08434 [hep-ph].
  - [328] R. D. Ball and R. L. Pearson, *Eur. Phys. J. C* **81**, 830 (2021), arXiv:2105.05114 [hep-ph].
  - [329] J. McGowan, T. Cridge, L. A. Harland-Lang, and R. S. Thorne, *Eur. Phys. J. C* **83**, 185 (2023), [Erratum: *Eur.Phys.J.C* 83, 302 (2023)], arXiv:2207.04739 [hep-ph].
  - [330] R. D. Ball *et al.* (NNPDF), *Eur. Phys. J. C* **84**, 517 (2024), arXiv:2401.10319 [hep-ph].
  - [331] B. Pasquini, S. Rodini, and S. Venturini (MAP (Multi-dimensional Analyses of Partonic distributions)), *Phys. Rev. D* **107**, 114023 (2023), arXiv:2303.01789 [hep-ph].
  - [332] Y. Hatta, B.-W. Xiao, F. Yuan, and J. Zhou, *Phys. Rev. Lett.* **126**, 142001 (2021), arXiv:2010.10774 [hep-ph].
  - [333] Y. Hatta, B.-W. Xiao, F. Yuan, and J. Zhou, *Phys. Rev. D* **104**, 054037 (2021), arXiv:2106.05307 [hep-ph].
  - [334] P. Caucal, F. Salazar, B. Schenke, and R. Venugopalan, *JHEP* **11**, 169 (2022), arXiv:2208.13872 [hep-ph].
  - [335] P. Taels, T. Altinoluk, G. Beuf, and C. Marquet, *JHEP* **10**, 184 (2022), arXiv:2204.11650 [hep-ph].
  - [336] M. Dasgupta, F. Dreyer, G. P. Salam, and G. Soyez, *JHEP* **04**, 039 (2015), arXiv:1411.5182 [hep-ph].
  - [337] M. Dasgupta, F. A. Dreyer, G. P. Salam, and G. Soyez, *JHEP* **06**, 057 (2016), arXiv:1602.01110 [hep-ph].
  - [338] A. Banfi, P. F. Monni, G. P. Salam, and G. Zanderighi, *Phys. Rev. Lett.* **109**, 202001 (2012), arXiv:1206.4998 [hep-ph].
  - [339] A. Banfi, F. Caola, F. A. Dreyer, P. F. Monni, G. P. Salam, G. Zanderighi, and F. Dulat, *JHEP* **04**, 049 (2016), arXiv:1511.02886 [hep-ph].
  - [340] X. Liu, S.-O. Moch, and F. Ringer, *Phys. Rev. Lett.* **119**, 212001 (2017), arXiv:1708.04641 [hep-ph].
  - [341] G. Luisoni and S. Marzani, *J. Phys. G* **42**, 103101 (2015), arXiv:1505.04084 [hep-ph].
  - [342] S. Caletti, O. Fedkevych, S. Marzani, D. Reichelt, S. Schumann, G. Soyez, and V. Theeuwes, *JHEP* **07**, 076 (2021), arXiv:2104.06920 [hep-ph].
  - [343] D. Reichelt, S. Caletti, O. Fedkevych, S. Marzani, S. Schumann, and G. Soyez, *JHEP* **03**, 131 (2022), arXiv:2112.09545 [hep-ph].
  - [344] E. Chapon *et al.*, *Prog. Part. Nucl. Phys.* **122**, 103906 (2022), arXiv:2012.14161 [hep-ph].
  - [345] A. Accardi *et al.* (LHCspin), (2025), arXiv:2504.16034 [hep-ex].
  - [346] L. A. Anchordoqui *et al.*, *Phys. Rept.* **968**, 1 (2022), arXiv:2109.10905 [hep-ph].
  - [347] I. Adachi *et al.* (ILC International Development Team and ILC Community), (2022), arXiv:2203.07622 [physics.acc-ph].
  - [348] C. Balazs *et al.* (Linear Collider), (2025), arXiv:2503.24049 [hep-ex].
  - [349] D. Attié *et al.* (Linear Collider Vision), (2025),

- arXiv:2503.19983 [hep-ex].
- [350] A. Arbuzov *et al.*, *Prog. Part. Nucl. Phys.* **119**, 103858 (2021), arXiv:2011.15005 [hep-ex].
  - [351] C. Accettura *et al.*, *Eur. Phys. J. C* **83**, 864 (2023), [Erratum: *Eur.Phys.J.C* 84, 36 (2024)], arXiv:2303.08533 [physics.acc-ph].
  - [352] C. Accettura *et al.* (International Muon Collider), **2/2024** (2024), 10.23731/CYRM-2024-002, arXiv:2407.12450 [physics.acc-ph].
  - [353] C. Accettura *et al.* (MuCoL), (2024), 10.5281/zenodo.13970100, arXiv:2411.02966 [physics.acc-ph].
  - [354] K. M. Black *et al.*, *JINST* **19**, T02015 (2024), arXiv:2209.01318 [hep-ex].
  - [355] C. Accettura *et al.* (International Muon Collider), (2025), arXiv:2504.21417 [physics.acc-ph].
  - [356] A. Accardi *et al.*, *Eur. Phys. J. A* **60**, 173 (2024), arXiv:2306.09360 [nucl-ex].
  - [357] T. Bose *et al.*, in *2022 Snowmass Summer Study* (2022) arXiv:2209.13128 [hep-ph].
  - [358] S. Gessner *et al.*, (2025), arXiv:2503.20214 [physics.acc-ph].
  - [359] J. Altmann *et al.*, *ECFA Higgs, electroweak, and top Factory Study*, CERN Yellow Reports: Monographs, Vol. 5/2025 (2025) arXiv:2506.15390 [hep-ex].
  - [360] F.-K. Guo, U.-G. Meißner, and W. Wang, *Commun. Theor. Phys.* **61**, 354 (2014), arXiv:1308.0193 [hep-ph].
  - [361] S. J. Brodsky, P. Hoyer, C. Peterson, and N. Sakai, *Phys. Lett. B* **93**, 451 (1980).
  - [362] S. J. Brodsky, A. Kusina, F. Lyonnet, I. Schienbein, H. Spiesberger, and R. Vogt, *Adv. High Energy Phys.* **2015**, 231547 (2015), arXiv:1504.06287 [hep-ph].
  - [363] P. Jimenez-Delgado, T. J. Hobbs, J. T. Londergan, and W. Melnitchouk, *Phys. Rev. Lett.* **114**, 082002 (2015), arXiv:1408.1708 [hep-ph].
  - [364] R. D. Ball, V. Bertone, M. Bonvini, S. Carrazza, S. Forte, A. Guffanti, N. P. Hartland, J. Rojo, and L. Rottoli (NNPDF), *Eur. Phys. J. C* **76**, 647 (2016), arXiv:1605.06515 [hep-ph].
  - [365] T.-J. Hou, S. Dulat, J. Gao, M. Guzzi, J. Huston, P. Nadolsky, C. Schmidt, J. Winter, K. Xie, and C. P. Yuan, *JHEP* **02**, 059 (2018), arXiv:1707.00657 [hep-ph].
  - [366] R. D. Ball, A. Candido, J. Cruz-Martinez, S. Forte, T. Giani, F. Hekhorn, K. Kudashkin, G. Magni, and J. Rojo (NNPDF), *Nature* **608**, 483 (2022), arXiv:2208.08372 [hep-ph].
  - [367] M. Guzzi, T. J. Hobbs, K. Xie, J. Huston, P. Nadolsky, and C. P. Yuan, *Phys. Lett. B* **843**, 137975 (2023), arXiv:2211.01387 [hep-ph].
  - [368] R. D. Ball, A. Candido, J. Cruz-Martinez, S. Forte, T. Giani, F. Hekhorn, G. Magni, E. R. Nocera, J. Rojo, and R. Stegeman (NNPDF), *Phys. Rev. D* **109**, L091501 (2024), arXiv:2311.00743 [hep-ph].
  - [369] R. Vogt, *Phys. Rev. D* **110**, 074036 (2024), arXiv:2405.09018 [hep-ph].
  - [370] Y. L. Dokshitzer, V. A. Khoze, and S. I. Troian, *J. Phys. G* **17**, 1602 (1991).
  - [371] S. Acharya *et al.* (ALICE), *Nature* **605**, 440 (2022), [Erratum: *Nature* 607, E22 (2022)], arXiv:2106.05713 [nucl-ex].
  - [372] W. A. Bardeen, A. J. Buras, D. W. Duke, and T. Muta, *Phys. Rev. D* **18**, 3998 (1978).
  - [373] D. Yu. Ivanov and A. Papa, *JHEP* **07**, 045 (2012), arXiv:1205.6068 [hep-ph].
  - [374] A. Tumasyan *et al.* (CMS), *JHEP* **03**, 189 (2022), arXiv:2111.04605 [hep-ex].